Ritmes dels processos geològics i ritmes de les activitats sobre el medi generats per la nostra espècie

"estem manipulant i precipitant els temps d'alguns processos geològics"

Pere Busquets – Facultat de Geologia de la Universitat de Barcelona

MIRADES DE LA CIÈNCIA SOBRE EL TEMPS
Facultat de Filologia de la Universitat de Barcelona
26 i 27 de maig de 2014

Com ens hem convertit en agents geològics importants?

- Alguns exemples:

-Canviant més ràpidament les superfícies continentals i les submarines

-Produint alguns terratrèmols

-Coneixent més els volcans i retocant-los

-Mesurant i començant a influir (?) en el cicle geològic (sísmica 4d)

-La biosfera fa milions d'anys que incideix en el cicle geològic i el cicle geològic en la biosfera

Annex

-L'Antropocè (edat geològica?) i el gran experiment

- Canviant les superfícies continentals i les submarines

Retenció de sediments

Table 1. Flux of river water (Q) and sediment (Q_s) for pre-Anthropocene and Anthropocene conditions *ca* late twentieth century (after [35]). These values represent continental coastline fluxes.

continent	Q (km^3 yr^{-1})	Q_s with humans[a] (Gt yr^{-1})	Q_s pre-humans[a] (Gt yr^{-1})
Africa	3797	1.1	1.6
Asia	9806	4.8 =4800000000 Tones	5.3
Australasia	608	0.28	0.24
Europe	2680	0.4	0.6
Indonesia	4251	2.4	2.4
North America	5819	1.5	1.7
Oceans	20	0.004	0.003
South America	11 529	2.4	3.3
Global	38 510	12.8	15.1

[a]Incorrect Q_s values were unfortunately published in a previous table [35].

Retencions d'entre el 10 i el 15% respecte al transport sense influència humana

- Canviant les superfícies continentals i les submarines

Retenció de sediments

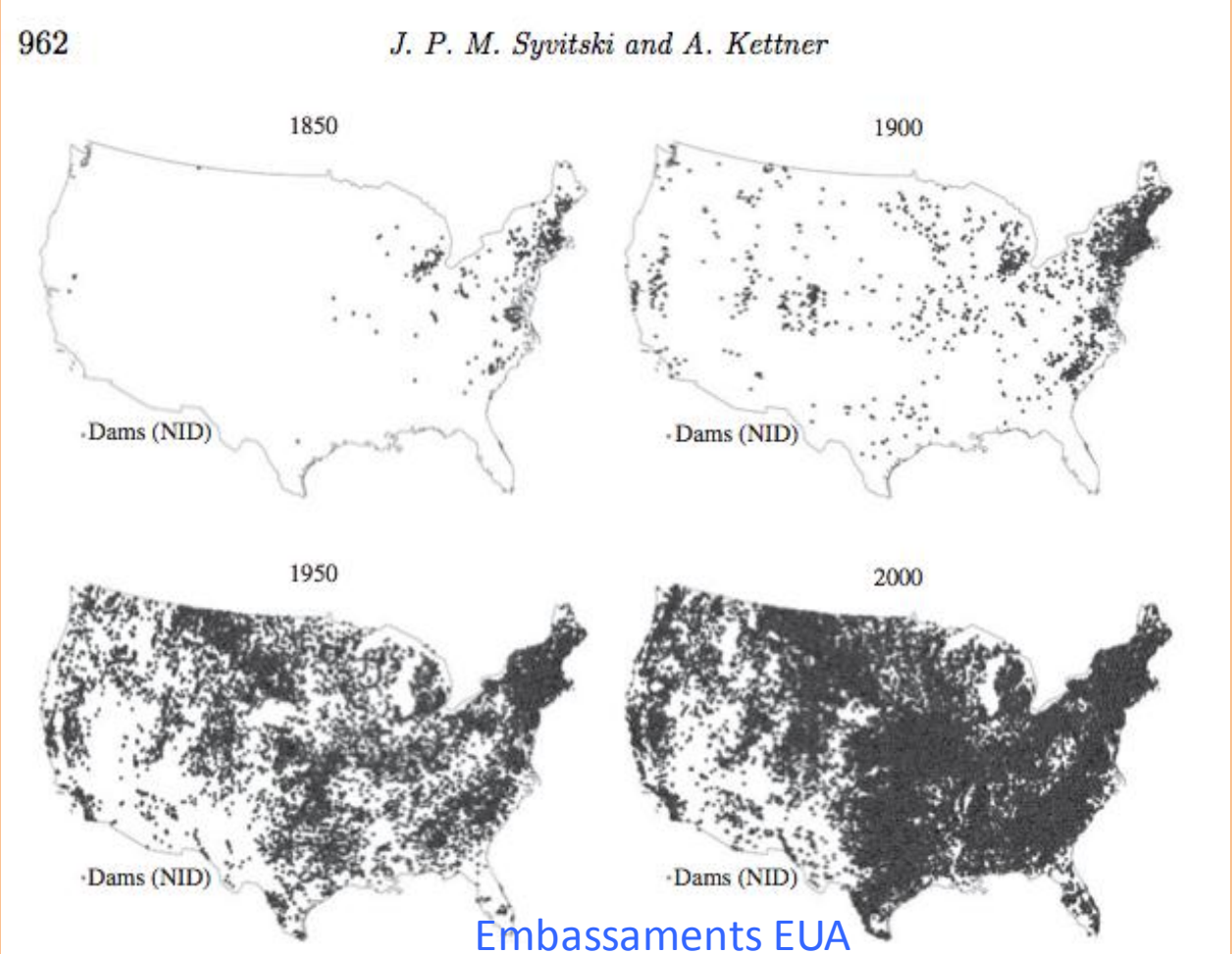

Embassaments EUA

Figure 3. The growth of US dams and reservoirs as recorded in the National Inventory of Dams (NID). Four periods shown: 1850, 1900, 1950 and 2000. There were no dams in 1800.

- Canviant les superfícies continentals i les submarines

Retenció de sediments

File:ThreeGorgesDam-China2009.jpg

Wikimedia Commons está disponible en español

From Wikimedia Commons, the free media repository

File | File history | File usage on Commons | File usage on other wikis

v: 800 × 474 pixels. Other resolutions: 320 × 190 pixels I 640 × 380 pixels I 1,024 × 607 pixels I 1,280 × 759 pixels I 2,900 × 1,720 pixels.

900 × 1,720 pixels, file size: 2.87 MB, MIME type: image/jpeg); ZoomViewer: flash/no flash

Capacidad total	39300 Hm³
Localización	
País	China
Río	Yangtsé
Coordenadas	30°49′48″N 111°0′36″E

- Canviant les superfícies continentals i les submarines

  Moviments de terres

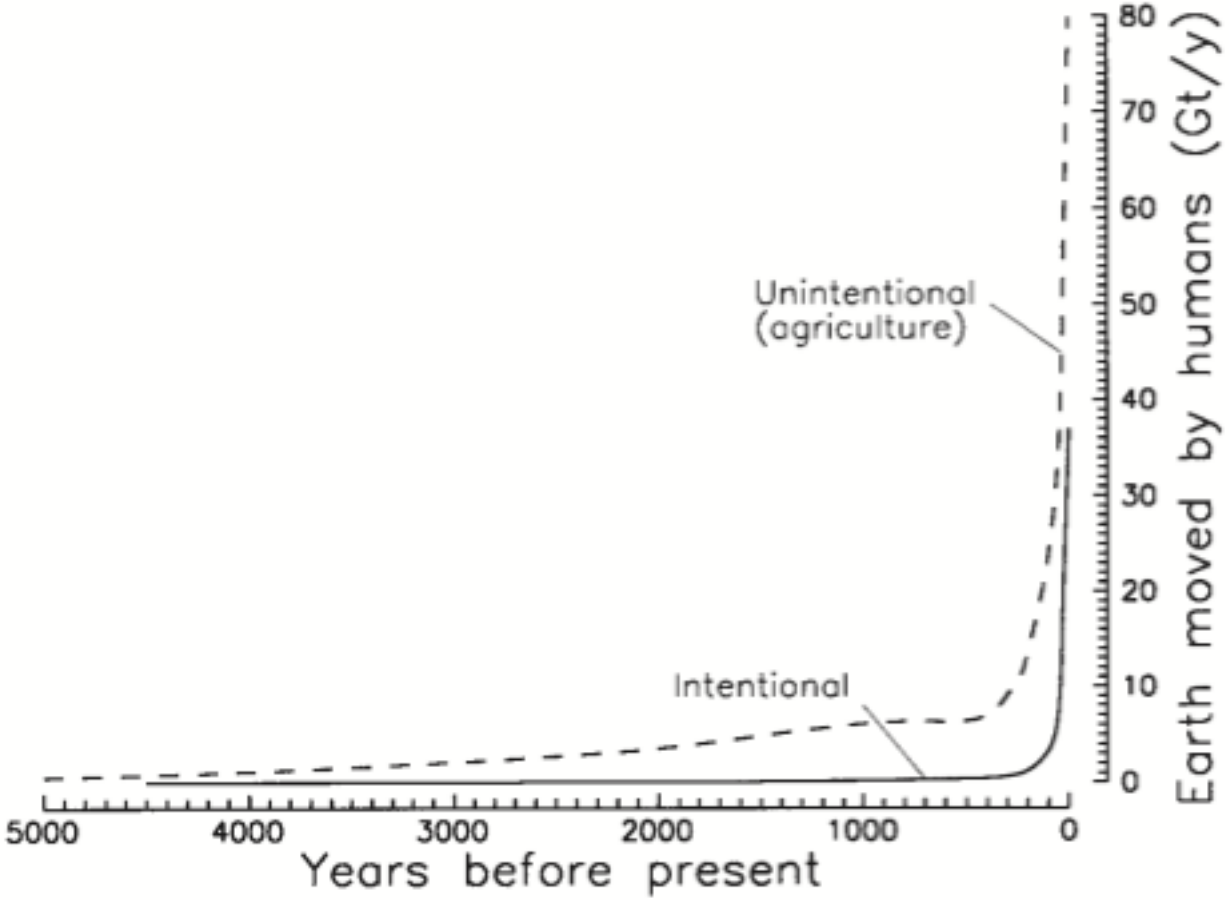

Figure 4. Estimate of total amount of earth moved annually by humans at various times in the past. Curves were obtained by multiplying earth moved per capita (Fig. 2) by population (Fig. 3).

GEOLOGY, September 2000

The Mediterranean Drainage basin

Anthropogenic versus natural contributions to river sediment loads

EROSION AND SEDIMENT YIELD IN MEDITERRANEAN RIVER BASINS

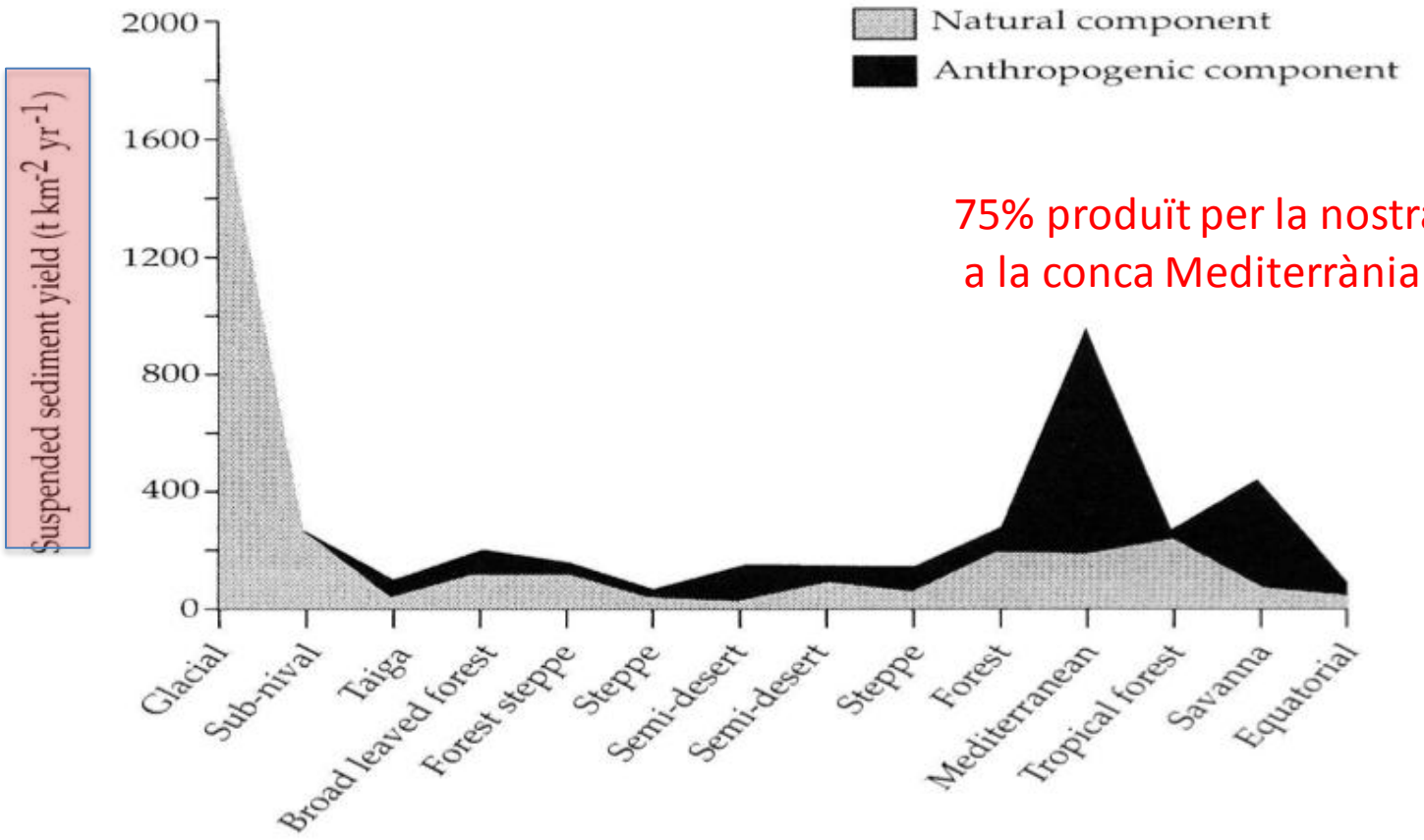

75% produït per la nostra activitat a la conca Mediterrània

The relative importance of natural and human contributions to the suspended sediment yield of mountain river basins in different climatic regions (after Dedkov and Mozzherin, 1992). These data indicate that around 75% of the sediment yield of Mediterranean headwater river basins may be attributed to human activity

Canviant les superfícies continentals i les submarines
Moviments de terres en mines a cel obert

Valle de Boinas, Asturias

- Canviant les superfícies continentals i les submarines
- La pesca d'arrossegament

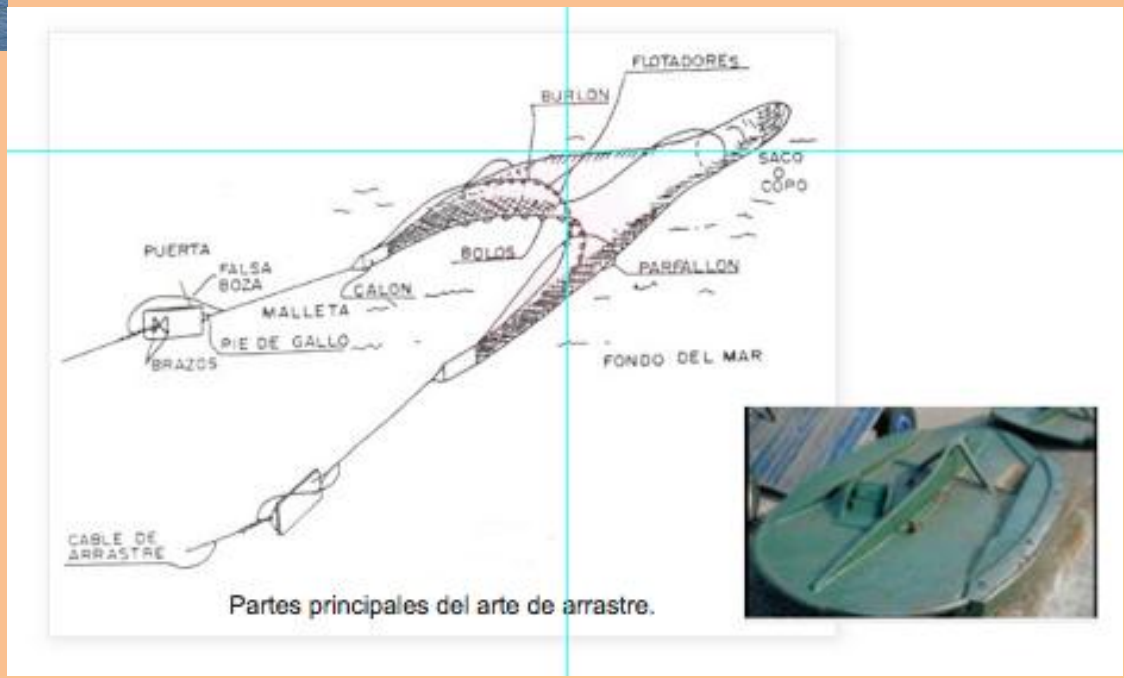

Partes principales del arte de arrastre.

- Canviant les superfícies continentals i les submarines
- La pesca d'arrossegament

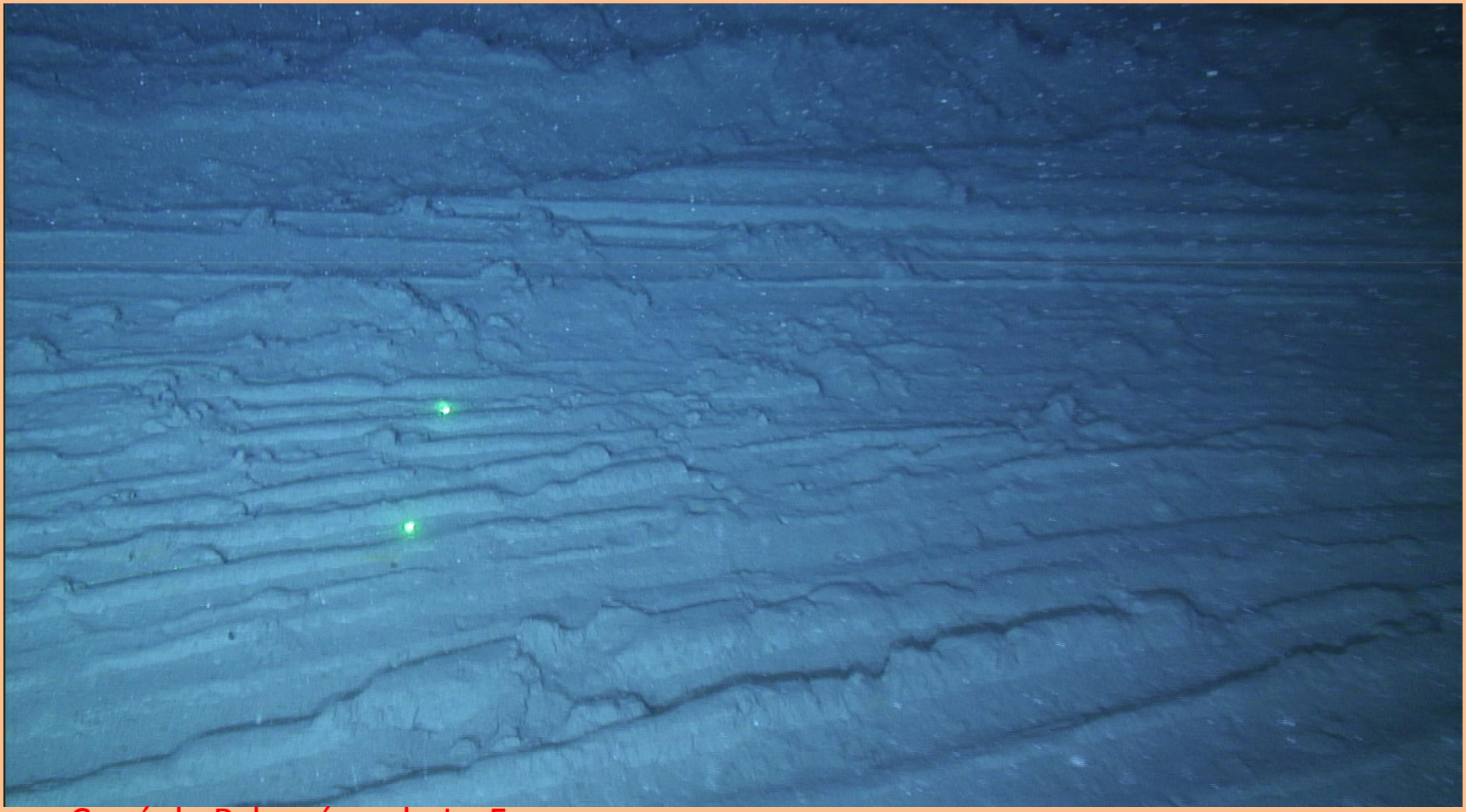

Canó de Palamós o de La Fonera

- Canviant les superfícies continentals i les submarines
- La pesca d'arrossegament

Pere Puig et al. 2012 *Nature 489*

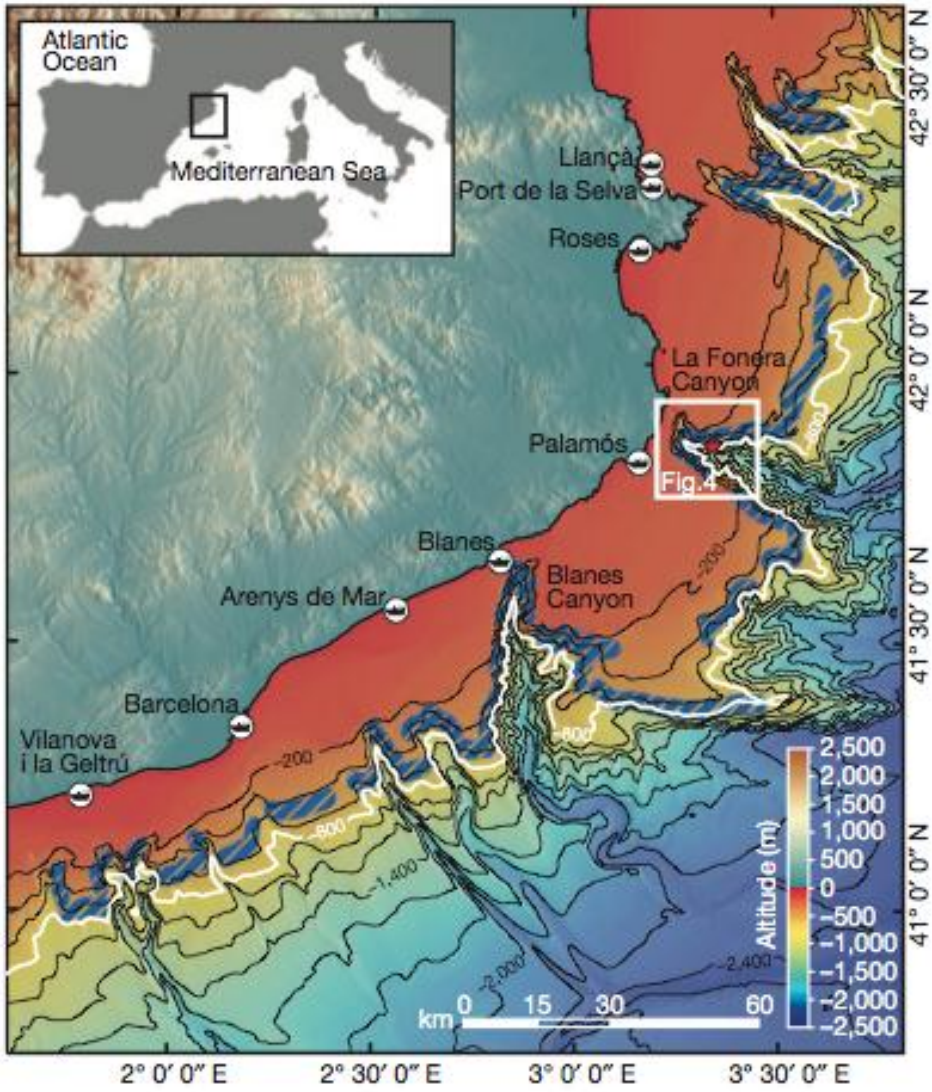

Figure 2 | Bathymetric map of the study area. Bathymetric map of the northern Catalan margin (northwestern Mediterranean) showing the main trawling grounds on the open continental slope and canyon flanks (blue hatching). Data was obtained from the VMS. The largest ports of the area (vessels in white circles) and the 800-m isobath (white thick contour) are highlighted. The location of Fig. 4 and the mooring station (red star in white box; see Fig. 3 and Supplementary Fig. 1) in La Fonera (also named Palamós) Canyon are indicated.

- Canviant les superfícies continentals i les submarines
- La pesca d'arrossegament

Pere Puig et al.2012 *Nature 489*

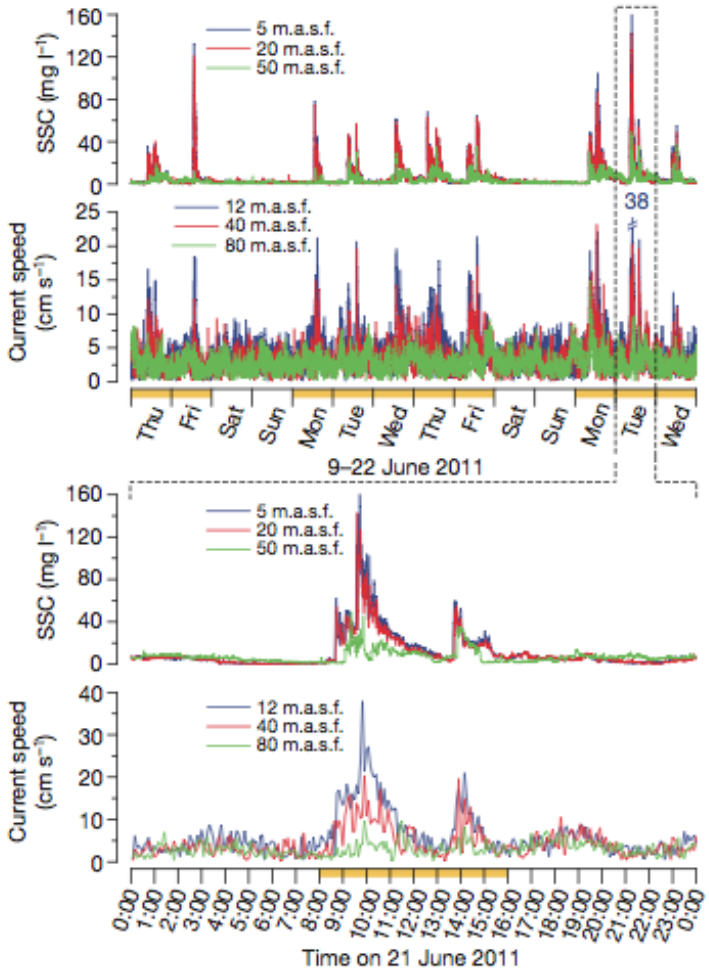

Figure 3 | Time series observations of trawling-induced sediment gravity flows. Graphs showing near-bottom suspended sediment concentration (SSC) and current speed records observed at the northern flank of La Fonera Canyon during a two-week period at different heights above the sea floor (m.a.s.f., metres above sea floor). Sediment transport events were observed during weekdays (that is, working days for the fishery), but not on weekends. The detail of a one-day record (21 June 2011) shows two sharp increases in SSC and the consequent intensification of the current speed (directed downslope towards 192°), with higher velocities closer to the sea floor that denote the occurrence of sediment gravity flows. The two peaks correspond to the two main hauls of the trawling fleet, the first one heading offshore and the second one heading to port. Orange bars on the *x* axes denote working days and working hours, respectively. Note the change in scale of the current-speed *y* axes. See mooring location in Figs 2 and 4 and Supplementary Figs 2 and 3.


Panama
Colombia
Venezuela
Barranquilla 85km
350 m
Mar Caribe
Cartagena 50km
1000 m
Volcán de lodo Totumo
Galerazamba (Colombia)
Image © 2007 DigitalGlobe
©2006 Google

Presents en alguns
fons marins i en àrees petrolíferes
(més de naturals que de provocats per la nostra activitat). Són freqüents els provocats per sismes.

- Canviant les superfícies continentals i les submarines
Canviant límits terra-mar

Retrogradation example: Holland coast

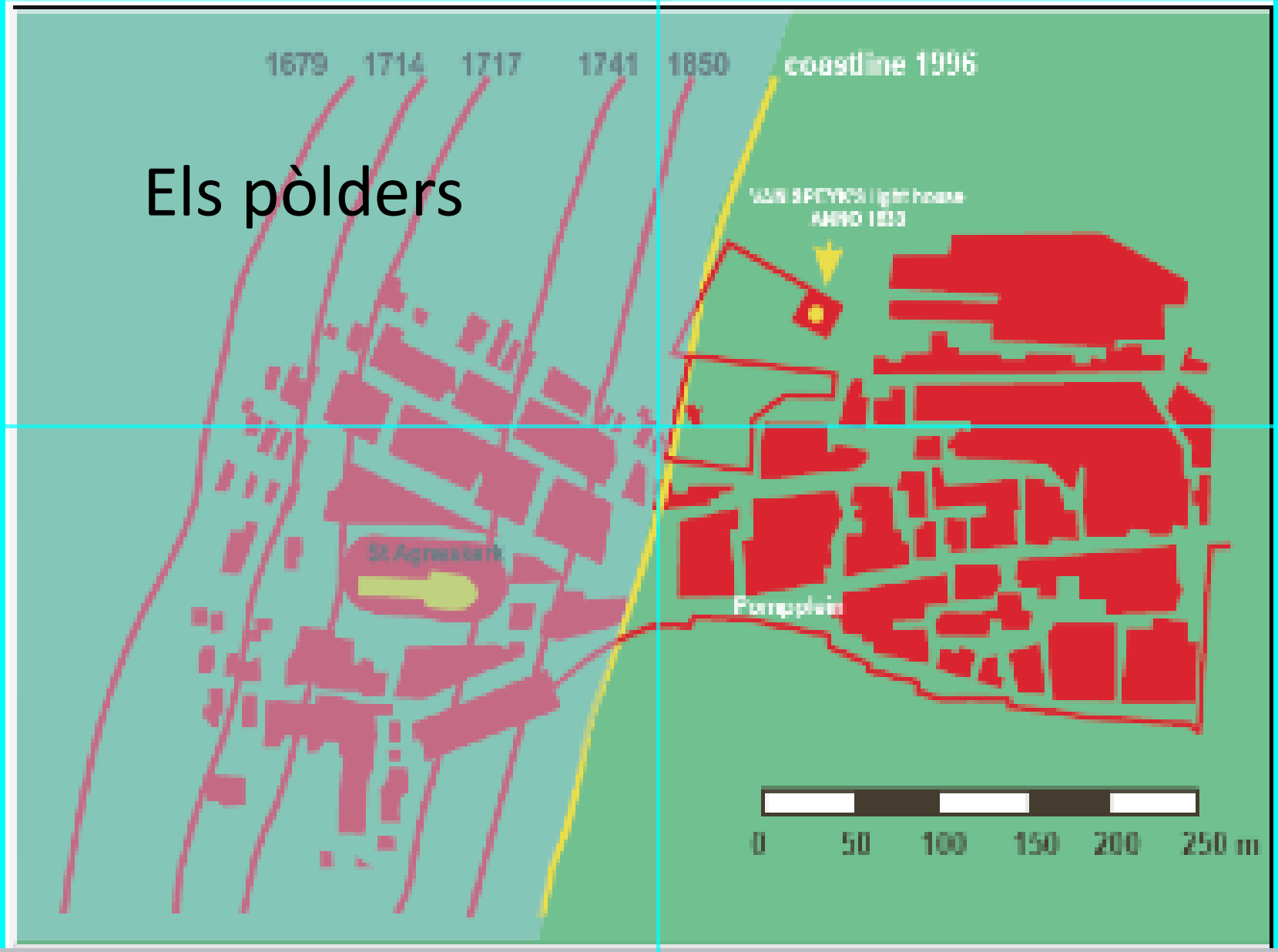

Els pòlders

- Canviant les superfícies continentals i les submarines
Canviant límits terra-mar.
De manera natural ja va canviant.

Gulpiyuri -Asturias

- Canviant les superfícies continentals i les submarines
- L'ensorrament de territoris

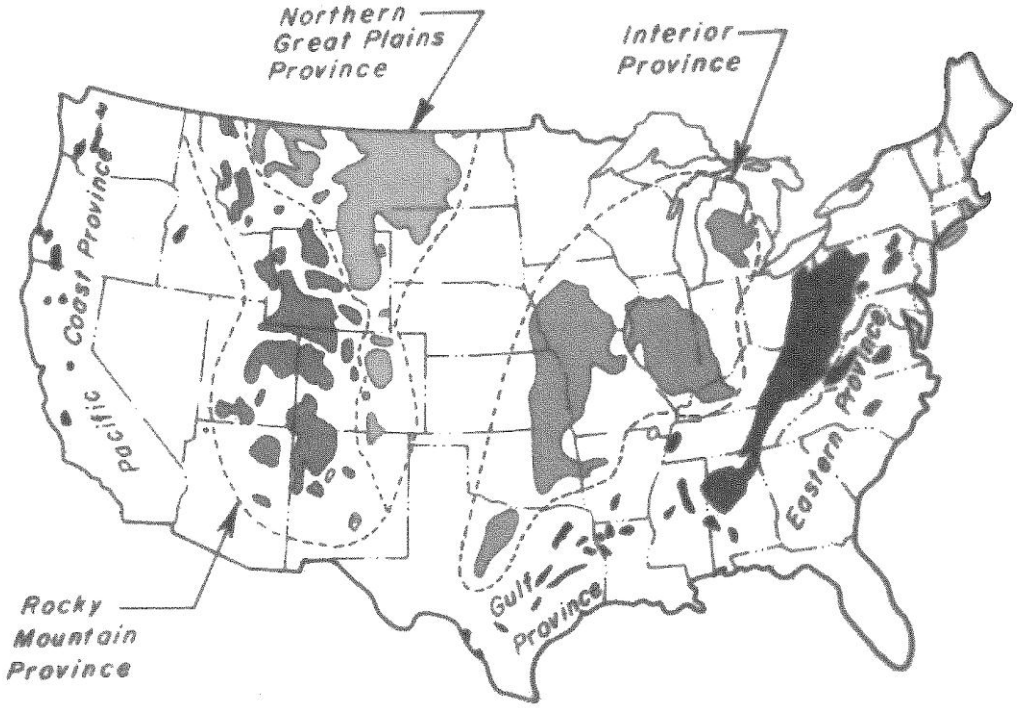

Figure 1. Coal fields in the conterminous United States (after Averitt, 1970).

Àrees amb carbó als EUA

- Canviant les superfícies continentals i les submarines
- L'ensorrament de territoris

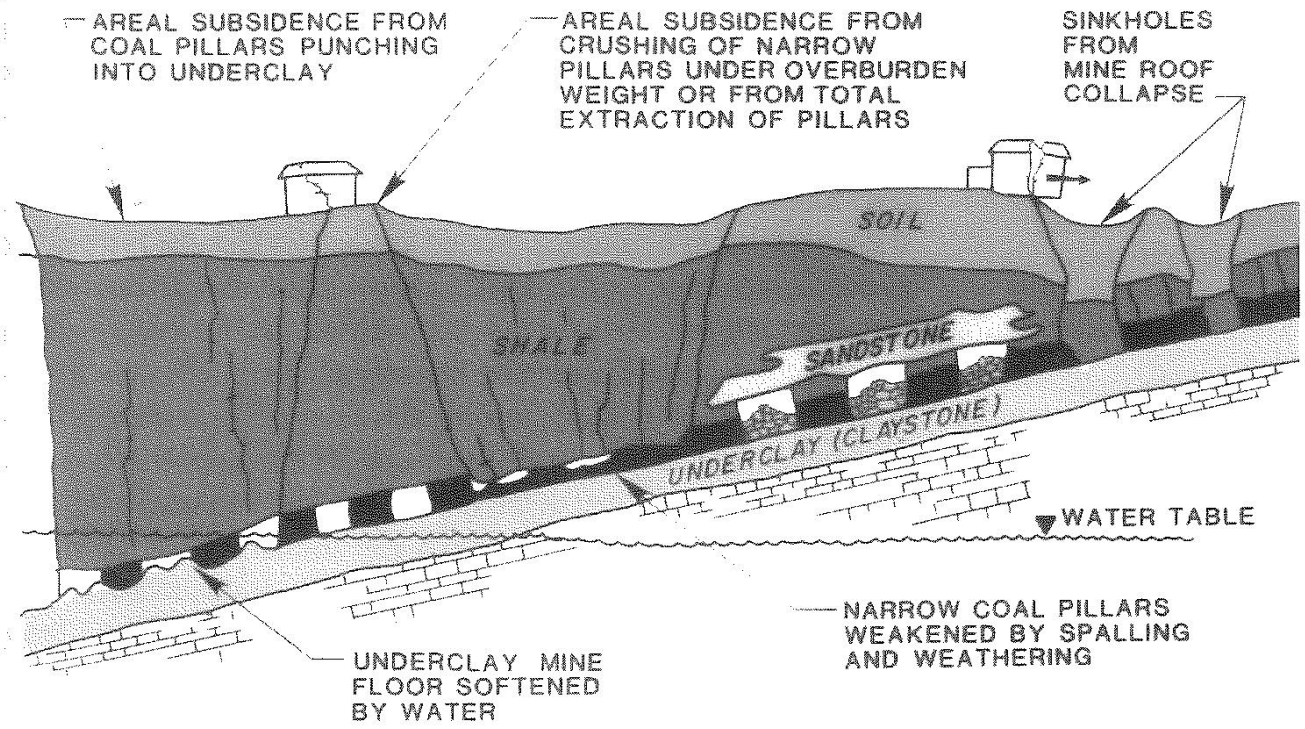

Figure 6. Modes of subsidence (Gray and Bruhn, 1984).

- Canviant les superfícies continentals i les submarines
- L'ensorrament de territoris

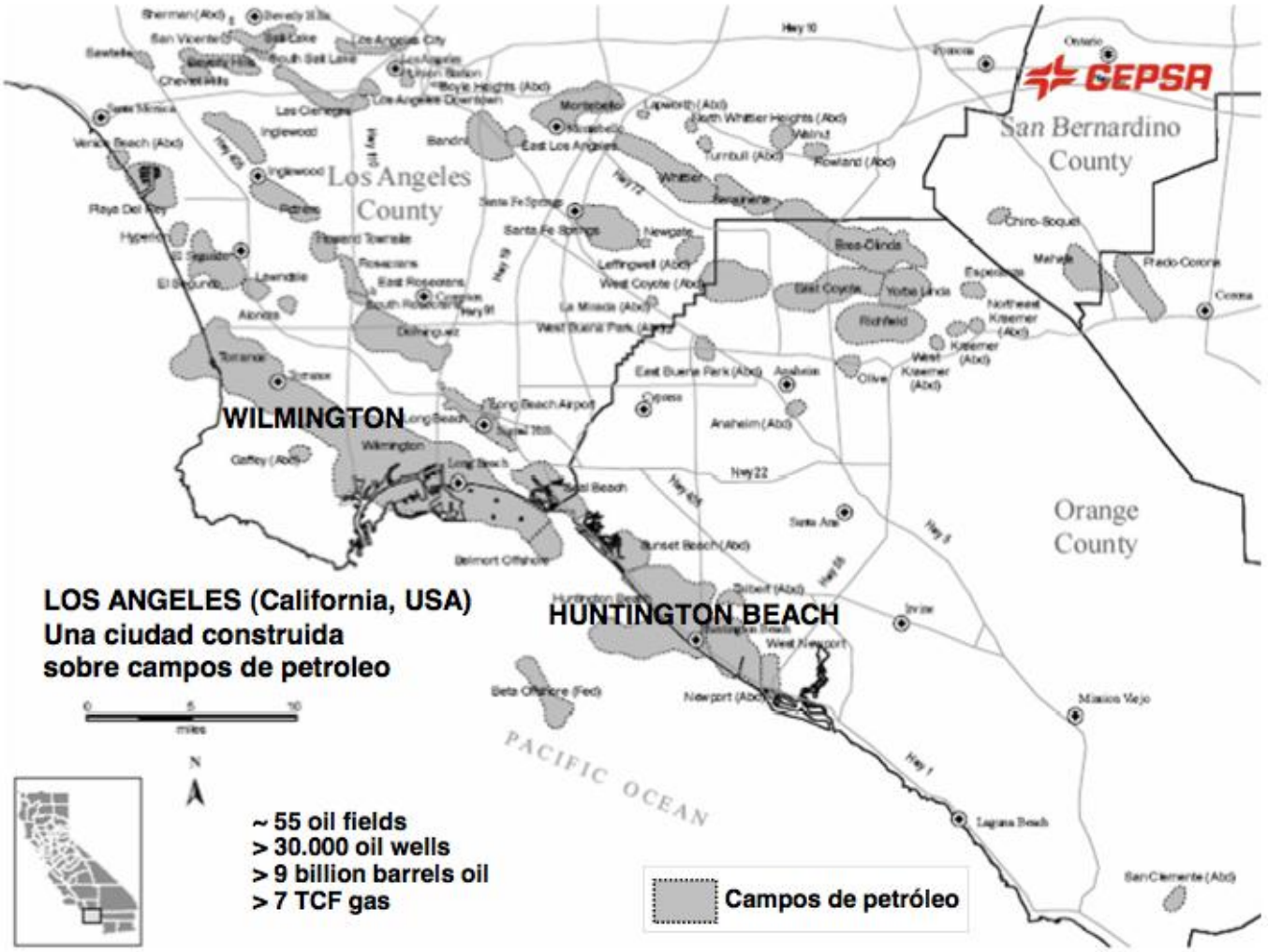

- Canviant les superfícies continentals i les submarines
- L'ensorrament de territoris

Aprox. 1500 km^2

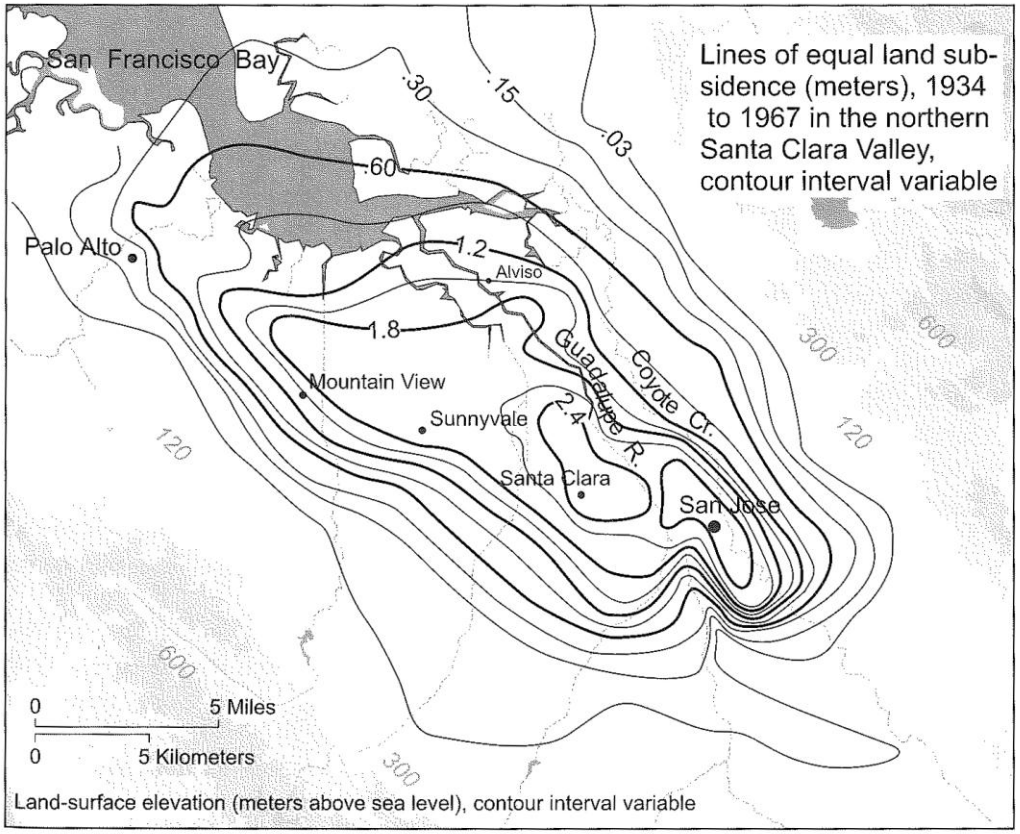

Lines of equal land subsidence (meters), 1934 to 1967 in the northern Santa Clara Valley, contour interval variable

Figure 5. Map of subsider
Clara Valley, California, 19
ified from Poland and Irel

Aprox 9 metres en 90 anys

Figure 4. Approximate point of maximum subsidence in the San Joaquin Valley, California. Land surface subsided ~9 m from 1925 to 1977 due to aquifer-system compaction. Signs on the telephone pole indicate the former elevations of the land surface in 1925 and 1955. Photograph by Richard Ireland.

(Geological Society of America. Holzer and Halllowayl 2005.Reviews in Engineering Geology, Volume XVI)

- Canviant les superfícies continentals i les submarines
- L'ensorrament de territoris

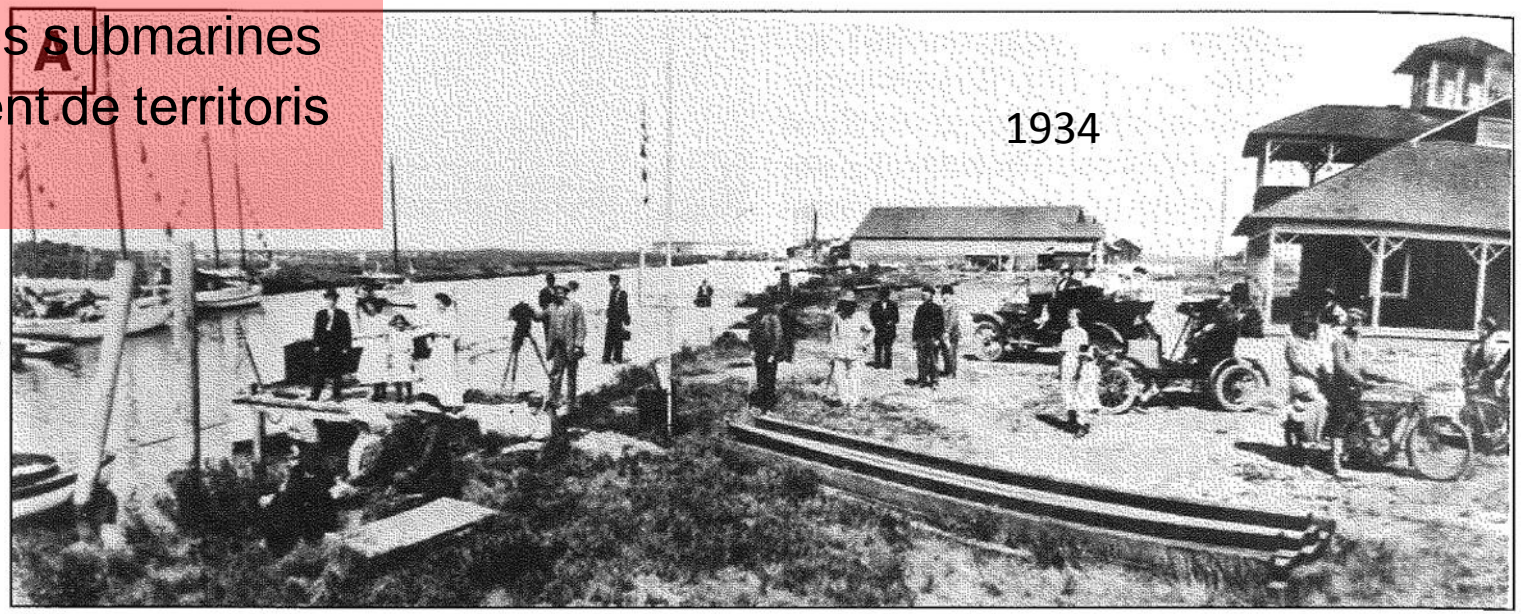

Figure 8. Alviso Yacht Club, Santa Clara Valley, California, in 1914 (A) and 1976 (B). Approximately 2 m of subsidence occurred at this site from 1934 to 1967. Photographs from archives of Alviso Yacht Club.

(Geological Society of America. Holzer and Hallloway1 2005.Reviews in Engineering Geology, Volume XVI)

- Canviant les superfícies continentals i les submarines
- L'ensorrament de territoris

(Geological Society of America.
Holzer and Hallloway l 2005.Reviews in Engineering Geology, Volume XVI)

Conseqüències: inundacions, canvis topogràfics, esquerdes, reducció de la capacitat dels aqüífers..)

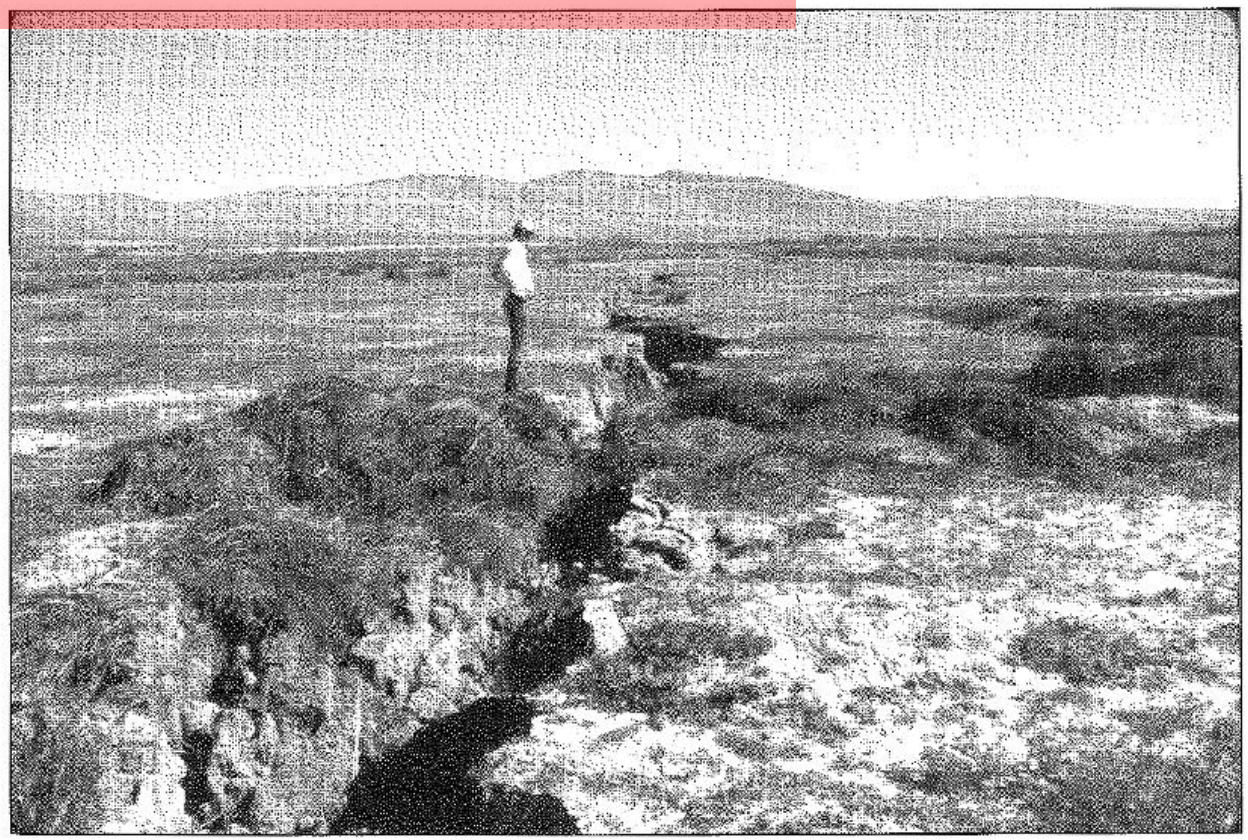

Figure 11. Earth fissure associated with land subsidence caused by pumping of groundwater in Fremont Valley, California. Photograph by Thomas L. Holzer, March 1978.

La part més positiva de la història…….

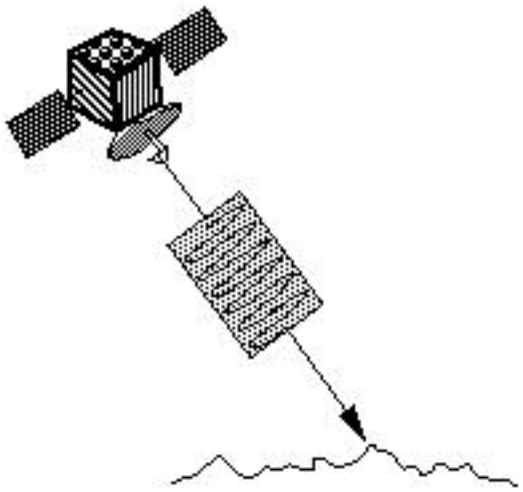

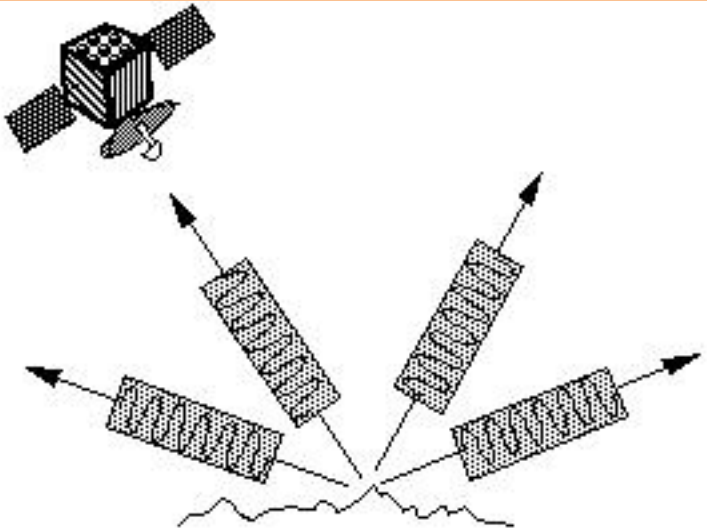

Figures from T. Freeman, Jet Propulsion Laboratory

Eva Asensio 2014
(tesi doctoral inèdita)

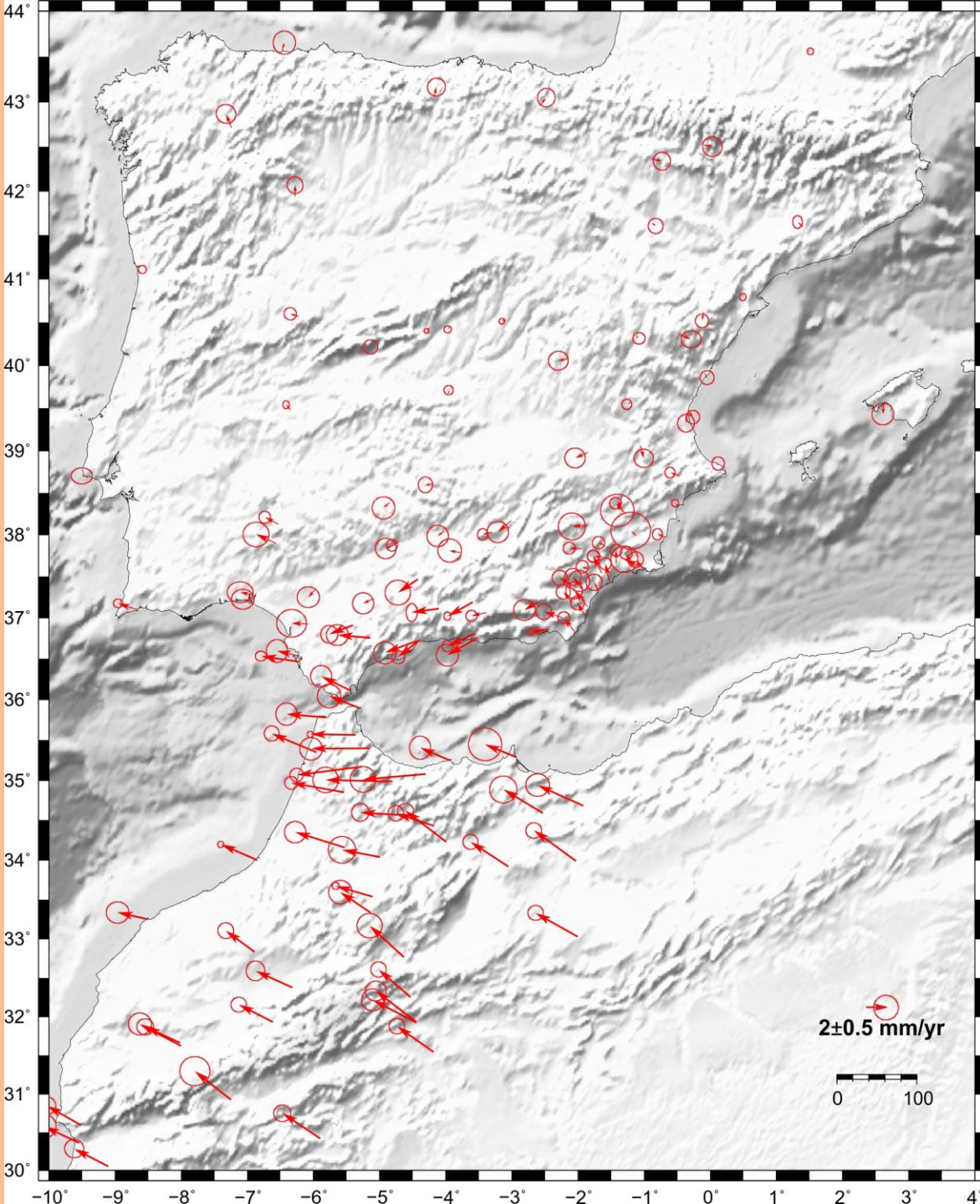

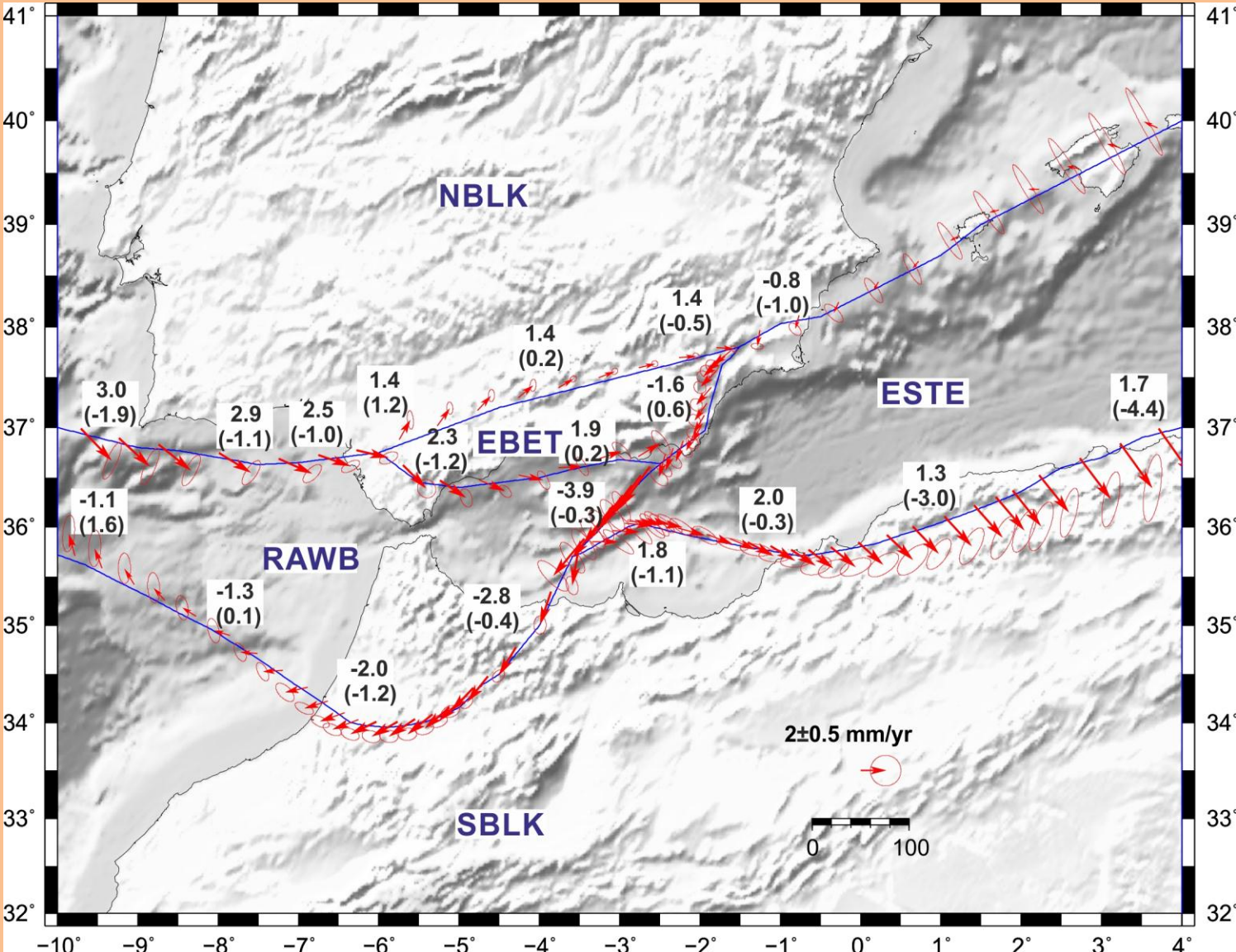

Eva Asensio 2014
(tesi doctoral inèdita)

LETTER

doi:10.1038/nature13275

Uplift and seismicity driven by groundwater depletion in central California

Colin B. Amos[1], Pascal Audet[2], William C. Hammond[3], Roland Bürgmann[4,5], Ingrid A. Johanson[4] & Geoffrey Blewitt[3]

Groundwater use in California's San Joaquin Valley exceeds replenishment of the aquifer, leading to substantial diminution of this resource[1–4] and rapid subsidence of the valley floor[5]. The volume of groundwater lost over the past century and a half also represents a substantial reduction in mass and a large-scale unburdening of the lithosphere, with significant but unexplored potential impacts on crustal deformation and seismicity. Here we use vertical global positioning system measurements to show that a broad zone of rock uplift of up to 1–3 mm per year surrounds the southern San Joaquin Valley. The observed uplift matches well with predicted flexure from a simple elastic model of current rates of water-storage loss, most of which is caused by groundwater depletion[3]. The height of the adjacent central Coast Ranges and the Sierra Nevada is strongly seasonal and peaks during the dry late summer and autumn, out of phase with uplift of the valley floor during wetter months. Our results suggest that long-term and late-summer flexural uplift of the Coast Ranges reduce the effective normal stress resolved on the San Andreas Fault. This process brings the fault closer to failure, thereby providing a viable mechanism for observed seasonality in microseismicity at Parkfield[6] and potentially affecting long-term seismicity rates for fault systems adjacent to the valley. We also infer that the observed contemporary uplift of the southern Sierra Nevada previously attributed to tectonic or mantle-derived forces[7–10] is partly a consequence of human-caused groundwater depletion.

Hydrospheric mass changes exert direct influence over lithospheric deformation. Both seasonal and long-term changes to ice, snow or water loads may induce displacements of the Earth's surface[11–15] and can create stress perturbations that modulate activity on seismogenic faults[16–19]. A volume of groundwater approaching approximately 160 km^3 in California's Central Valley has been lost through pumping, irrigation and evapotranspiration over the past 150 years or so[3,4]. Historical and modern records demonstrate that groundwater depletion occurs primarily in the drier, hotter, southern portion of the basin[1,3] (the San Joaquin Valley), parallel to the central San Andreas Fault and adjacent to the high topography of the southern Sierra Nevada (Fig. 1). Previous studies demonstrating sensitivity to small-scale stress changes across this section of the San Andreas point to seasonal hydrologic[6] or temperature[20] variations to explain observed changes in seismicity rates[6] or strain in shallow boreholes[20].

Modest contemporary uplift rates of the southern Sierra Nevada observed using space geodesy[7–9] have been attributed to various tectonic and geomorphic drivers, such as buoyant response to mantle delamination[10], Basin and Range extensional faulting[21], and erosional mass transfer from Pleistocene glaciation[22]. Inferred stress change from epeirogenic uplift in the southern Sierra Nevada is also potentially linked to the transition from locked to creeping sections of the San Andreas Fault[23]. Here we seek to explore potential human impacts on contemporary deformation across this region through global positioning system (GPS) constraints on lithospheric flexure induced by anthropogenic groundwater level changes.

Continuous GPS networks spanning the southwestern USA provide a high-resolution framework for analysing crustal motion in three dimensions (Fig. 1). Longer available records and recently improved processing techniques enable determination of reliable GPS vertical velocities with a precision[24] of less than a millimetre per year, tied to the Earth system's centre of mass to within 0.5 mm yr^{-1} (refs 24 and 25). GPS station data were processed to create individual time series of vertical position and were then fitted with an empirical mo
locity, and the amplitude and phase
monic components (to model seasona
only stations with at least two-and-a-h
uncertainties of ≤1.0 mm yr^{-1} (566 s
lysis and processing techniques are i

Figure 1 shows the distribution of
California and east of the Sierra Nevad
rates exclude GPS stations located with
water basin that display comparativ
position on soft sediment. These stati
driven subsidence through loss of pore
related to groundwater level fluctuati
processes unrelated to solid earth mo

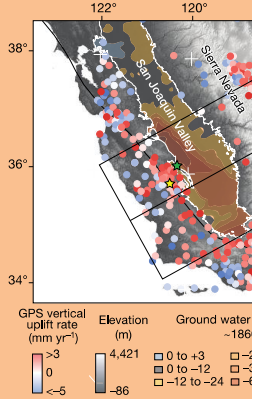

Figure 1 | Contemporary GPS vertical ra
of vertical uplift rates from GPS stations (
the western Great Basin. Stations in the v
signals and local irrigation effects are excl
changes in the deep, confined aquifer[1]. Th
configuration of the Central Valley groun
Valley; SJV, San Joaquin Valley), and the

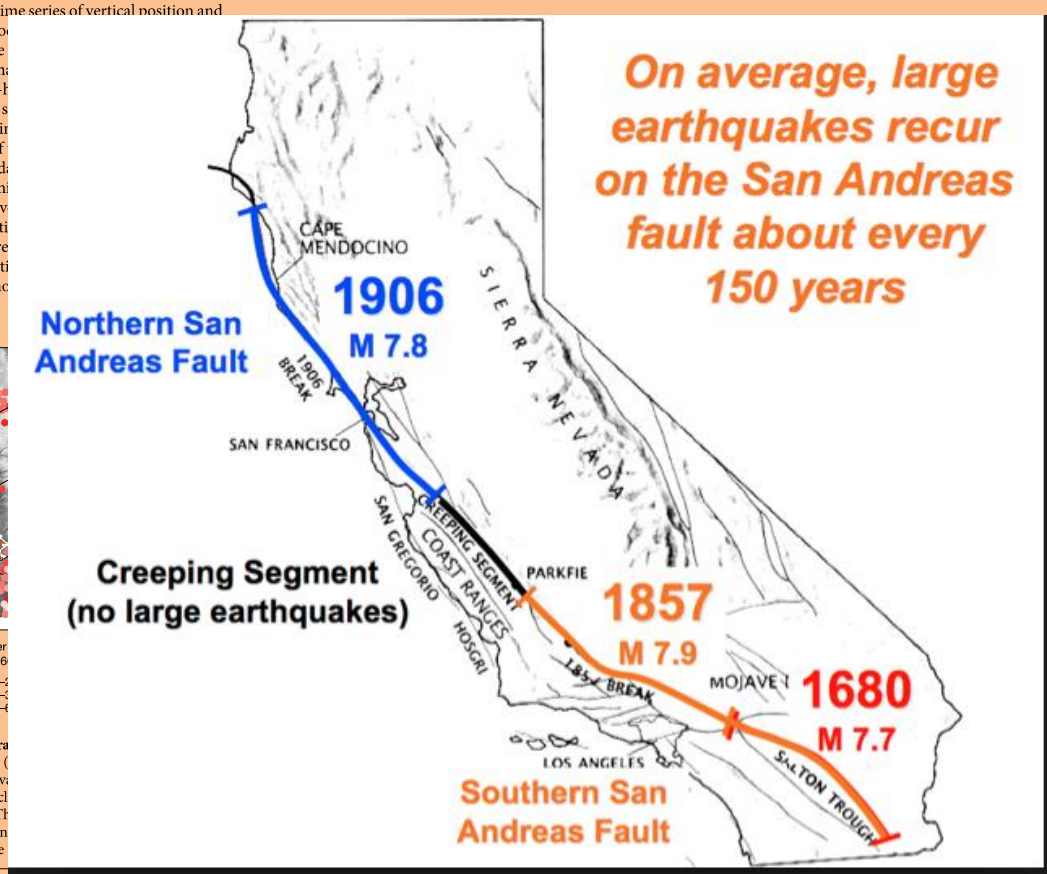

[1]Geology Department, Western Washington University, Bellingham, Washington 98225-9080, USA. [2]Department of Earth Sciences, University of Ottawa, Ottawa, Ontario K1N 6N5, Canada. [3]Nevada Geodetic Laboratory, Nevada Bureau of Mines and Geology and Nevada Seismological Laboratory, University of Nevada, Reno, Nevada 89557, USA. [4]Berkeley Seismological Laboratory, University of California, Berkeley, California 94720-4760, USA. [5]Department of Earth and Planetary Science, University of California, Berkeley, California 97720-4767, USA.

Com coneixem les zones que s'estàn tensionant

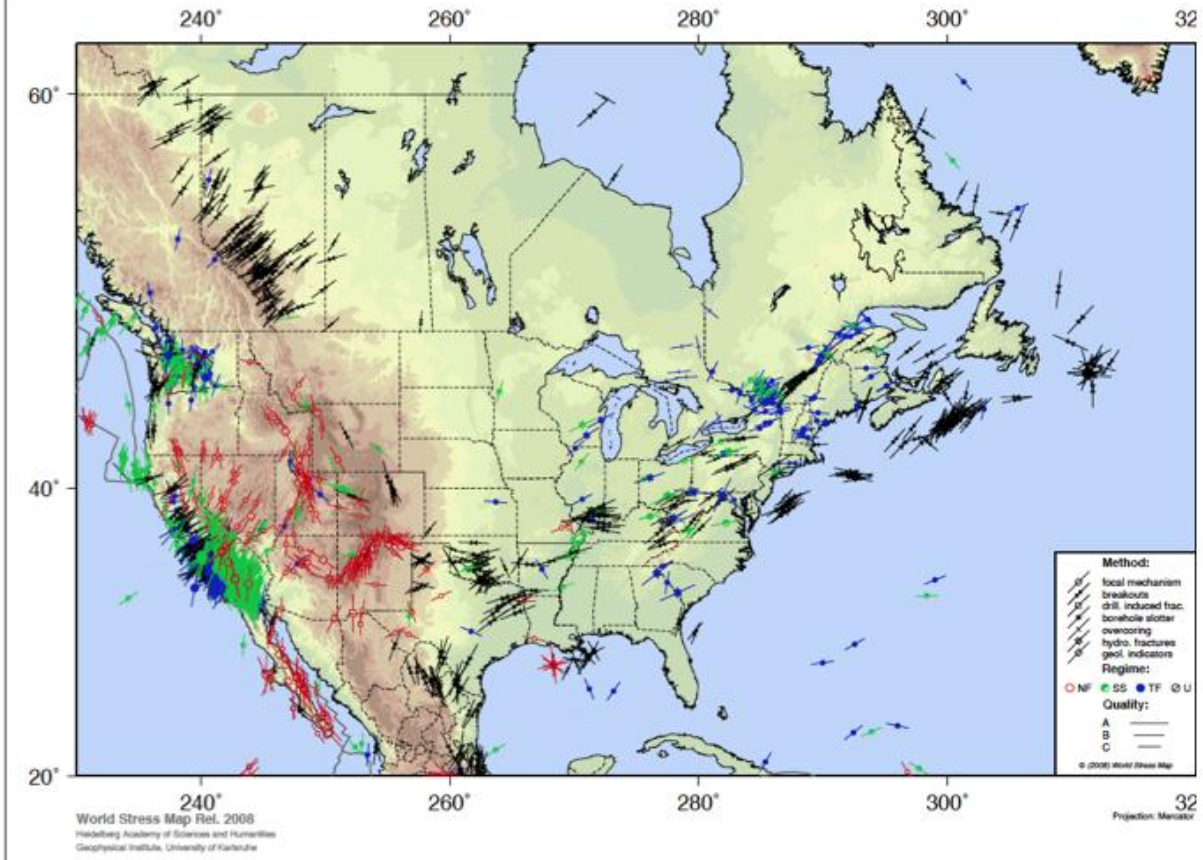

Figure 4. North America stress map. The stress map displays the orientations of the maximum horizontal compressive stress (σ_H). The length of the stress symbols represents the data quality, with A being the best quality. Quality A data are assumed to record the orientation of σ_H to within 10°-15°, quality B data to within 15°-20°, and quality C data to within 25°. As can be seen from this global dataset, stress measurements are absent in many parts of North America and the offshore. Because stress measurements are important in the consideration of induced seismicity, their measurement, particularly in areas where data are sparse, could usefully contribute to understanding the potential for induced seismicity related to energy development. The tectonic regimes are: NF for normal faulting, SS for strike-slip faulting, TF for thrust faulting, and U for an unknown regime. Topographic relief is indicated by green (lower elevations) to brown (higher elevations) shading. Data used to plot this map were accessed from www.world-stress-map.org/ (see Heidbach et al., 2008).

- Canviant les superfícies continentals i les submarines
- L'ensorrament de territoris

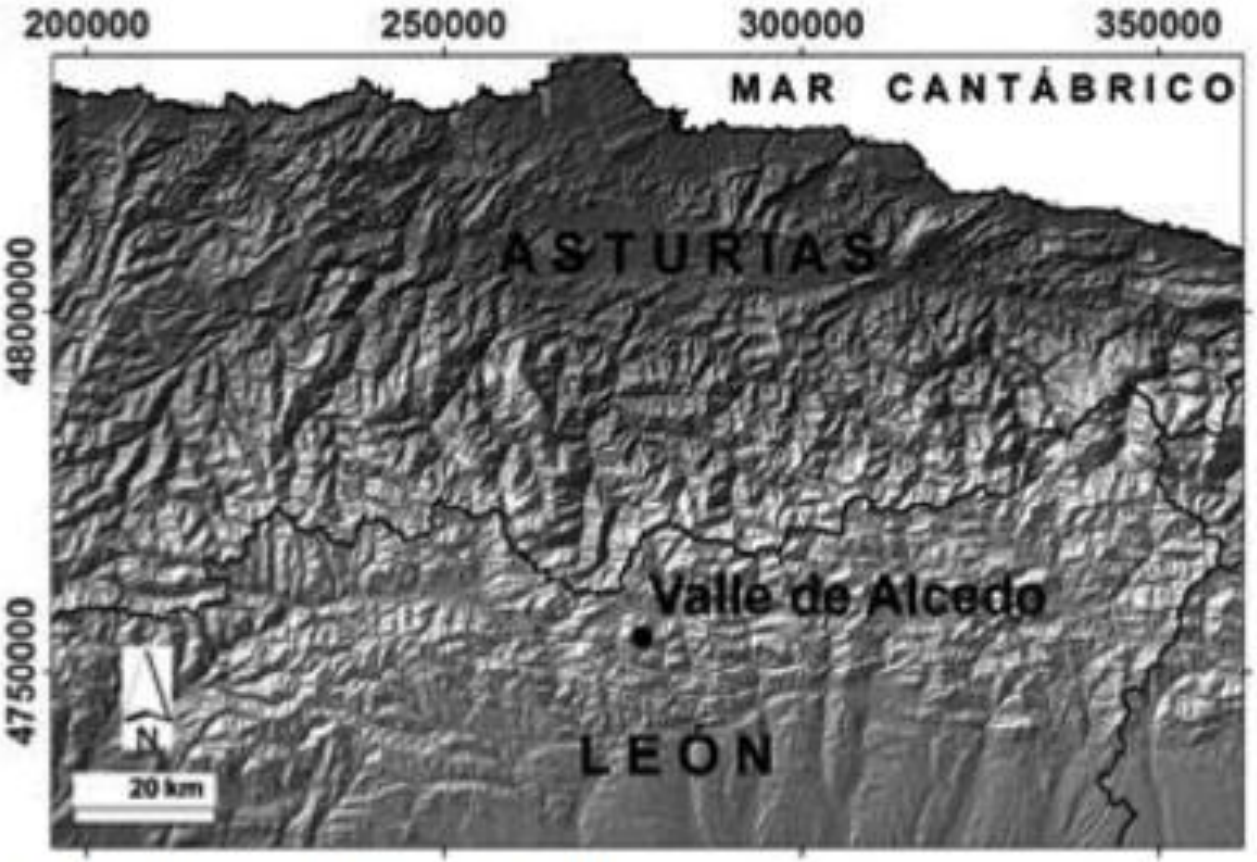

Fig. 1.- Situación del área de estudio.

Fig. 1.- Studying area situation.

Pablo Valenzuela et al. 2013. Geogaceta, 54)

- Canviant les superfícies continentals i les submarines
- L'ensorrament de territoris

(Pablo Valenzuela et al. 2013. Geogaceta, 54)

Fig. 2.- Fractura de la canalización sobre el socavón de mayor cota en el arroyo de Alcedo. En la fotografía se observan dos sumideros activos (a y b).

Fig. 2.- Broken canal over the highest sinkhole in Alcedo stream. The picture shows two active infiltration areas (a and b).

Súria i sal

- Canviant les superfícies continentals i les submarines
- L'ensorrament de territoris

Desplazamientos debidos a explotación minera

- Zona: Suria

- Periodo cubierto: 35 días

- Obtenido a partir de imágenes SAR ERS

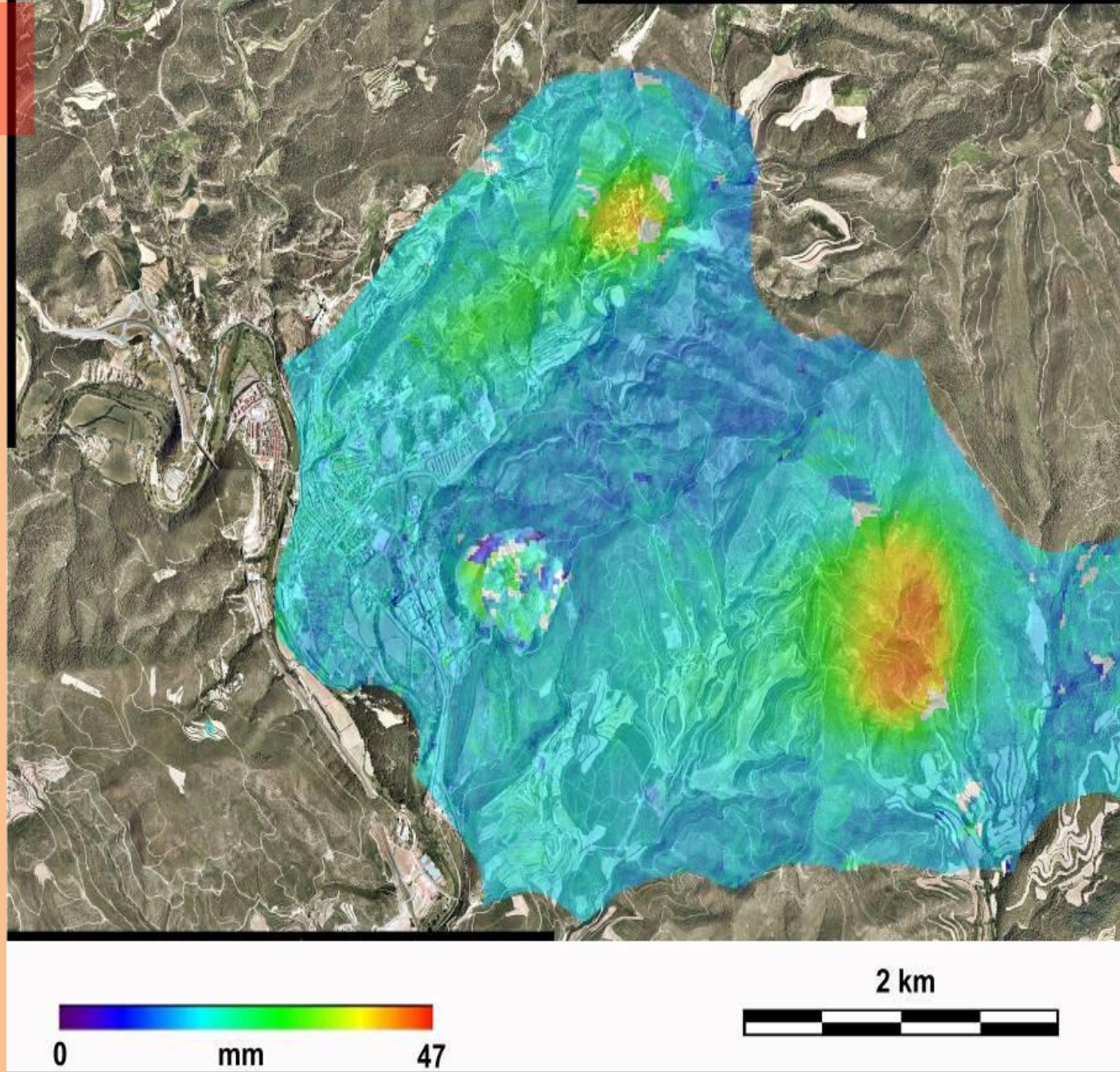

INSTITUT DE GEOMÀTICA

Produint terratrèmols

Coneixem on s'originen
Coneixem la intensitat aproximada
I anem afinant quan es produiran

I en produïm

Produint terratrèmols

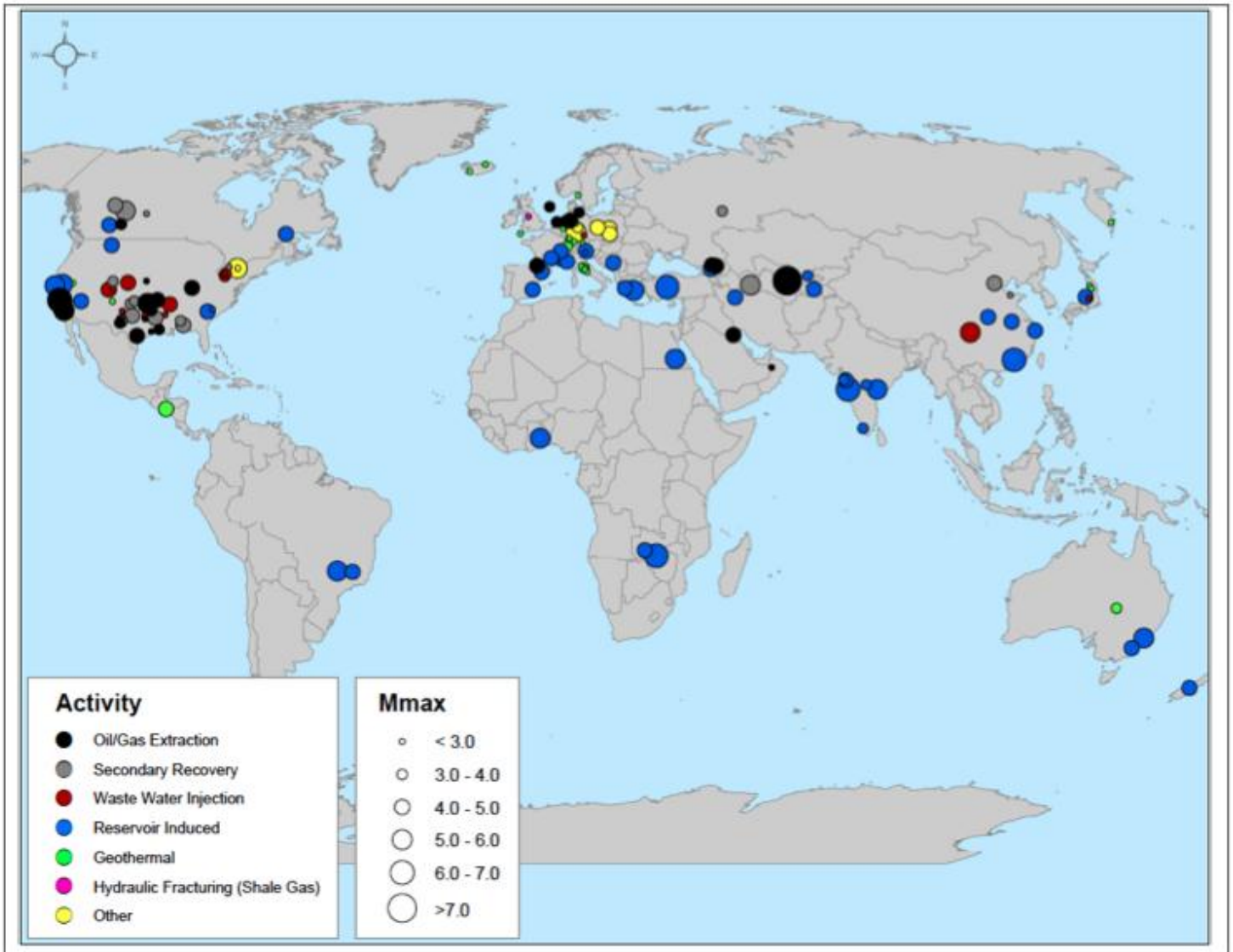

Figure Worldwide locations of seismicity reported in the technical literature caused by or likely related to human activities, with the maximum magnitude reported to be induced at each site.

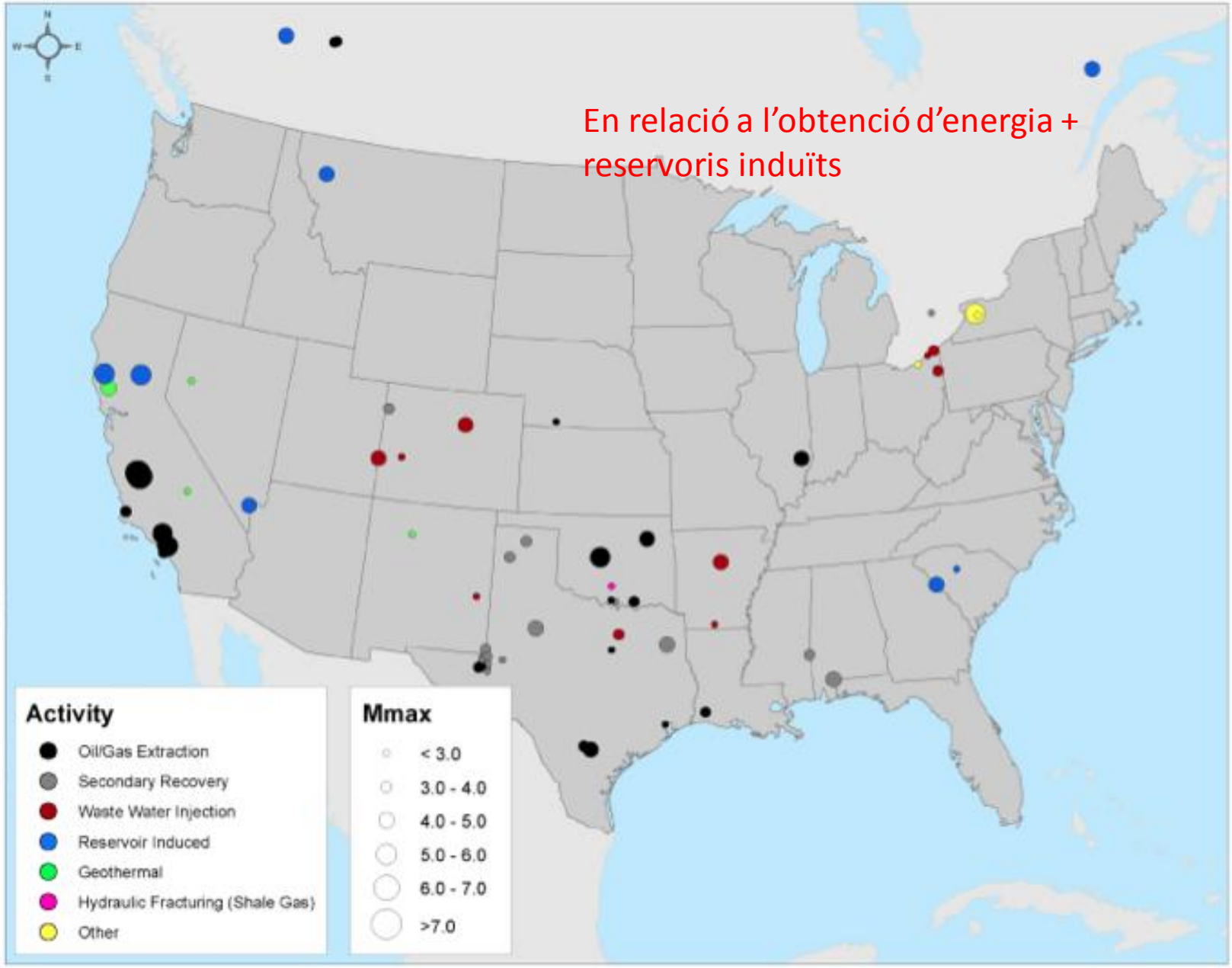

Figure Locations of seismic events caused by or likely related to human activities within the coterminous United States and portions of Canada as documented in the technical literature.

Produint terratrèmols

En relació a l'obtenció d'energia

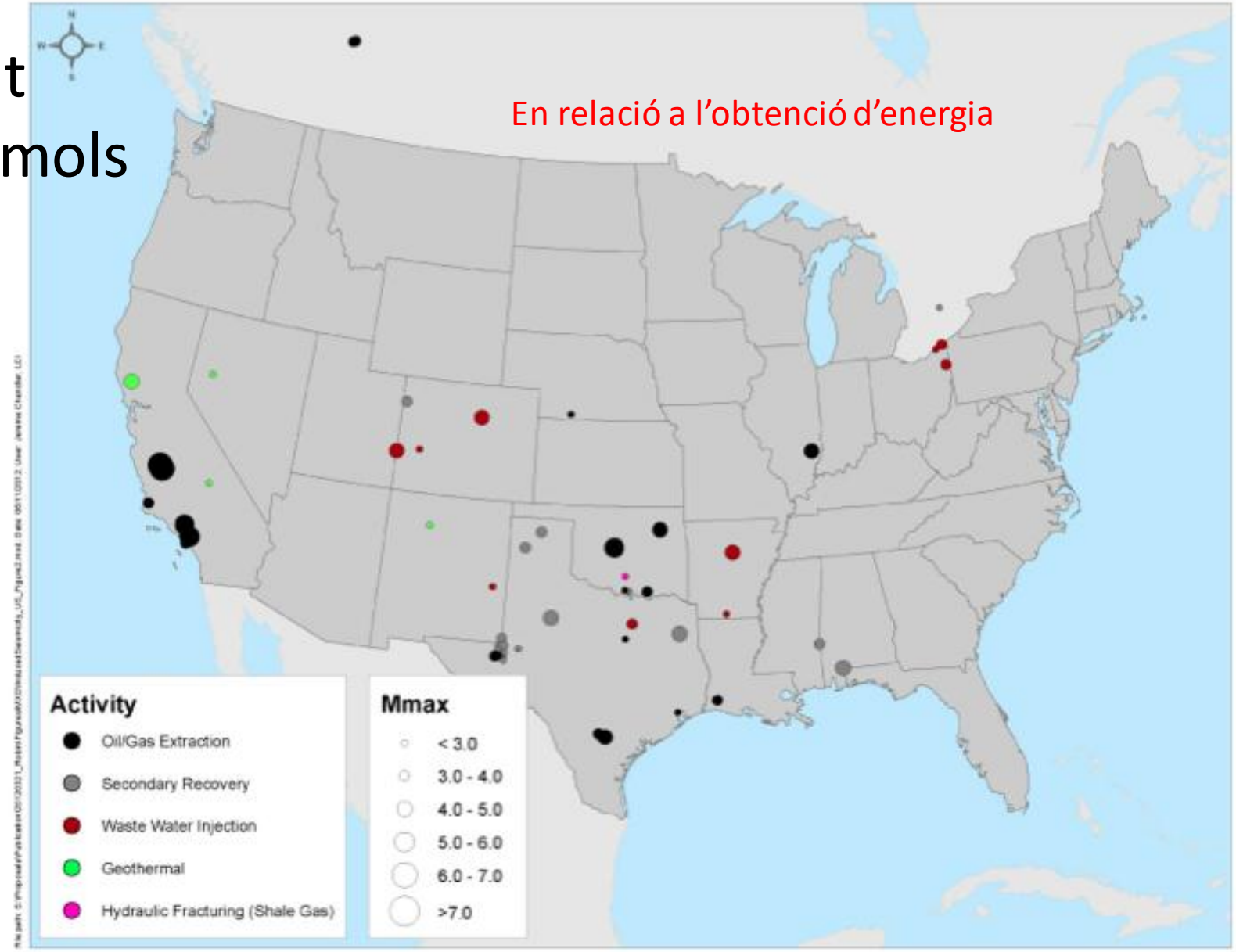

Figure S.1 Sites in the United States and Canada with documented reports of seismicity caused by or likely related to energy development from various energy technologies. The reporting of the occurrence of small induced seismic events is limited by the detection and location thresholds of local surface-based seismic monitoring networks.

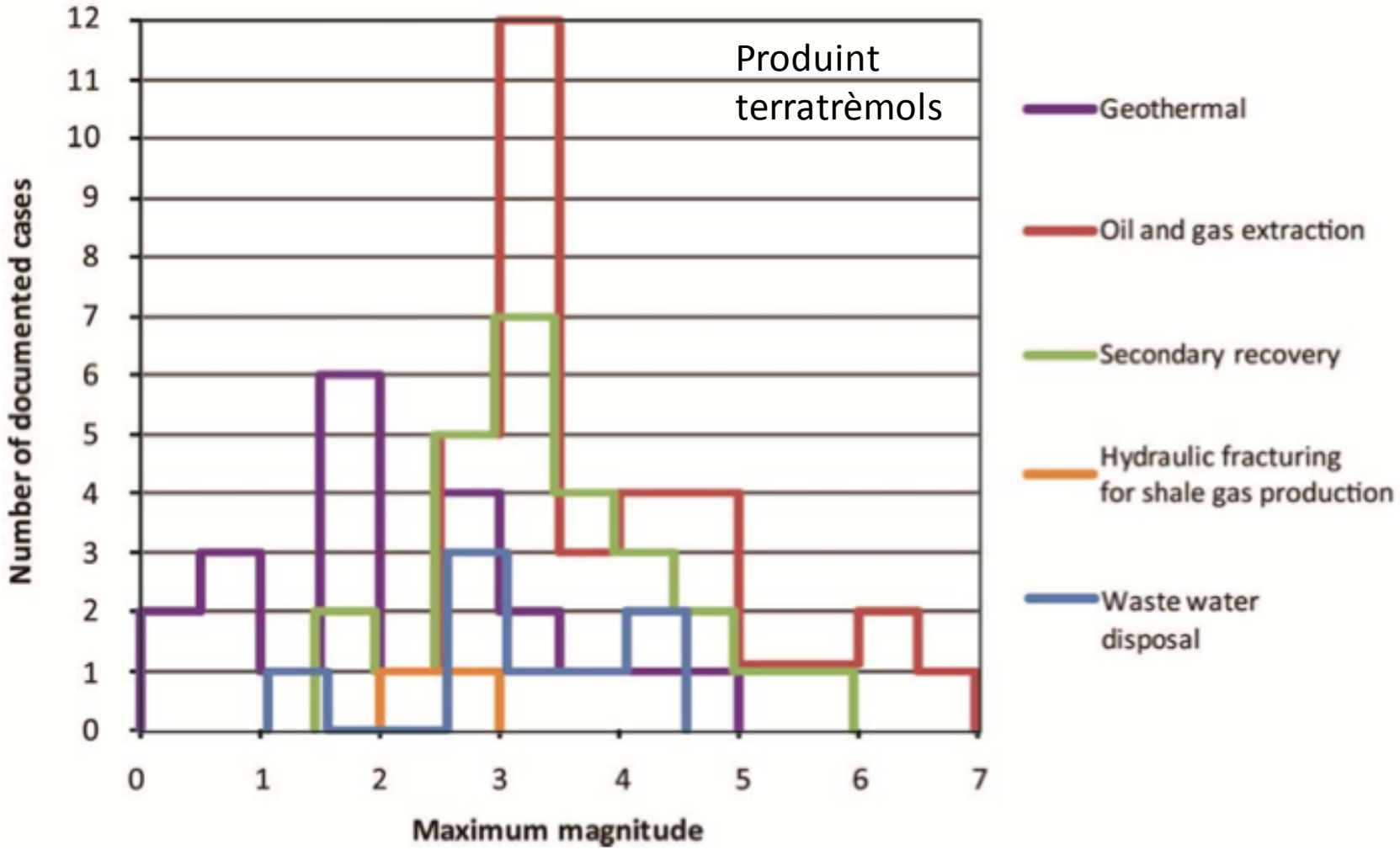

Figure 3.15 Histograms of maximum magnitudes documented in technical literature caused by or likely related to subsurface energy production globally. Note: Many gas and oil fields undergo extraction of hydrocarbons along with injection of water for secondary recovery, but if the reported total volume of extracted fluids exceeds that of injection, the site is categorized as extraction. Some cases of induced seismicity in the list above do not have reported magnitudes associated with earthquakes, and those cases are not included in the counts used to develop this figure. No induced seismic events have been recognized related to existing CCS projects. SOURCE: See Appendix C.

geotèrmia

Produint terratrèmols

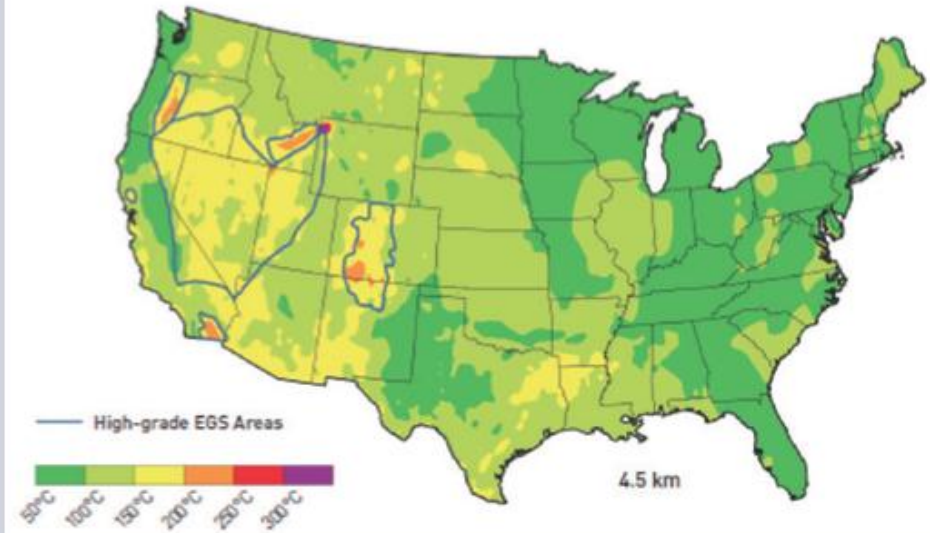

Figure 1: Average temperature at 4.5 km, conterminous United States. (Tester, et al., 2006, after Blackwell and Richards, 2004)

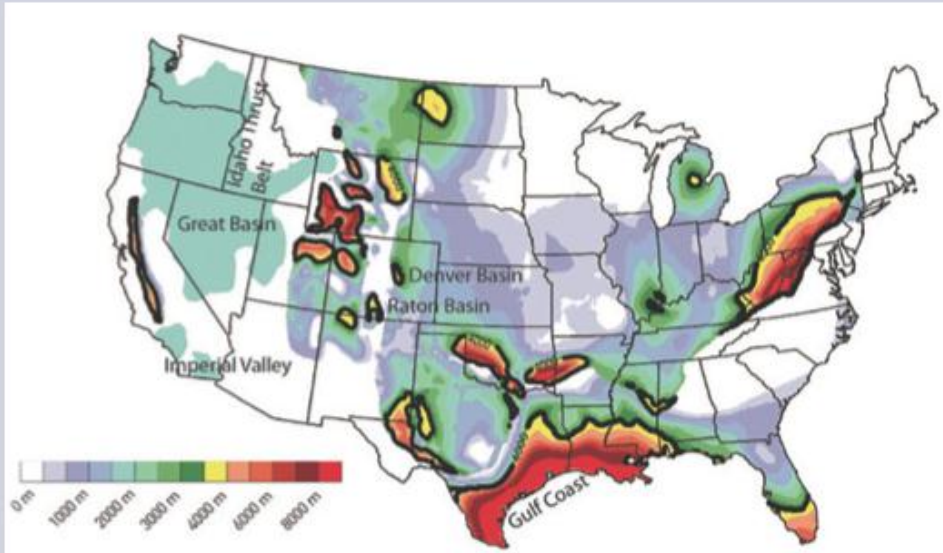

Figure 2: Distribution of sediment thickness in the conterminous U.S. 4 km isopach in black. Numerous basin-and-range basins over 4 km excluded for small resolution (Tester, et al., 2006)

Geotèrmia

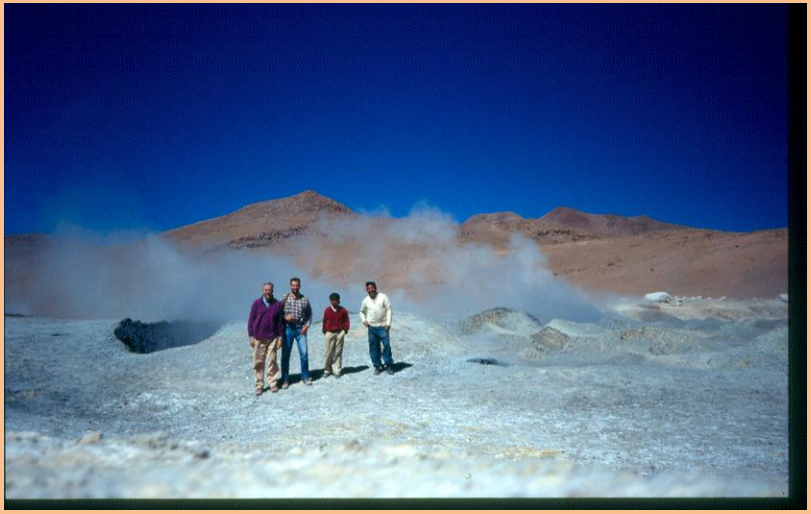

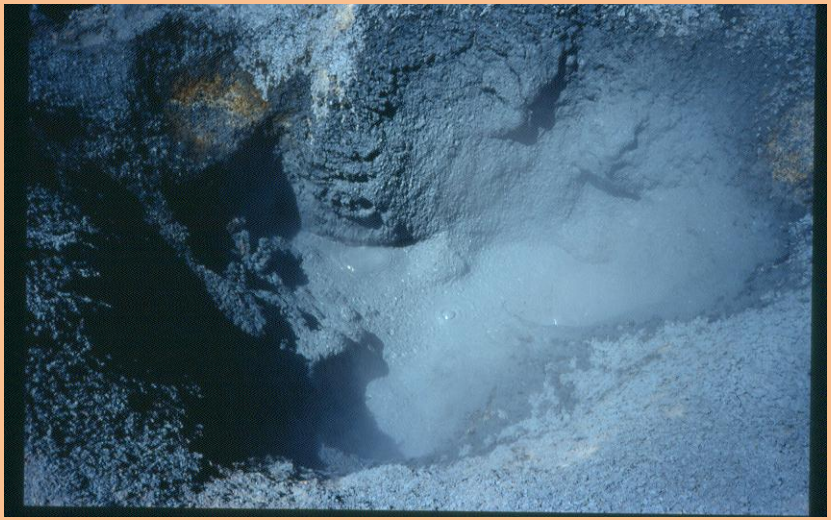

Altipla andí – Bolivia

Guèisers de Sol de Mañana

geotèrmia

Figure 3.3 Ridgeline Unit 7 and 8 Power Plant (rated at 69 MW) in the left foreground at The Geysers in California. The turbine building, housing the two turbine-generator sets, the operator's control room and various plant auxiliaries are on the left. The evaporative cooling tower with steam emanating from the top is on the right of the main complex. The beige pipelines along the roads (with square expansion loops) are the steam pipelines that gather the steam from the production pads and bring it to the plant. A high-voltage transmission line (denoted by lattice towers) is in the middle foreground of the picture. SOURCE: Calpine.

geotèrmia

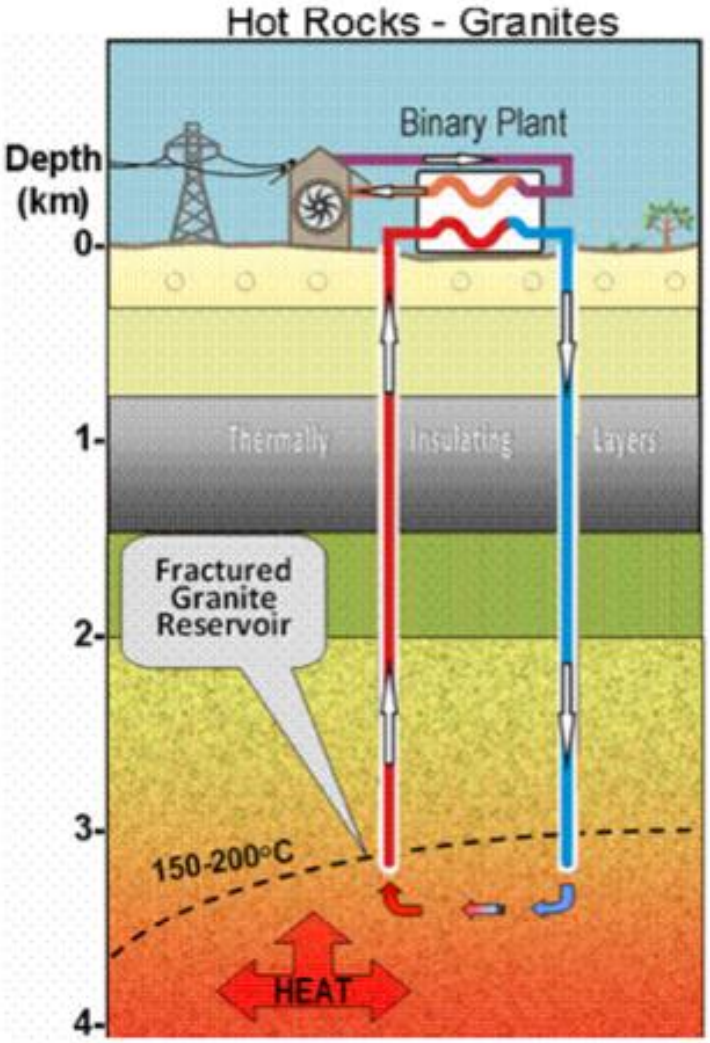

Figure 3.7 Schematic of an EGS development with an injection-production well pair and a power plant. The injection well (blue) is accompanied by a second (production) well (red) that is drilled to intersect the fractures generated by the injection well at a depth and appropriate lateral distance from the injection well. The distance allows the injected water to be sufficiently heated by the surrounding rock as it is circulated to the production well and pumped to the surface. Once at the surface the hot water can be flashed to steam or used to heat a secondary fluid that can be used in a binary cycle process. SOURCE: Courtesy of Clean Energy Australia Pty Ltd.

geotèrmia

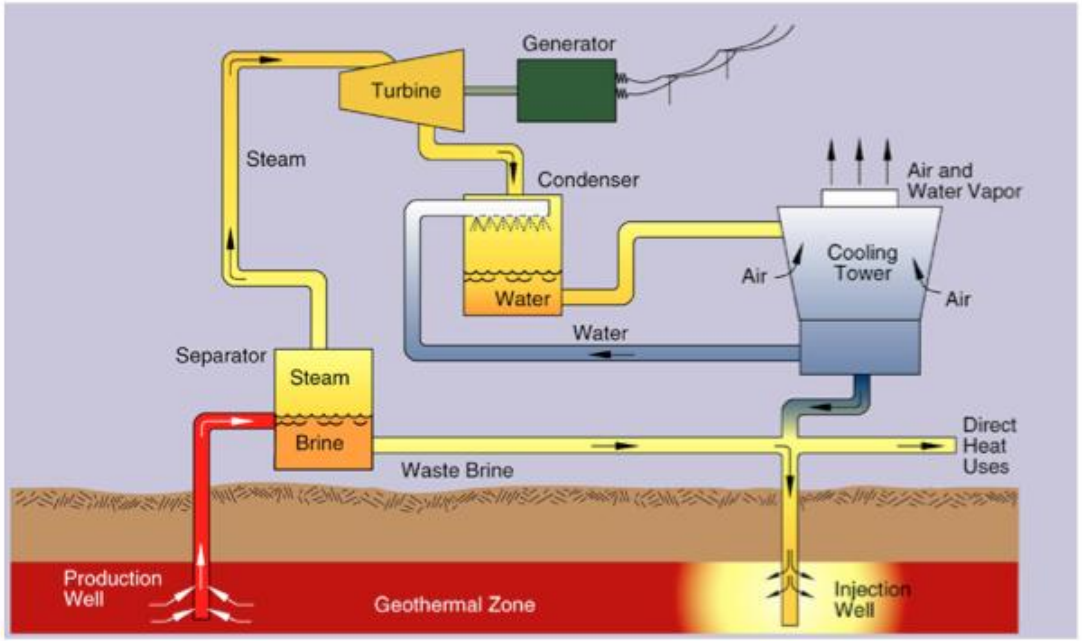

a)

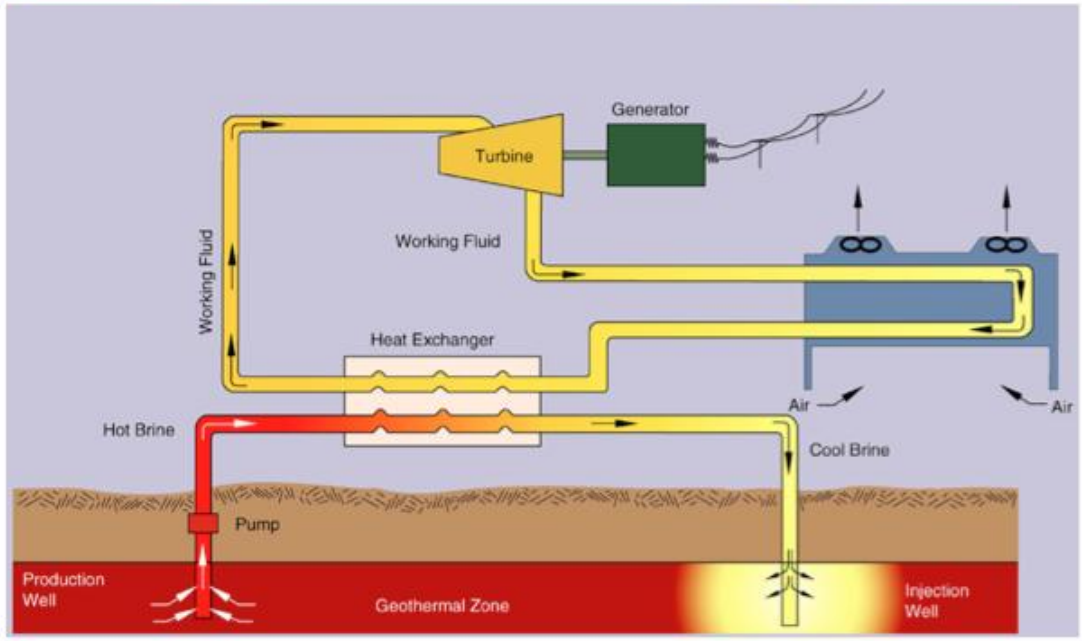

b)

igure 3.6 a and b. (a) The fluids delivered to the surface by the production wells in a Flash Steam ower Cycle are passed through a flash vessel or separator; the separated steam that flows out of the top directed into a power plant where it is used to spin a steam turbine connected to a generator that roduces an electrical output. The spent steam travels through a condenser and the condensate is then

Box 3.1

Geysers Annual Steam Production, Water Injection, and Observed Seismicity, 1965-2010

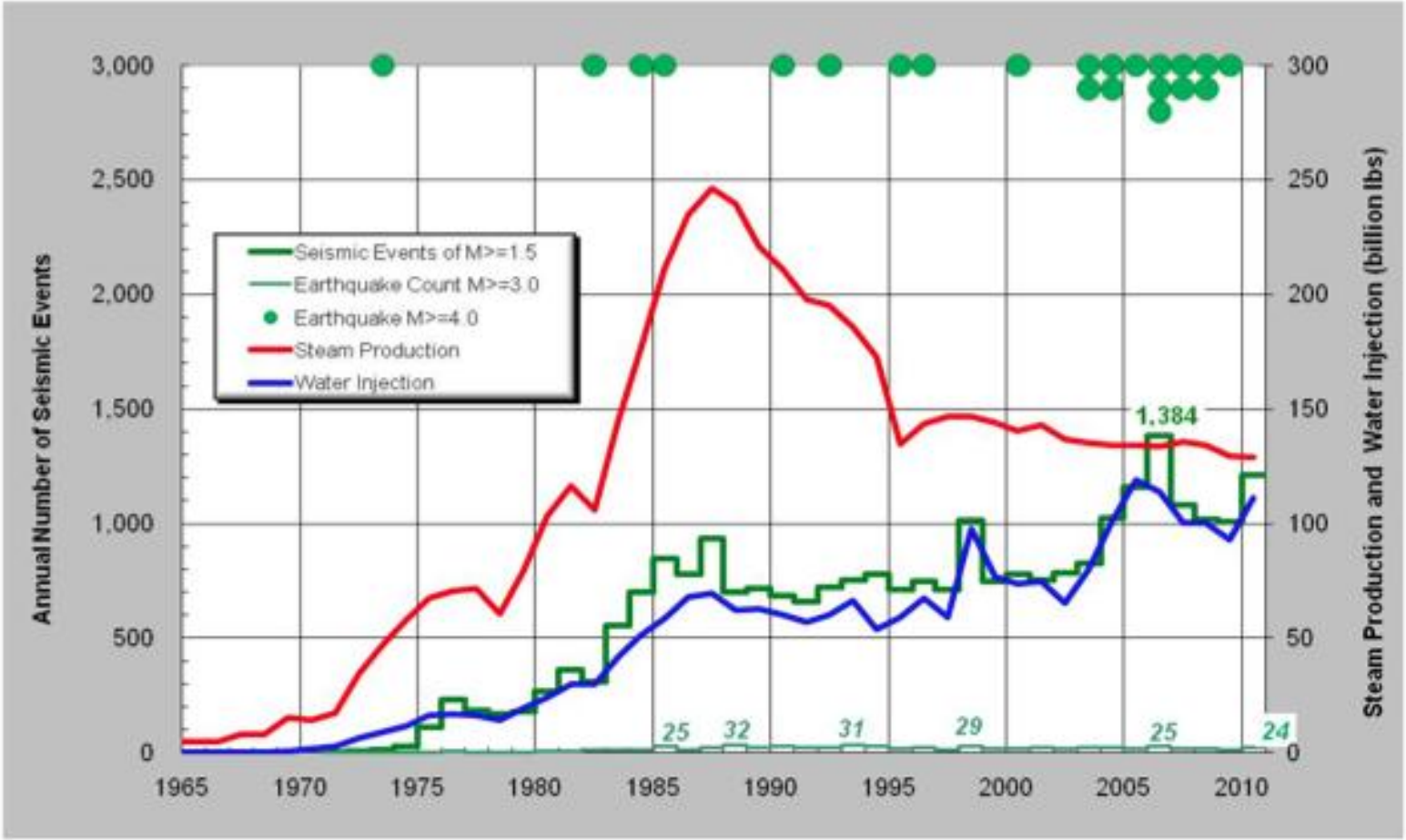

Figure The history of induced seismicity at The Geysers is shown in three forms. First, the number of recorded events of **M** 1.5* and greater is shown to have increased from almost none in the 1960s to 112 in 1975 and then to as many as 1,384 in 2006 (thick green line). Second, the annual number of earthquakes of **M** 3.0 and greater is shown along the bottom of the graph (pale green line). By 1985 25

geotèrmia

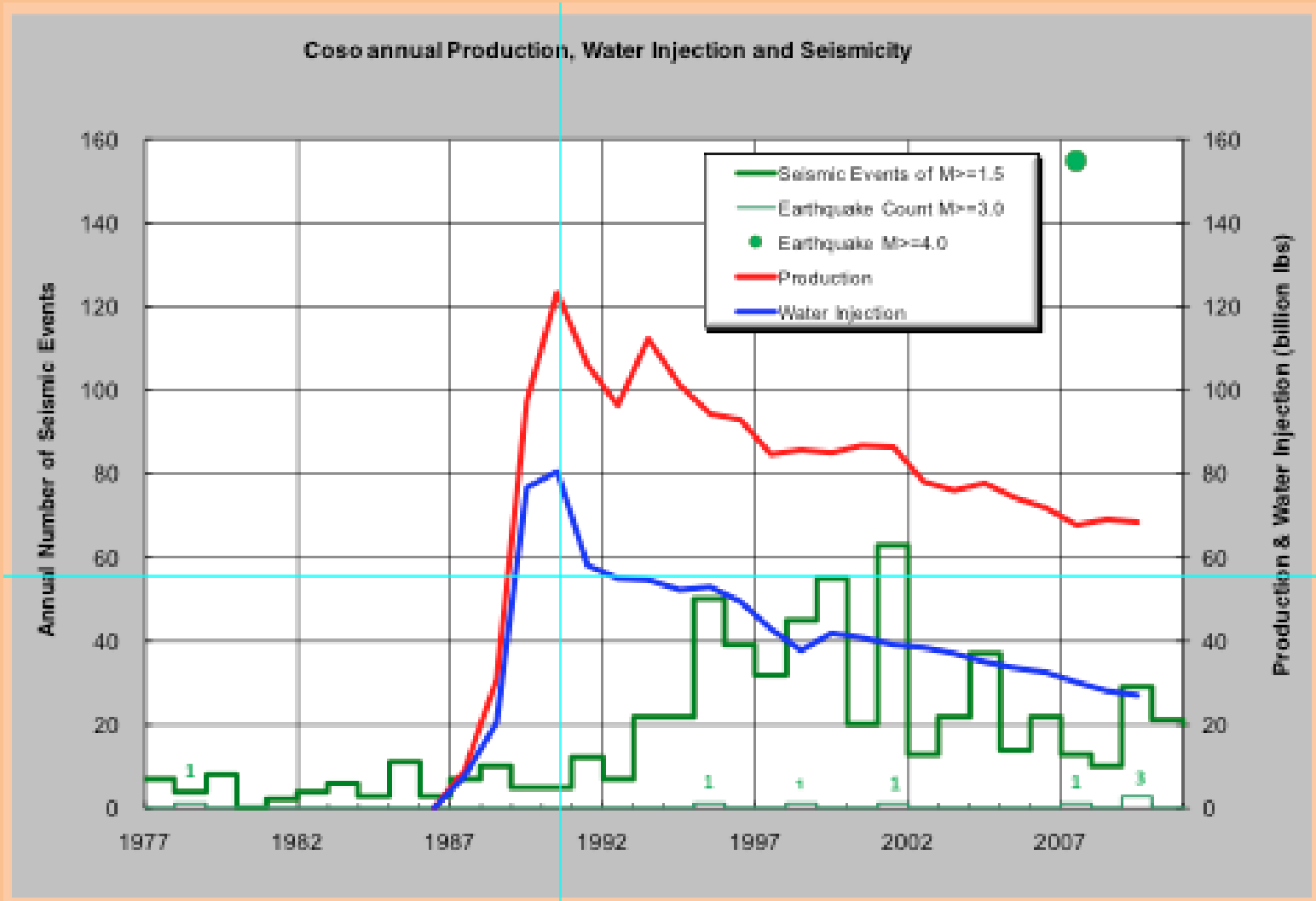

Figure 2 Annual Production, Water Injection and Seismicity at the Coso Geothermal Field. SOURCE: Generated by the study committee from available data.

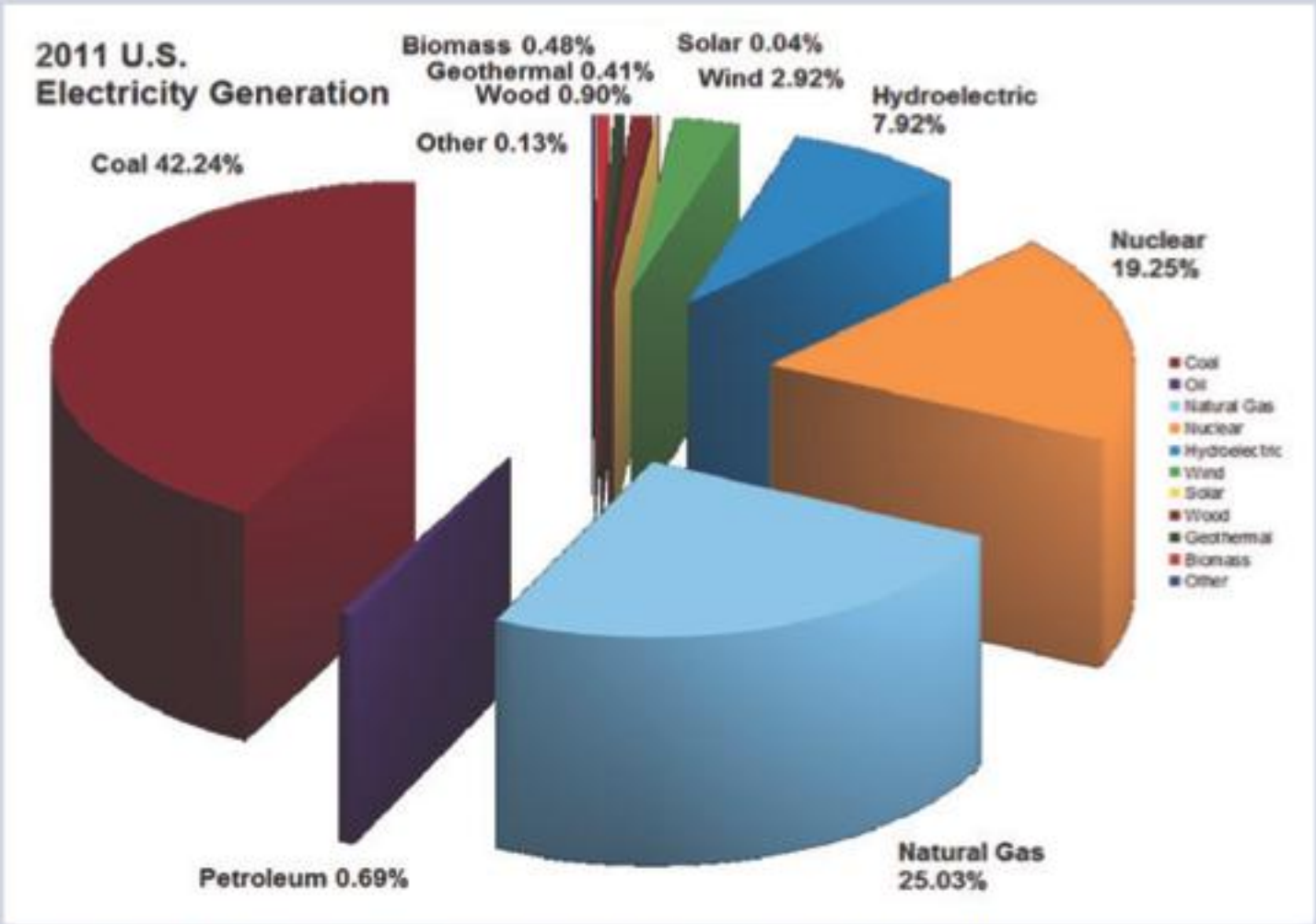

Figure 3: Distribution of electric generation by source in the U.S.for 2011. (Figure from http://earthdesk.blogs.pace.edu/tag/clean-water-act/; raw data available at http://www.eia.gov/totalenergy /data/monthly/#electricity)

geotèrmia

Figure 1 Drilling activity in the middle of the city of Basel. SOURCE: KEYSTONE/Georgios Kefalas.

geotèrmia

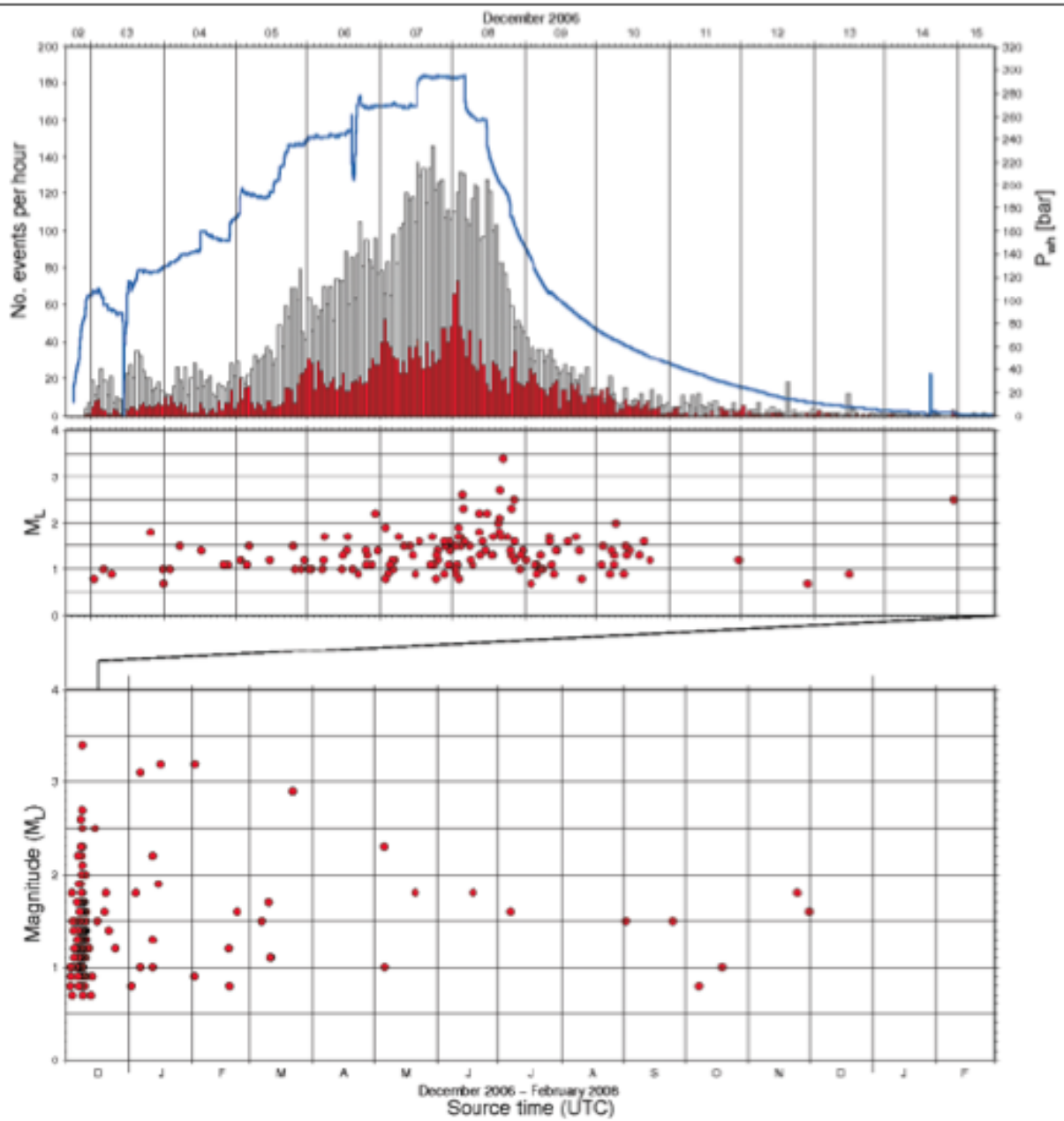

Figure 2 Seismic events and wellhead pressure at Basel. SOURCE: Kraft et al. (2009).

hidrocarburs

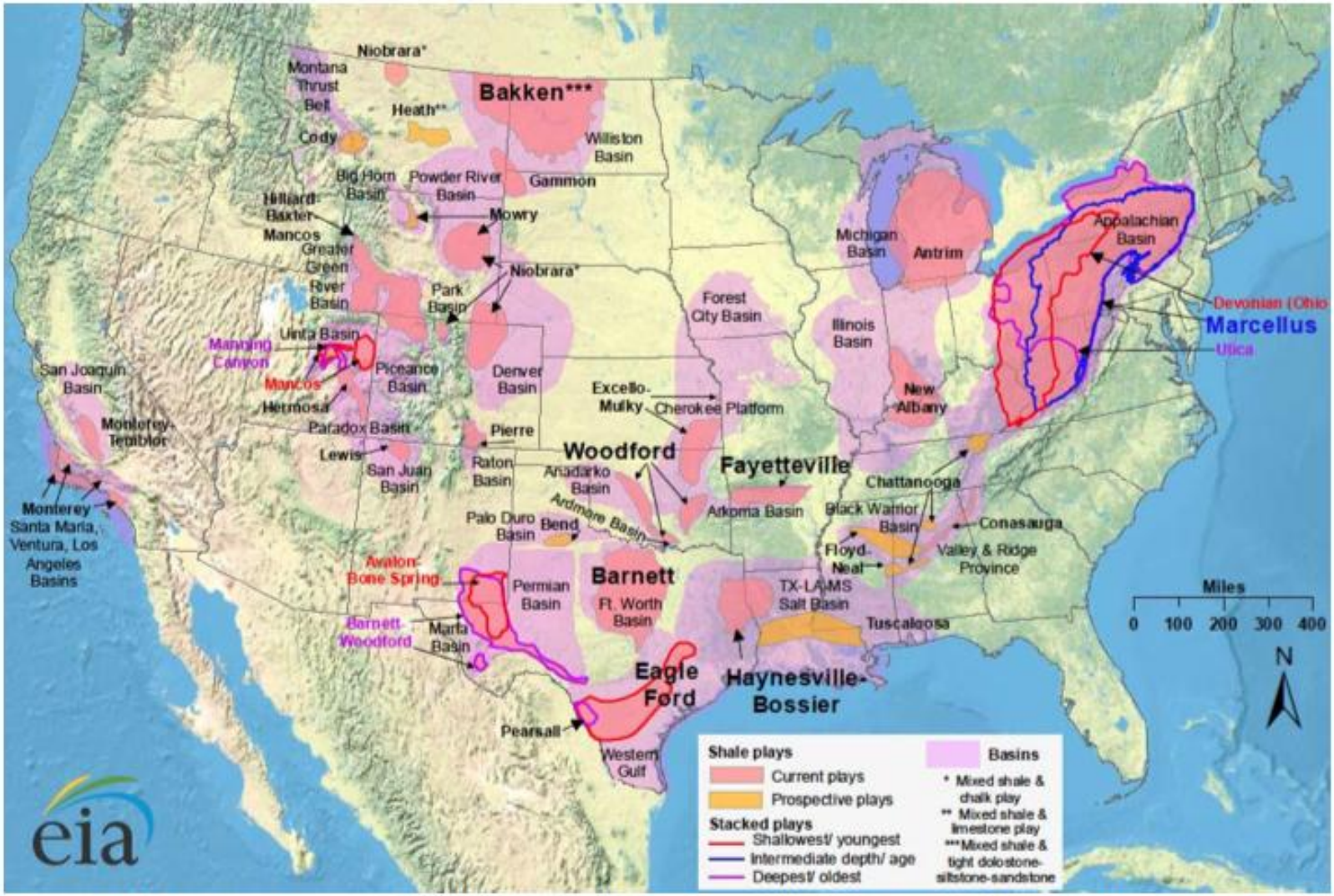

Figure 3.11 Location of areas of active exploration and/or production for shale hydrocarbons (oil and gas) in the contiguous United States. Light pink areas are major sedimentary basins; dark pink areas (e.g. Eagle Ford, Barnett) are under active development and production for gas or oil from shale; orange areas are prospective regions currently being explored for potential oil or gas development from shale. Several shale units of different ages may overlie one another and these units are outlined in thick red, blue, and purple lines representing youngest to oldest shale units, respectively. SOURCE: EIA (2011). Available at www.eia.gov/pub/oil_gas/natural_gas/analysis_publications/maps/maps.htm.

hidrocarburs

Periodos geológicos y rocas madre

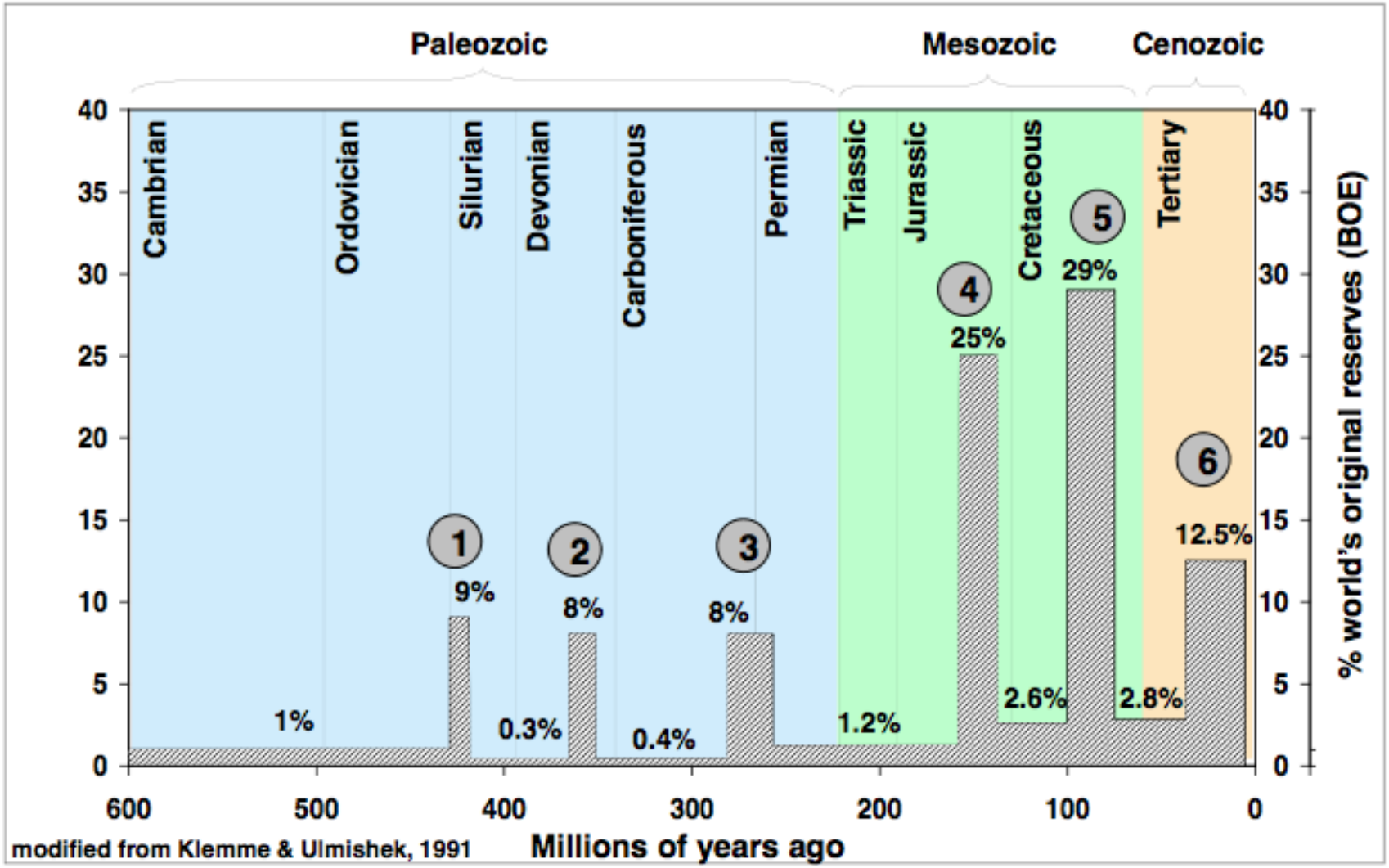

hidrocarburs

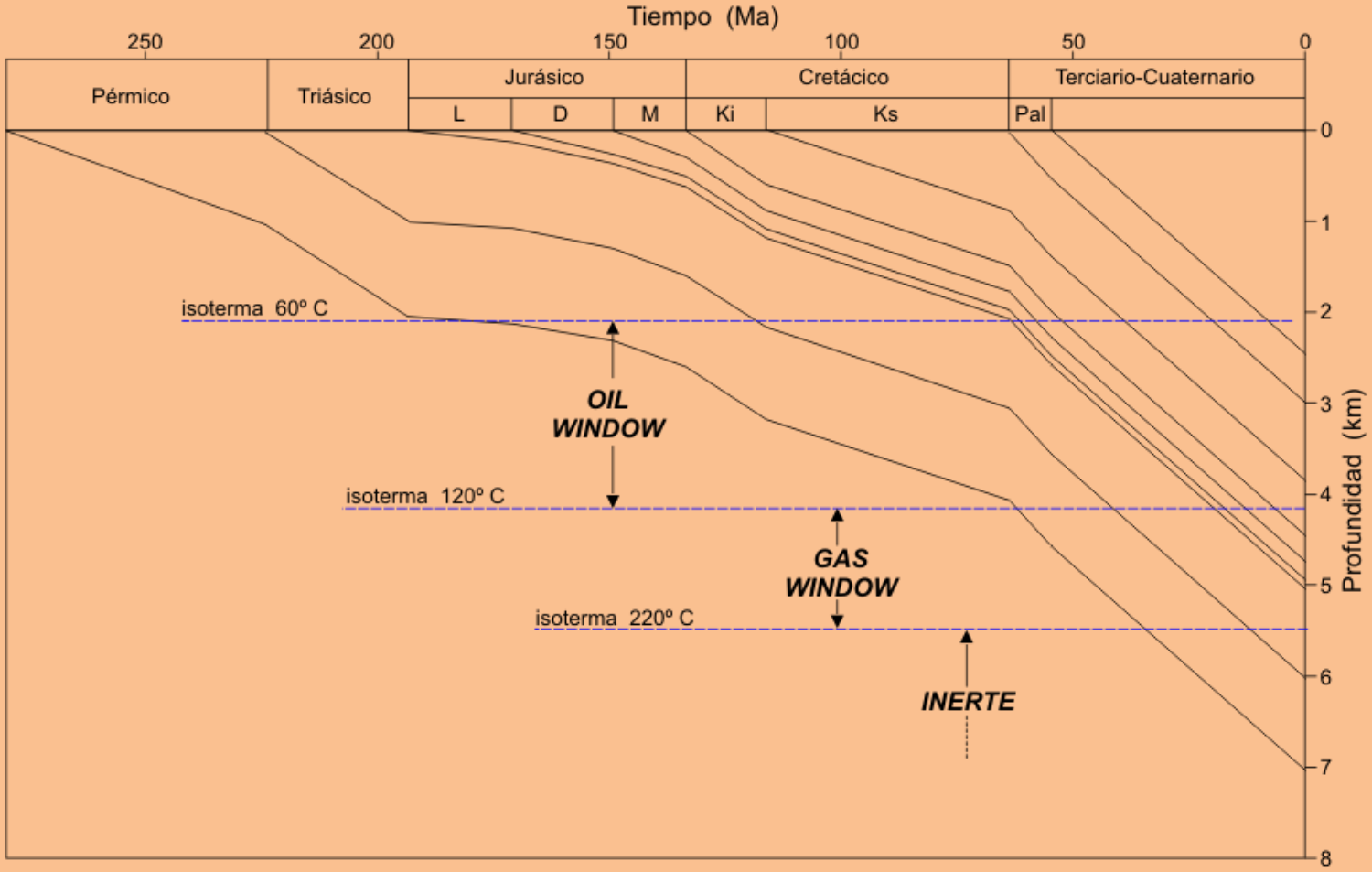

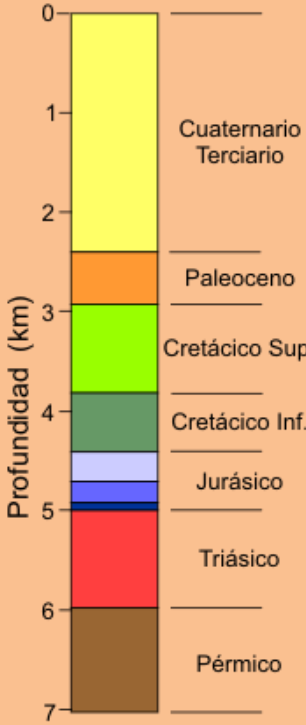

Mariano Marzo

hidrocarburs

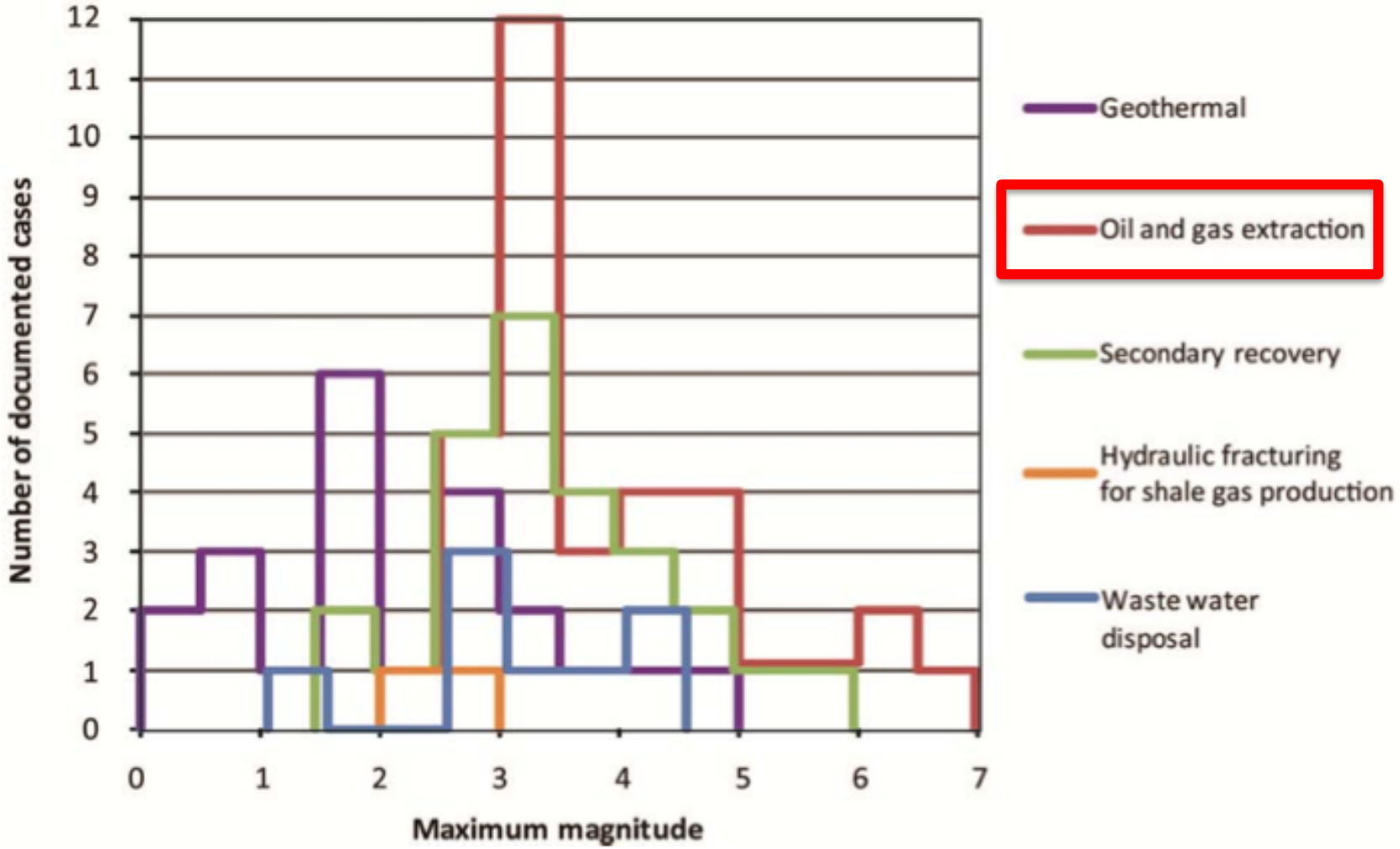

Figure 3.15 Histograms of maximum magnitudes documented in technical literature caused by or likely related to subsurface energy production globally. Note: Many gas and oil fields undergo extraction of hydrocarbons along with injection of water for secondary recovery, but if the reported total volume of extracted fluids exceeds that of injection, the site is categorized as extraction. Some cases of induced seismicity in the list above do not have reported magnitudes associated with earthquakes, and those cases are not included in the counts used to develop this figure. No induced seismic events have been recognized related to existing CCS projects. SOURCE: See Appendix C.

hidrocarburs

Shock waves. The 2012 earthquakes in Emilia-Romagna killed 27 people and caused major damage.

CREDIT: (TOP) ASSOCIATED PRESS

SEISMOLOGY

Human Activity May Have Triggered Fatal Italian Earthquakes, Panel Says

ROME—A pair of deadly earthquakes that struck the north of Italy in 2012 could have been triggered by the extraction of petroleum at a local oil field, according to an international panel of geoscientists.

The group's long-awaited and as-yet-unpublished report, commissioned in the wake of the disaster that killed 27 and injured hundreds in the Emilia-Romagna region, could have important political and economic ramifications, some scientists say. While previous studies in other countries have linked earthquakes to gas and oil exploration, human casualties have been very rare. Fear of humanmade seismicity has already triggered fierce opposition against new oil and gas drilling efforts in Italy, and Vasco Errani, the president of the Emilia-Romagna region, announced in May last year that all new requests for hydrocarbon exploration in the quake area would be put on hold until the commission delivered its report.

Sources with close knowledge of the study say it was presented to the Emilia-Romagna regional government at least a month ago, but that politicians at both the regional and national level are nervous about its effects and are delaying its release. Although phrased cautiously, the panel's conclusions could lead the presidents of Italy's regions to turn down new requests for fossil-fuel exploration; existing production could also be hit.

The panel, known as ICHESE, was asked in late 2012 to review possible links between hydrocarbon production and the earthquakes, a magnitude-5.9 event on 20 May 2012, and a magnitude-5.8 event 9 days later. ICHESE consists of two Italian and three foreign geoscientists—including the chair, Peter Styles of Keele University in the United Kingdom—as well as Franco Terlizzese, an engineer at Italy's Ministry of Economic Development.

In its report, dated February 2014, ICHESE refutes one alleged factor: the development of a 3.7-billion-m^3 natural gas deposit in an aquifer above an active geological fault near the village of Rivara in the Po Valley, close to the two epicenters. Drilling for the facility had yet to begin when the quakes struck. But the panel does finger another site: the Cavone oil field, owned and operated by Gas Plus. *Science* has seen the conclusions of the report, which says it "cannot be excluded" that activities there initiated the 20 May quake, whose epicenter lies about 20 km away.

Changes in stress and pressure within Earth's crust resulting from both the removal of oil and the injection of fluids to enhance oil flow would almost certainly not have been sufficient on their own to have induced a major earthquake, the experts explain. But it is possible that the fault involved in the 20 May tremor was close to the breaking point, and that the human-induced changes in the crust, although extremely small, were enough to "trigger" the earthquake. That quake could in turn have triggered the 29 May event by further altering crustal stress.

The group reached this conclusion on the basis of a correlation between increased output from the Cavone field beginning in April 2011 and rising seismicity in the area before 20 May 2012. They say this link should now be backed up by a physical model incorporating "the fluid dynamics in the reservoir and in the surrounding rocks."

Styles did not respond to questions about the report, and a spokesperson for Gas Plus says the company cannot comment on the findings. But an earth scientist who asked not to be named argues that several factors rule out a connection between crude oil production at Cavone and the 20 May earthquake: an absence of small quakes induced directly by the oil production, the significant distance between oil field and epicenter, and the plant's modest output of about 500 barrels a day.

Geoffrey Abers of Columbia University cautions that these factors wouldn't necessarily rule out a link. Three tremors with magnitudes between 4.5 and 5 in Denver in 1967 have been attributed to chemicals being pumped down a deep well, he notes, even though injection had stopped more than a year earlier and taken place up to 10 kilometers from the quakes' epicenters. And three quakes with magnitudes 5 and above that occurred in Oklahoma in November 2011 were probably a result of wastewater being pumped into a depleted oil well, even though the volumes involved were quite small. "We think that in Oklahoma the injected water was jacking up the pressure in just the right place," Abers says, "and that caused a cascading sequence of earthquakes."

Some Italian geologists worry the political noise that the report could generate will discourage rational and open discussion about the seismic risks of oil and gas development. Similar fears were aired after the L'Aquila earthquake, which killed more than 300 people 5 years ago this week. In its aftermath, seven experts were each sentenced to 6 years in prison for downplaying seismic risk ahead of the deadly event, a sentence that some, though by no means all, scientists believed betrayed ignorance by the public and the judiciary about the uncertainties inherent in science. An appeal in the L'Aquila case is pending.

–EDWIN CARTLIDGE

Edwin Cartlidge is a science writer in Rome.

Published by AAAS

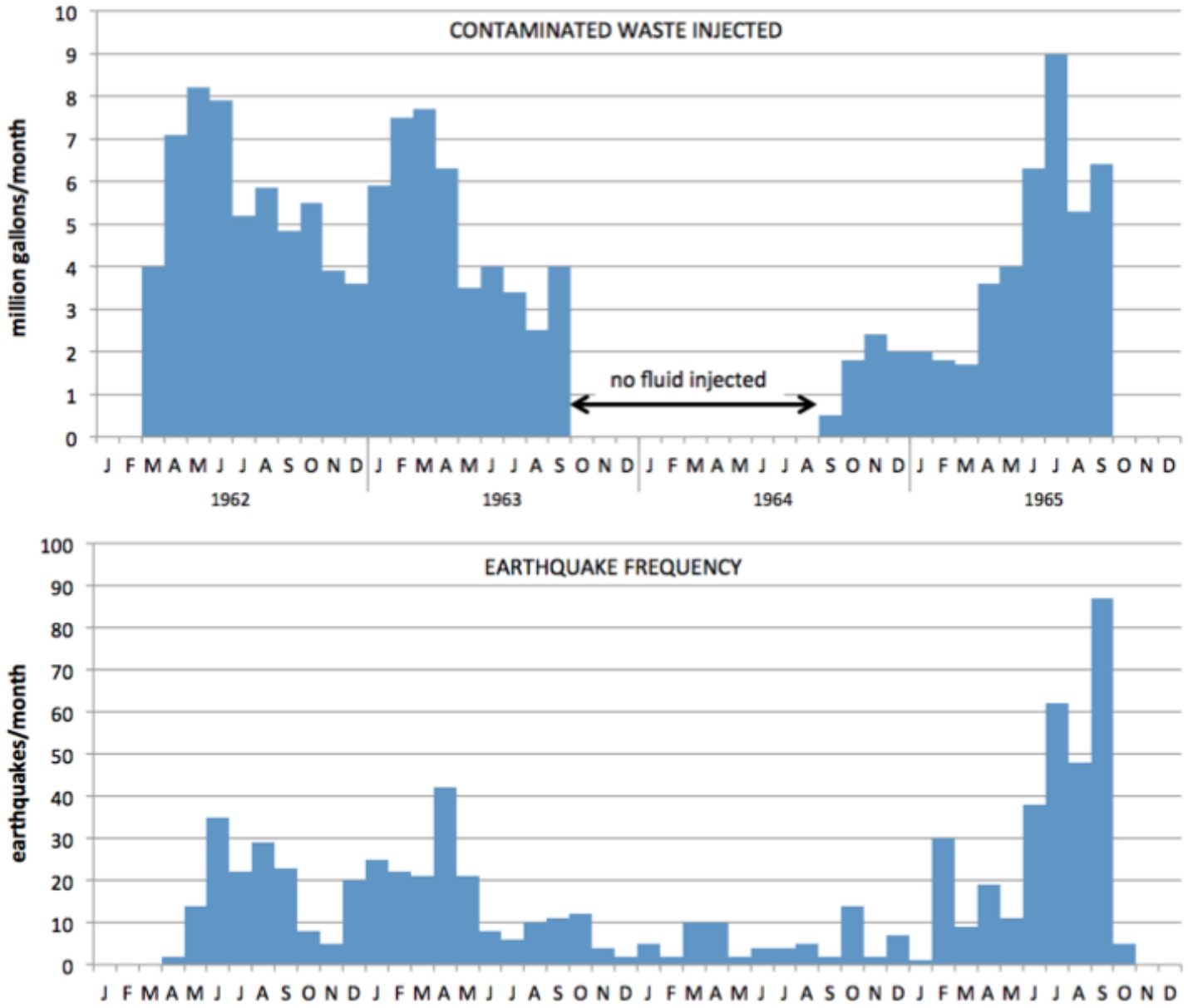

Figure Histograms showing relation between volume of waste injected into the Rocky Mountain Arsenal well and earthquake frequency. SOURCES: Adapted from Evans (1966); Healy et al. (1968); McClain (1970); Hsieh and Bredehoeft (1981).

Font d'informació de primer ordre per qüestions de sismicitat induïda

Induced Seismicity Potential in Energy Technologies

ISBN
978-0-309-25367-3

300 pages
7 x 10
PAPERBACK (2012)

Committee on Induced Seismicity Potential in Energy Technologies; Committee on Earth Resources; Committee on Geological and Geotechnical Engineering; Committee on Seismology and Geodynamics; Board on Earth and Sciences and Resources; Division on Earth and Life Studies; National Research Council

El perquè de tot plegat…..

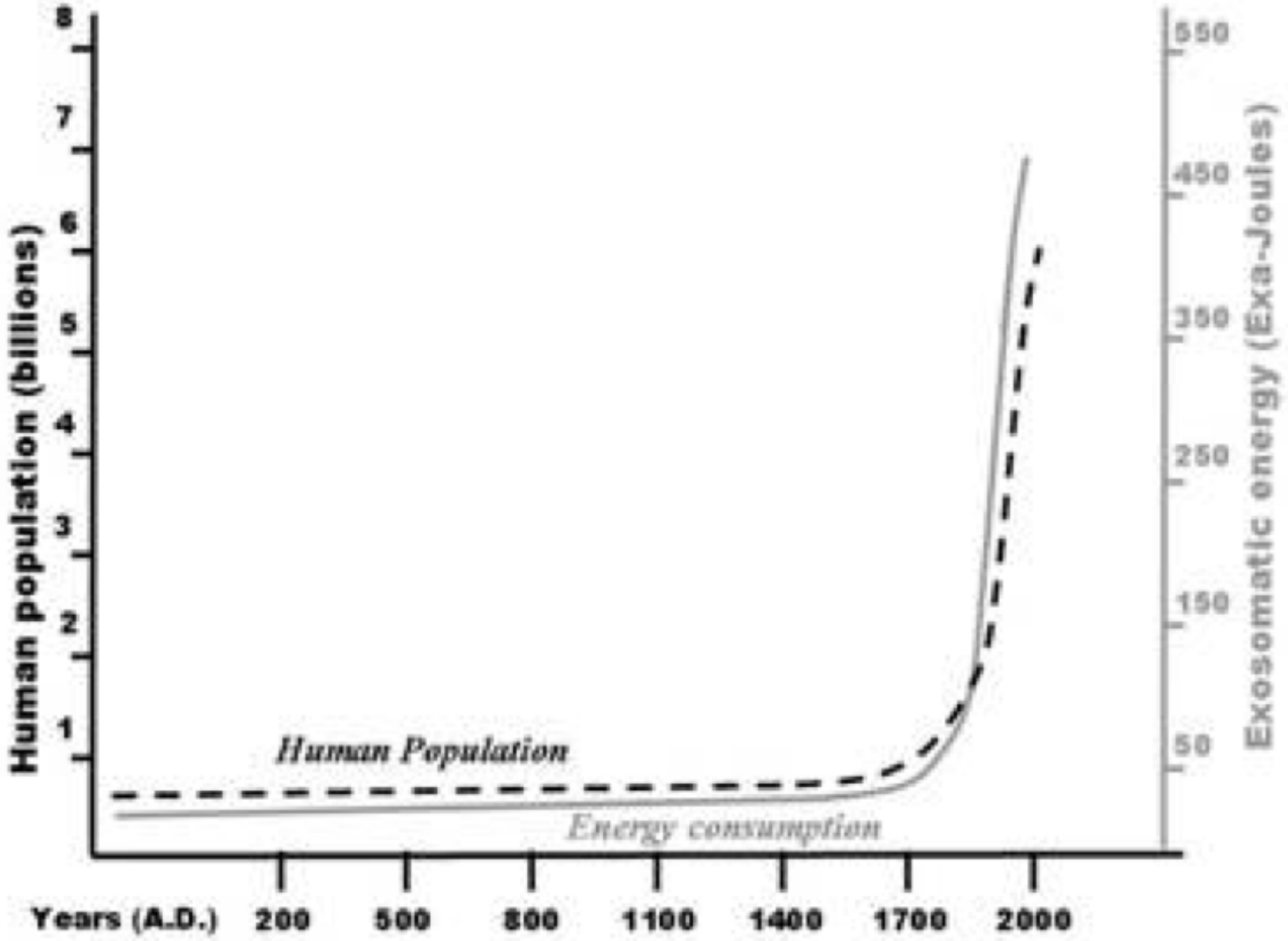

La situació actual

El perquè de tot plegat……

Productivity of labor:
700 kg of grain per hour

Productivity of labor:
1 kg of grain per hour

El perquè de tot plegat……

Productivity of labor:
1,400 trucks of coal
per worker per day

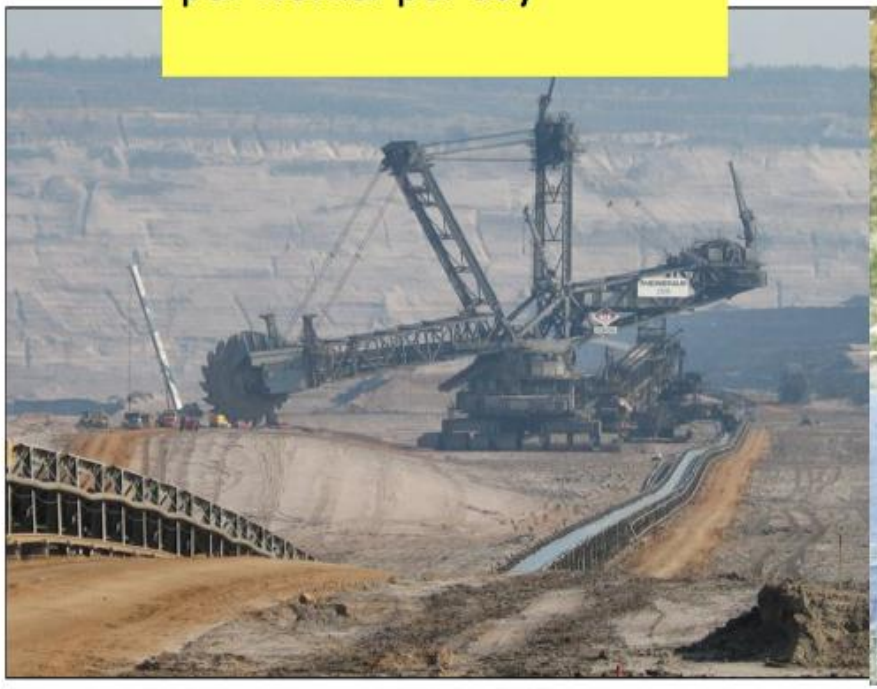

Productivity of labor:
0.01 truck of coal-equivalent
needing **two** workers . . .

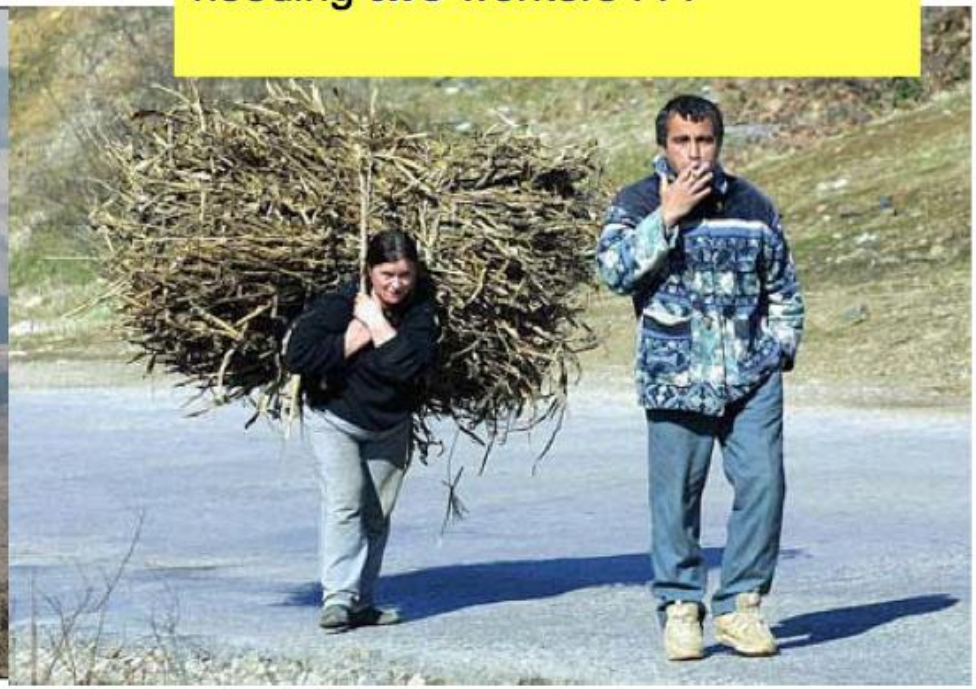

Com ens hem convertit en agents geològics importants?

- Alguns exemples:

-Canviant les superfícies continentals i les submarines
-Produint terratrèmols

MOLTES GRÀCIES!

-Coneixent mes els volcans i retocant-los
-Mesurant i començant a incidir (?) en el cicle geològic
-La biosfera fa milions d'anys que incideix en el cicle geològic i el cicle geològic en la biosfera

Anex
-L'Antropocè (edat geològica?) i el gran experiment

Annexos

1 Castor-Ebre

2 Asuncion 2012 Chile

3 Escales de Ritchter

CASTOR
EBRE

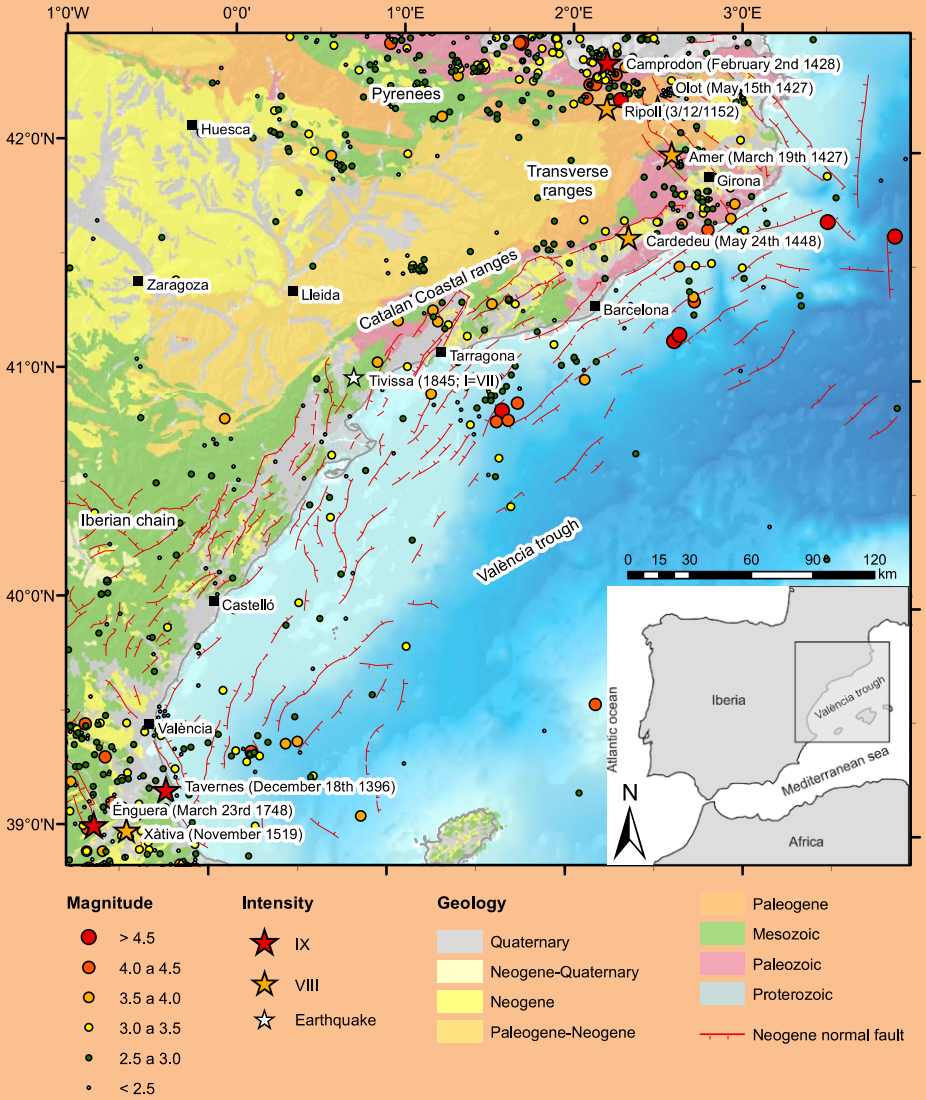

Fig. 1.- Simplified geological map of the northeastern Iberian Peninsula (modified from IGME, 1994), showing the position of the Neogene normal faults (Roca, 1992; Roca and Guimerà, 1992) and the historical earthquakes with intensity equal to and higher than VIII. Instrumental seismicity reported by the Instituto Geográfico Nacional earthquakes catalog.

Fig. 1.- Mapa geológico simplificado del noroeste de la Península Ibérica (modificado del IGME, 1994), donde se muestra la posición de las fallas normales Neógenas (Roca, 1992; Roca y Guimerà, 1992) y de los terremotos históricos con intensidad igual o mayor a VIII. Sismicidad instrumental dada en el catálogo de terremotos del Instituto Geográfico Nacional.

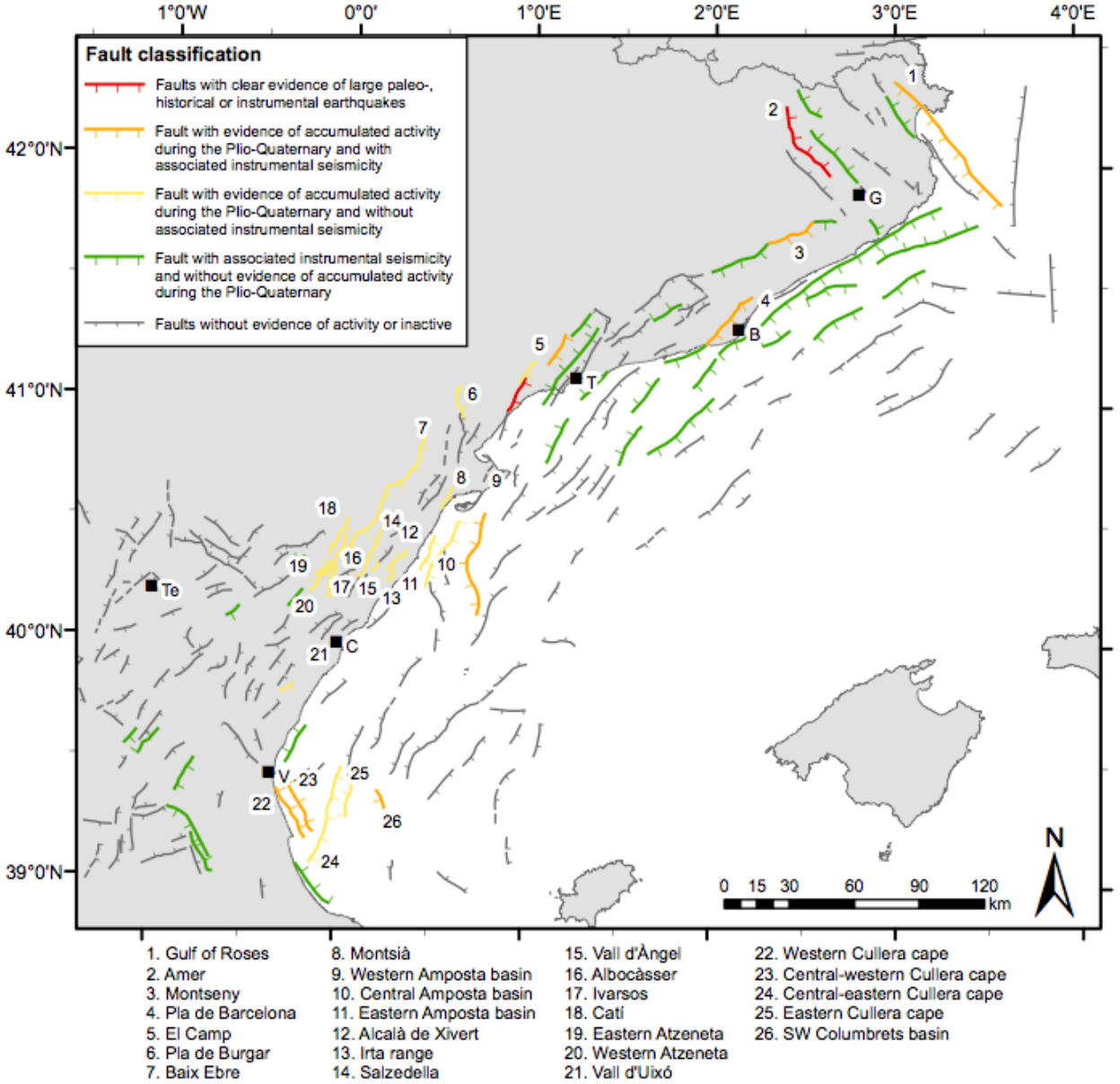

Fig. 8.- Map (modified from Perea *et al.*, 2006) showing the location of the faults corresponding to each of the different types of active faults (Fig. 7): a) faults with clear evidence of large paleo-, historic or instrumental earthquakes (red lines); b) faults with evidence of accumulated activity during the Plio-Quaternary and with associated instrumental seismicity (orange lines); c) faults with evidence of accumulated activity during the Plio-Quaternary and without associated instrumental seismicity (yellow lines); d) faults with associated instrumental seismicity and without evidence of accumulated activity during the Plio-Quaternary (green lines), and e) faults without evidence of activity or inactive faults (gray lines). B: Barcelona; C: Castelló; G: Girona; T: Tarragona; Te: Teruel; V: València. The seismic parameters of the numbered faults and their description are given in table 1 and in the text, respectably.

Onshore faults

Fault	With large earthquakes	With Plio-Quaternary activity and associated instrumental seismicity	With Plio-Quaternary activity and without associated instrumental seismicity	With associated instrumental seismicity and without Plio-Quaternary activity	Without evidence of activity or inactive
Instrumental seismicity	✕	✕		✕	
Large earthquakes	✕				
Mountain fronts showing recent activity	✕	✕	✕		
Scheme					

Offshore faults

Fault	With large earthquakes	With Plio-Quaternary activity and associated instrumental seismicity	With Plio-Quaternary activity and without associated instrumental seismicity	With associated instrumental seismicity and without Plio-Quaternary activity	Without evidence of activity or inactive
Instrumental seismicity	✕	✕		✕	
Large earthquakes	✕				
Plio-Quaternary reflectors offseted	✕	✕	✕		
Scheme	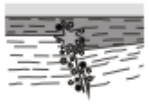	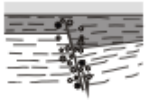	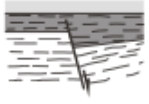	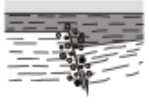	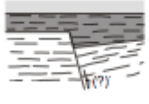

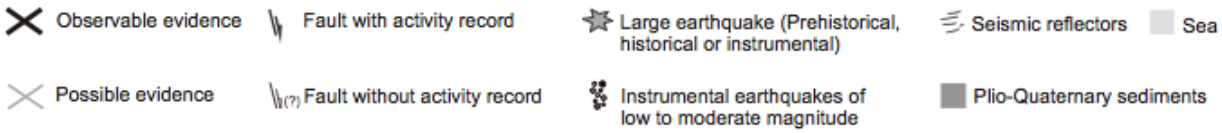

Fig. 7.- Classification of the normal faults located in the northwestern margin of the València trough (Perea, 2006). The cross symbols indicate observable (black bold) or possible observable (gray) evidence of Plio-Quaternary activity that characterizes each type of faults.

Fig. 7.- Clasificación de las fallas normales localizadas en el margen noroccidental del surco de Valencia (Perea, 2006). Las aspas indican la presencia de evidencias de actividad Plio-Cuaternaria observadas (negras gruesas) o posibles (gris) que caracterizan cada uno de los tipos de fallas descritos.

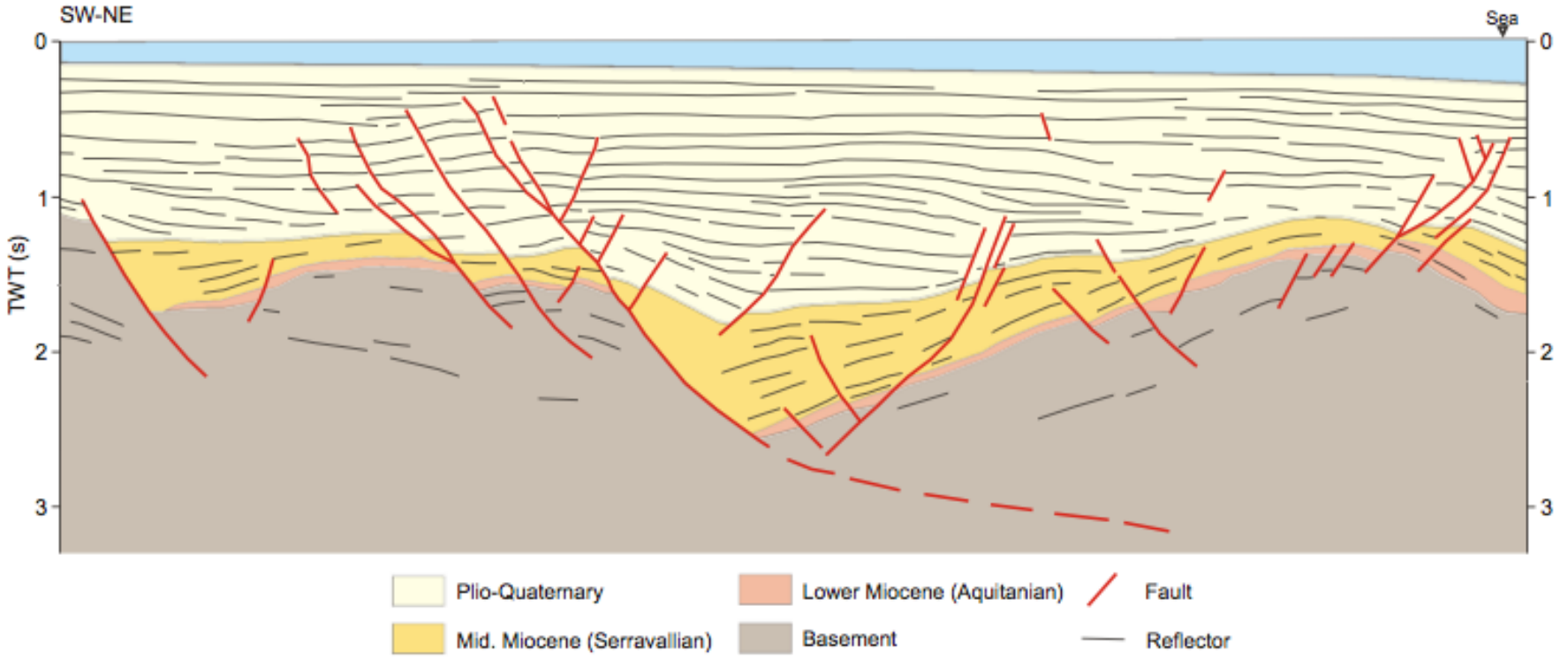

Fig. 6.- Cullera cape fault zone. Line drawing of the industrial reflection seismic profile GV-71 in the Cullera cape fault zone (modified from Roca, 1992). Note that the main normal faults offset the lower boundary of the Plio-Quaternary reflectors and that these faults show evidence of long term activity. See section 3.1 for more information about the approach and section 4 for the description of the fault zone. The location of the faults is in Fig. 8 and their parameters are in table 1.

Fig. 6.- Zona de falla del Cabo de Cullera. Interpretación del perfil de sísmica de reflexión con fines industriales GV-71 en la zona de falla del Cabo de Cullera (modificado de Roca, 1992). Nótese que las fallas normales principales desplazan los reflectores localizados en la base de la unidad Plio-Cuaternaria y que estas fallas también muestran evidencias de una actividad de larga duración. Ver la sección 3.1 para más información sobre la aproximación utilizada y la sección 4 para la descripción de la zona de falla. La localización de las fallas se puede ver en la figura 8 y sus parámetros en la tabla 1.

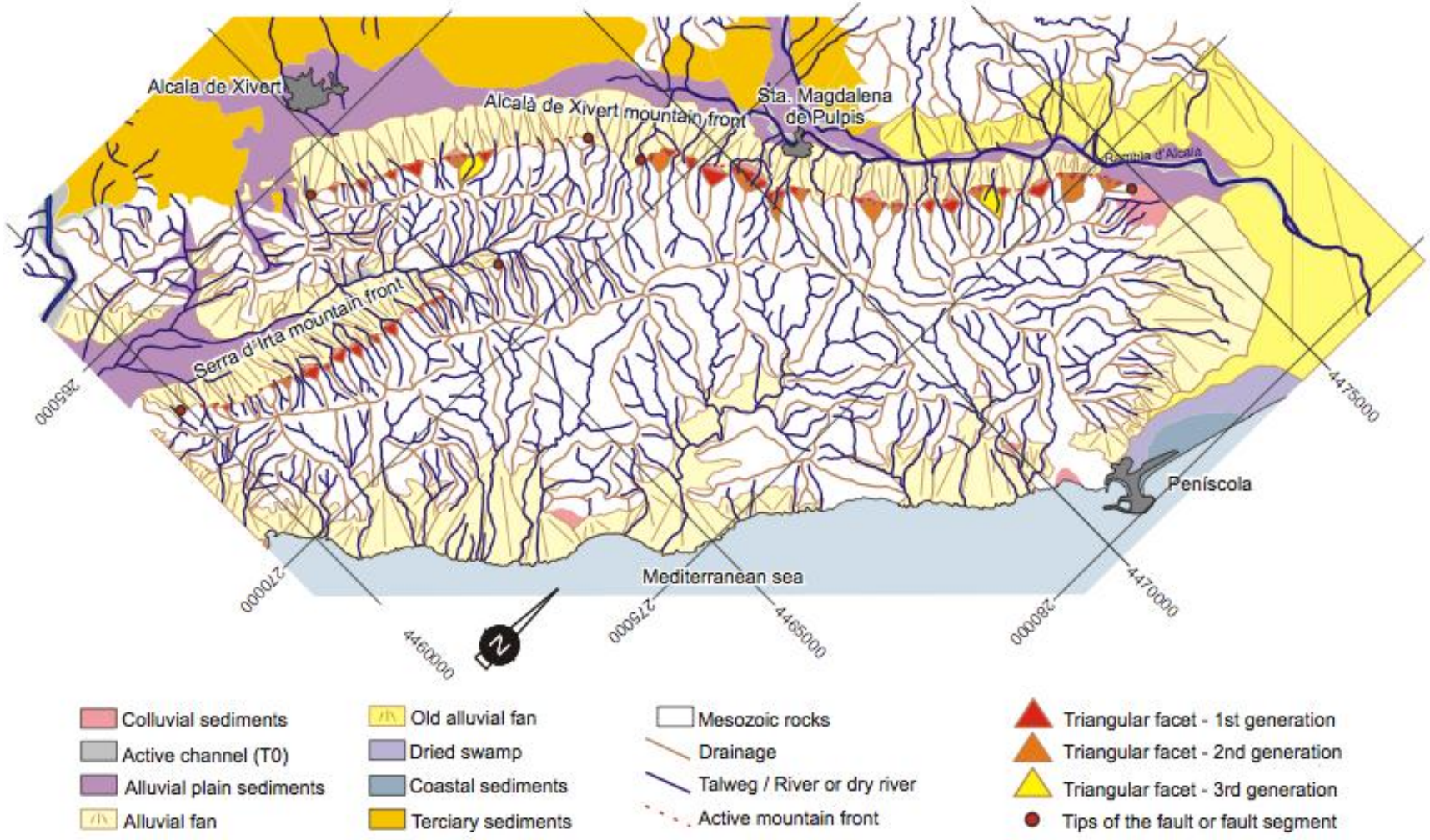

Fig. 5.- Geomorphological map of the Serra d'Irta range (modified from Perea, 2006).The Alcalà de Xivert and Serra d'Irta mountain fronts show gromorphologic features that point to the Plio-Quaternary activity of the faults with which they are associated (Perea, 2006; Perea *et al.*, 2006). Note the presence of different generations of triangular facets and the low sinuosity of the front. The basins are wineglass shaped and regularly spaced (see section 4 and table 1 for further information and their location in Fig. 8)

Fig. 5.- Mapa geomorfológico de la Sierra de Irta (modificado de Perea, 2006). Los frentes de montaña de Alcalá de Xivert i de la Sierra de Irta muestran características geomorfológicas que indican una actividad Plio-Cuaternaria de las fallas a las cuales están asociados (Perea, 2006; Perea *et al.*, 2006). Nótese la presencia de diferentes generaciones de facetas triangulares y la baja sinuosidad del frente. Las cuencas tienen forma de copa y muestran un espaciado regular (ver la sección 4 y la tabla 1 para más información y la figura 8 para su localización).

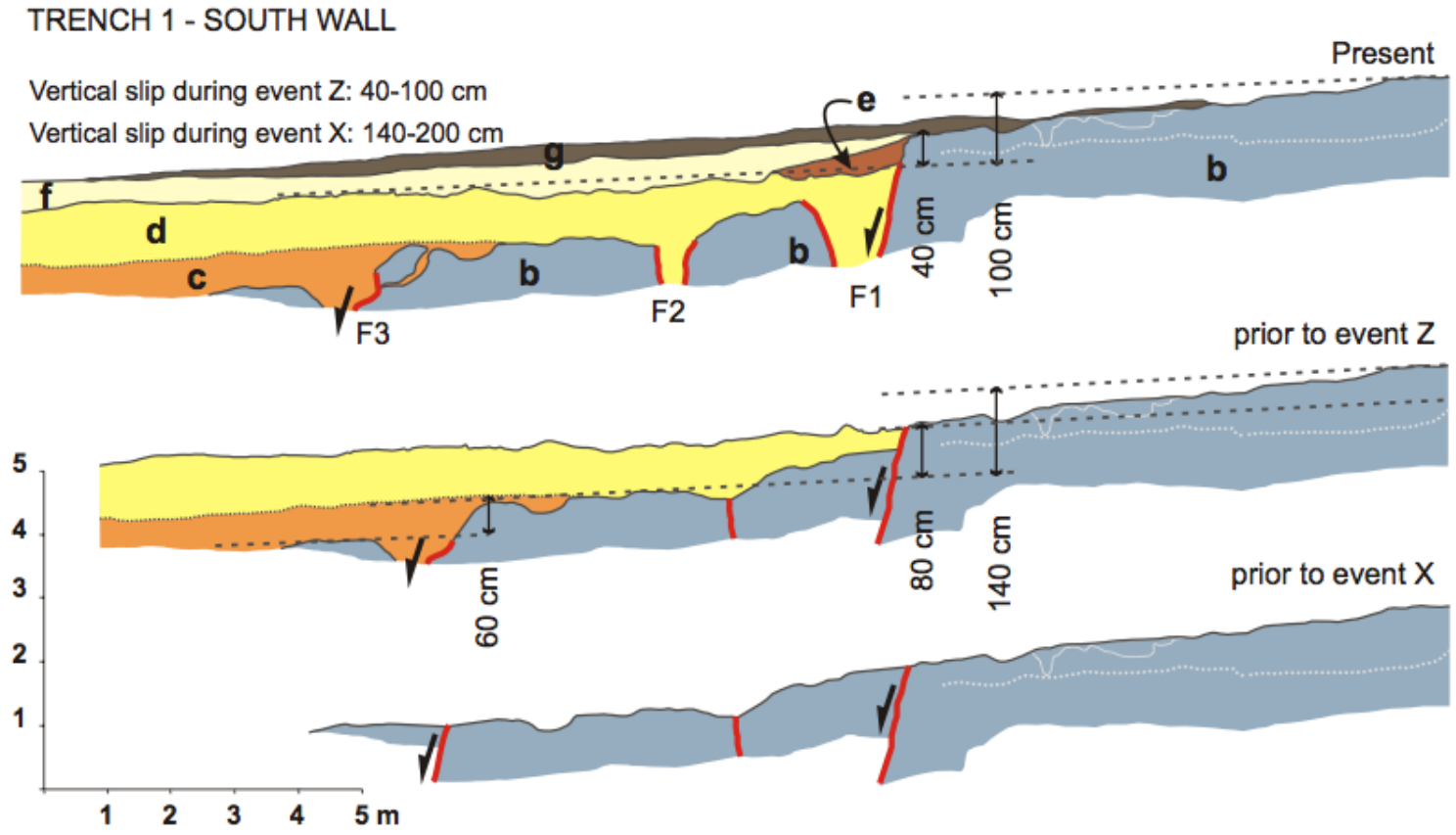

Fig. 2.- Restoration of the deformation produced by two paleoseismic events, events X and Z, recognized in trench 1 (southern wall) dug at the site of the Golf court on the El Camp fault (modified from Masana *et al.*, 2001b). Event X, the older one, is evidenced by a buried fault scarp. This event was dated between 125000 and 50000 years BP and the restoration allowed us to calculate a dip-slip of 140 to 200 cm. Event Z with a vertical slip ranging between 40 and 100 cm is evidenced by the presence of a colluvial wedge and its preferred age is 3000 years BP (Masana, 1995 and 1996; Masana *et al.*, 2001a and 2001b; Santanach *et al.*, 2001; Perea *et al.*, 2003; Perea, 2006; Perea *et al.*, 2006; Santanach *et al.*, 2010).

Fig. 2.- Restitución de la deformación producida por los dos eventos paleosísmicos, eventos X y Z, reconocidos en la trinchera 1 (pared sur) escavada en el sitio del Campo de Golf en la falla de El Camp (modificado de Masana *et al.*, 2001b). El evento X, el más antiguo, está evidenciado por un escarpe de falla enterrado. Este evento fue datado entre 125000 y 50000 años BP y la restitución permitió calcular un desplazamiento vertical de 140 a 200 cm. El evento Z con un desplazamiento vertical entre 40 y 100 cm está evidenciado por la presencia de una cuña coluvial y su edad mas probable sería de 3000 años BP (Masana, 1995 and 1996; Masana *et al.*, 2001a and 2001b; Santanach *et al.*, 2001; Perea *et al.*, 2003; Perea, 2006; Perea *et al.*, 2006; Santanach *et al.*, 2010).

ASUNCION
CHILE 2012

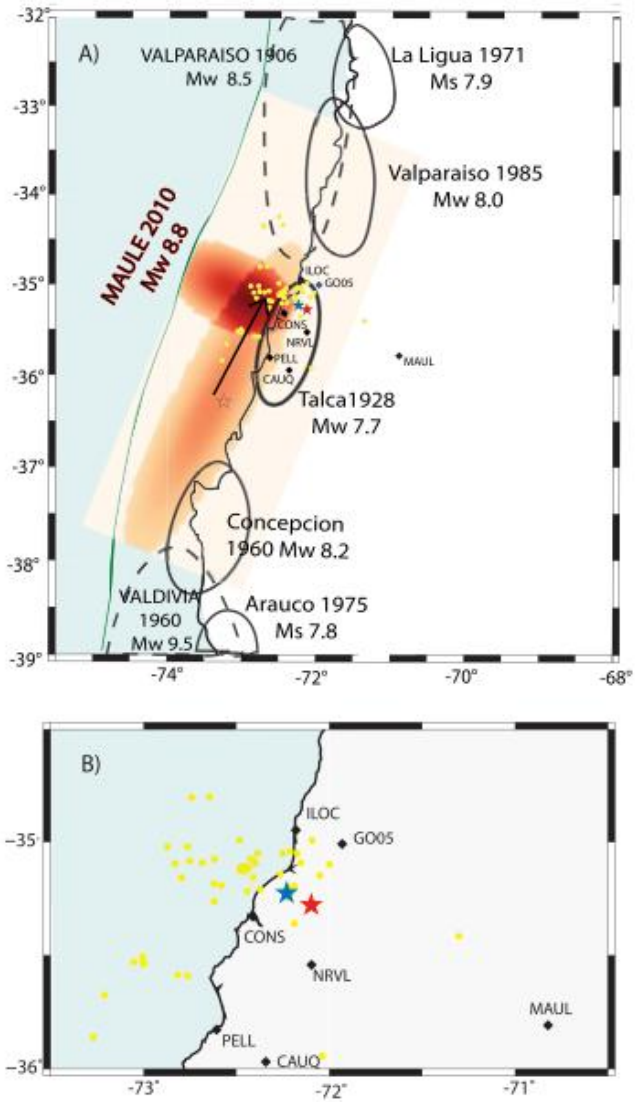

Fig. 1. The Mw 7.0 Constitución earthquake of 25 March 2012 in its context. At the top we show a simplified version of the slip distribution of the Maule 2012 mega earthquake determined by Ruiz et al. (2012). At the bottom we show an expanded map of the region of the 2012 Constitución earthquake. The red and blue stars are the *epicenters* of the 2012 earthquake computed using the P_1 and P_2 waves, respectively. The small green dots are the aftershocks of Constitución 2012 earthquakes located by SSN. The diamonds are the high-rate GPS stations and the GO05 accelerograph. The rupture area of the Talca 1928 earthquake is indicated by the thick black line. Other historical events are indicated by ellipses. (For interpretation of the references to color in this figure legend, the reader is referred to the web version of this article.)

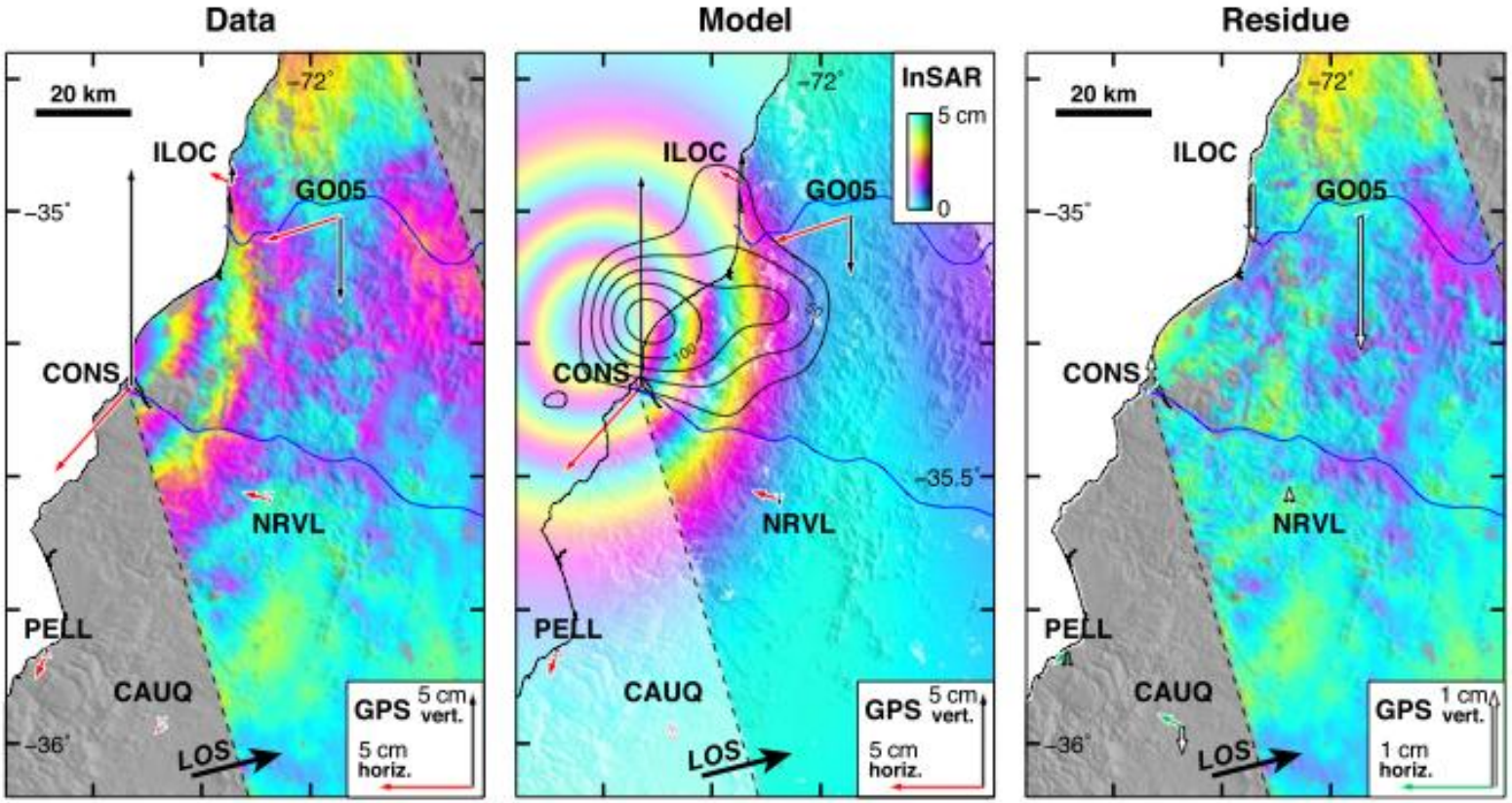

Fig. 9. Surface deformation due to the 2012 Constitución earthquake determined by InSAR, static GPS and integrated strong motion data. The left panel shows the measured displacement, the middle panel shows the synthetic displacements computed from inversion of the geodetic data; superposed on this image we plot the contour lines of slip for the inverted model. The right panel shows the residues. Vertical and horizontal GPS vectors are indicated by the arrows. Note that a different scaling of the GPS vectors is used in the right panel. Color cycles correspond the line-of-sight (LOS) component of the ground displacement derived from InSAR. Positive LOS displacement indicates motion towards the satellite. (For interpretation of the references to color in this figure legend, the reader is referred to the web version of this article.)

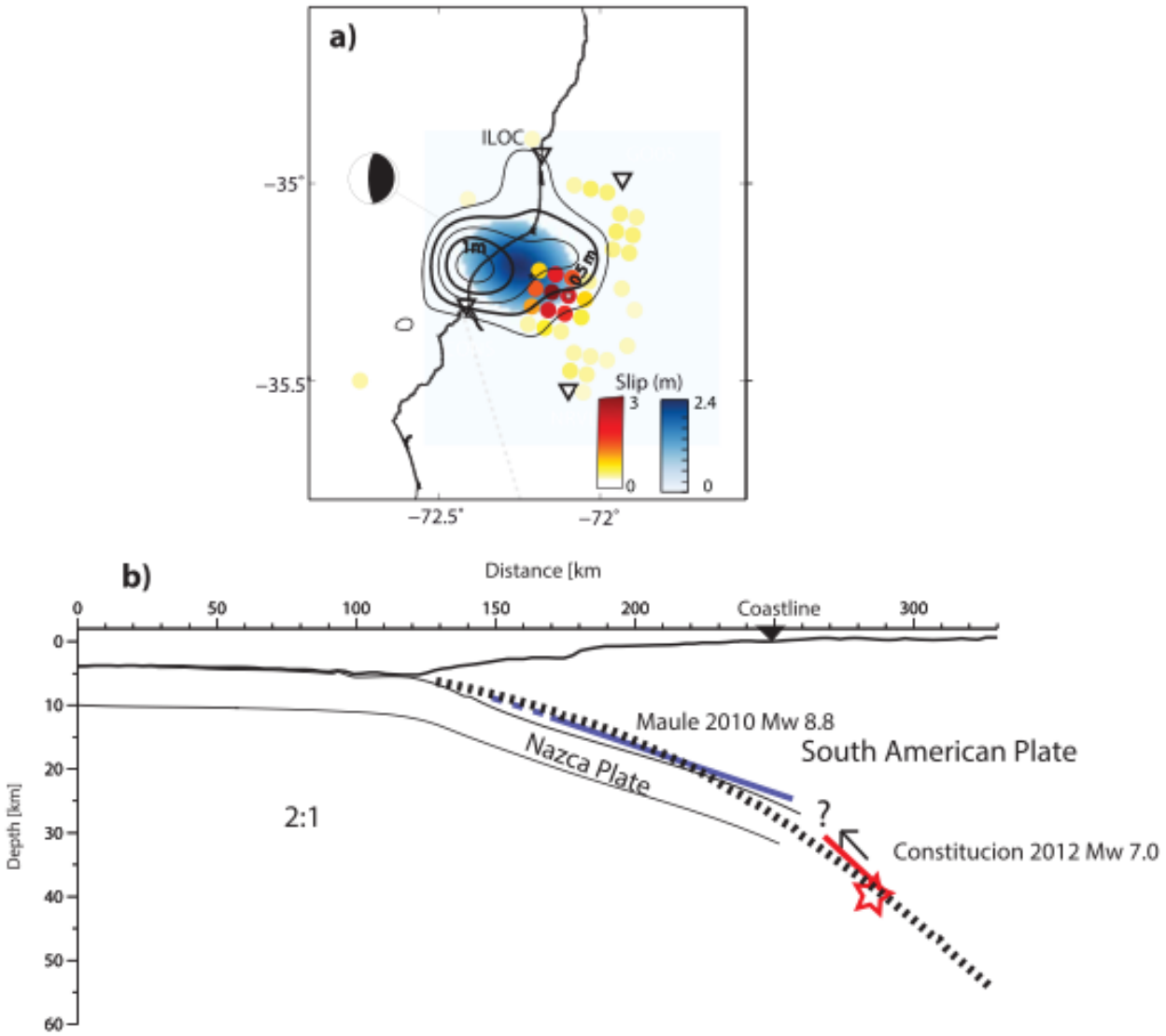

Fig. 10. (a) Slip distribution obtained from teleseismic records (color dots), together with InSAR images and GPS data (contour lines) and from GPS and strong motion records (gray shading). Color and gray scales are saturated to 4 m. (b) Geometry of the subducting Nazca plate modified from Moscoso et al. (2011) (black line). The black dashed line is the geometry of the slab interface proposed by Hayes et al. (2012). The thick blue line shows the Maule 2010 rupture zone (Ruiz et al., 2012). Red line is the Constitución 2012 rupture zone; red star is the hypocenter derived from P_I waves (2:1/V:H scale). (For interpretation of the references to color in this figure legend, the reader is referred to the web version of this article.)

6. Conclusions

The Mw 7.0 25 of March 2012 Constitución earthquake is one of the largest interplate thrust aftershocks of 2010 Maule earthquake. The rupture of the 2012 earthquake has an area of roughly 10 × 20 km, and is located near the bottom of the seismogenic zone of the interface between the Nazca and South American plates. The Constitución earthquake has a complex initiation with a deep hypocenter at 39 km depth and a shallower main rupture. The latter coincides with the depth determined by moment tensor analysis. The earthquake occurred down-dip of the region of maximum co-seismic slip of the 2010 Maule earthquake, and up-dip of the region of rapid afterslip following that event. The nucleation phase of the 2012 earthquake lasted 6 s, which is unusually long for an earthquake of that magnitude (Ellsworth and Beroza, 1995). The different techniques used in this work produce consistent results, with up-dip propagation of the rupture from southeast to northwest. Fig. 10a summarizes the slip distribution proposed for the 25 March 2012 earthquake using teleseismic records, InSAR image, GPS data and strong motion records. We observed that the largest slip is concentrated in a zone of less than 20 km radius in the deeper part of the interface between the Nazca and South American plates, as sketched in Fig. 10b, where the location of Constitución 2012 rupture is compared with the Maule 2010 rupture.

MAGNITUD RICHTER	EQUIVALENCIA EN TNT	EJEMPLOS (aproximado)
-1.5	6 onzas (170 gramos)	Romper una roca en una mesa de laboratorio
1.0	30 libras (13 kilogramos)	Una pequeña explosión en un sitio de construcción
1.5	320 libras (145 kg)	
2.0	1 tonelada	Una gran explosión minera
2.5	4,6 toneladas	
3.0	29 toneladas	
3.5	73 toneladas	
4.0	1.000 toneladas	Arma Nuclear pequeña
4.5	5.100 toneladas	Tornado promedio
5.0	32.000 toneladas	
5.5	80.000 toneladas	Terremoto de Little Skull Mtn., NV, 1992
6.0	1.000.000 de toneladas (un megatón)	Terremoto de Double Spring Flat, NV, 1994
6.5	5.000.000 de toneladas	Terremoto de Northridge, CA, 1994
7.0	32.000.000 de toneladas	Terremoto de Hyogo-Ken Nanbu, Japon, 1995
7.5	160.000.000 de toneladas	Terremoto de Landers, CA, 1992
8.0	1.000.000.000 de toneladas (un gigatón)	Terremoto de San Francisco, CA, 1906
8.5	5.000.000.000 de toneladas	Terremoto de Anchorage, AK, 1964
9.0	32.000.000.000 de toneladas	Terremoto de Chile, 1960
10.0	1 billón (1.000.000.000.000) de toneladas (1 teratón)	Energía acumulada en Falla tipo San Andrés
12.0	160 billones (160.000.000.000.000) de toneladas	¡¡Fracturar la tierra en la mitad por el centro !! o la energía solar recibida diariamente en la tierra

Extraído de The Nevada Seismological Laboratory at the University of Nevada, Reno

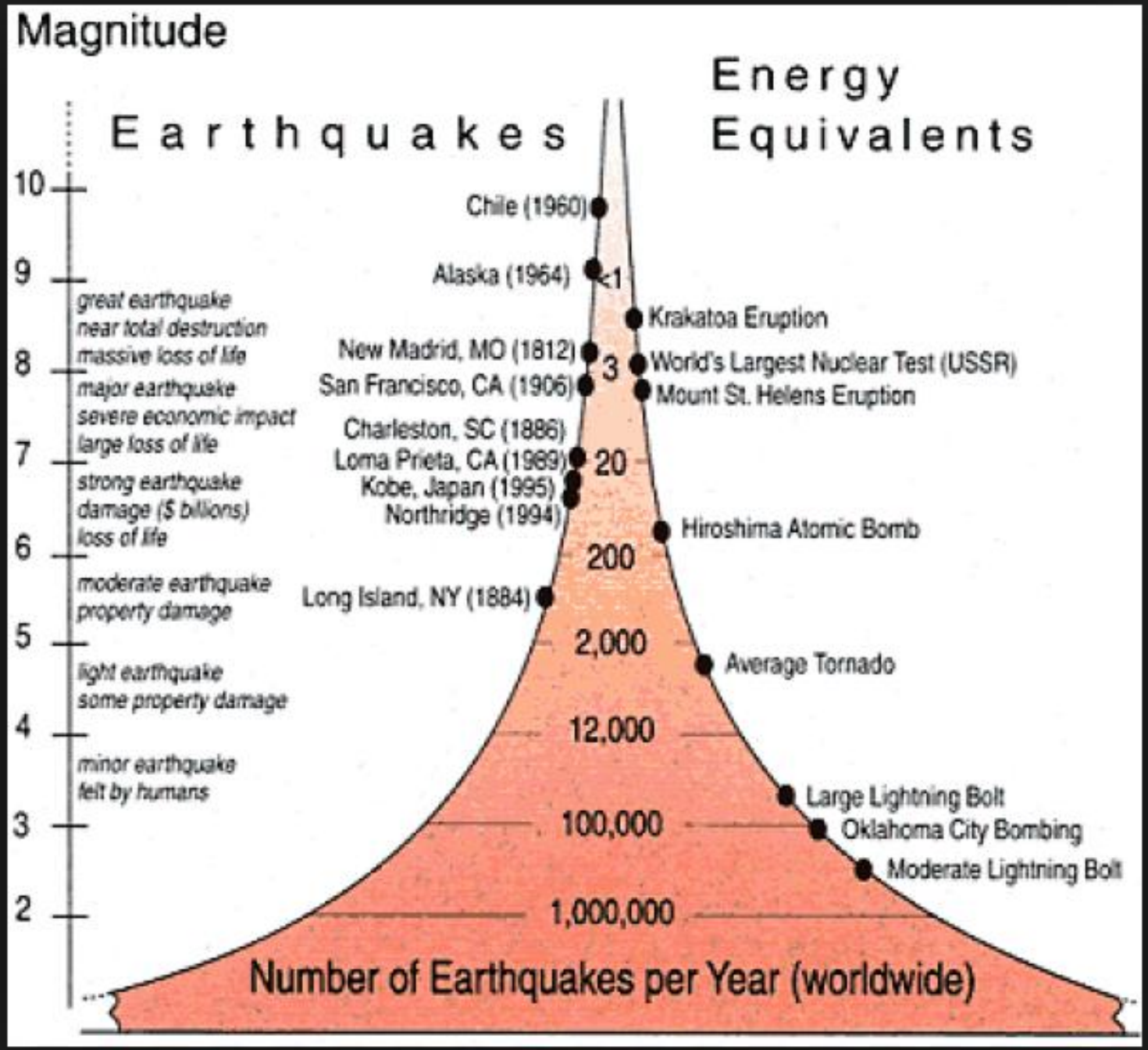
Magnitude
Earthquakes
Energy Equivalents
10
9
8
7
6
5
4
3
2
great earthquake
near total destruction
massive loss of life
major earthquake
severe economic impact
large loss of life
strong earthquake
damage ($ billions)
loss of life
moderate earthquake
property damage
light earthquake
some property damage
minor earthquake
felt by humans
Chile (1960)
Alaska (1964)
New Madrid, MO (1812)
San Francisco, CA (1906)
Charleston, SC (1886)
Loma Prieta, CA (1989)
Kobe, Japan (1995)
Northridge (1994)
Long Island, NY (1884)
<1
3
20
200
2,000
12,000
100,000
1,000,000
Krakatoa Eruption
World's Largest Nuclear Test (USSR)
Mount St. Helens Eruption
Hiroshima Atomic Bomb
Average Tornado
Large Lightning Bolt
Oklahoma City Bombing
Moderate Lightning Bolt
Number of Earthquakes per Year (worldwide)

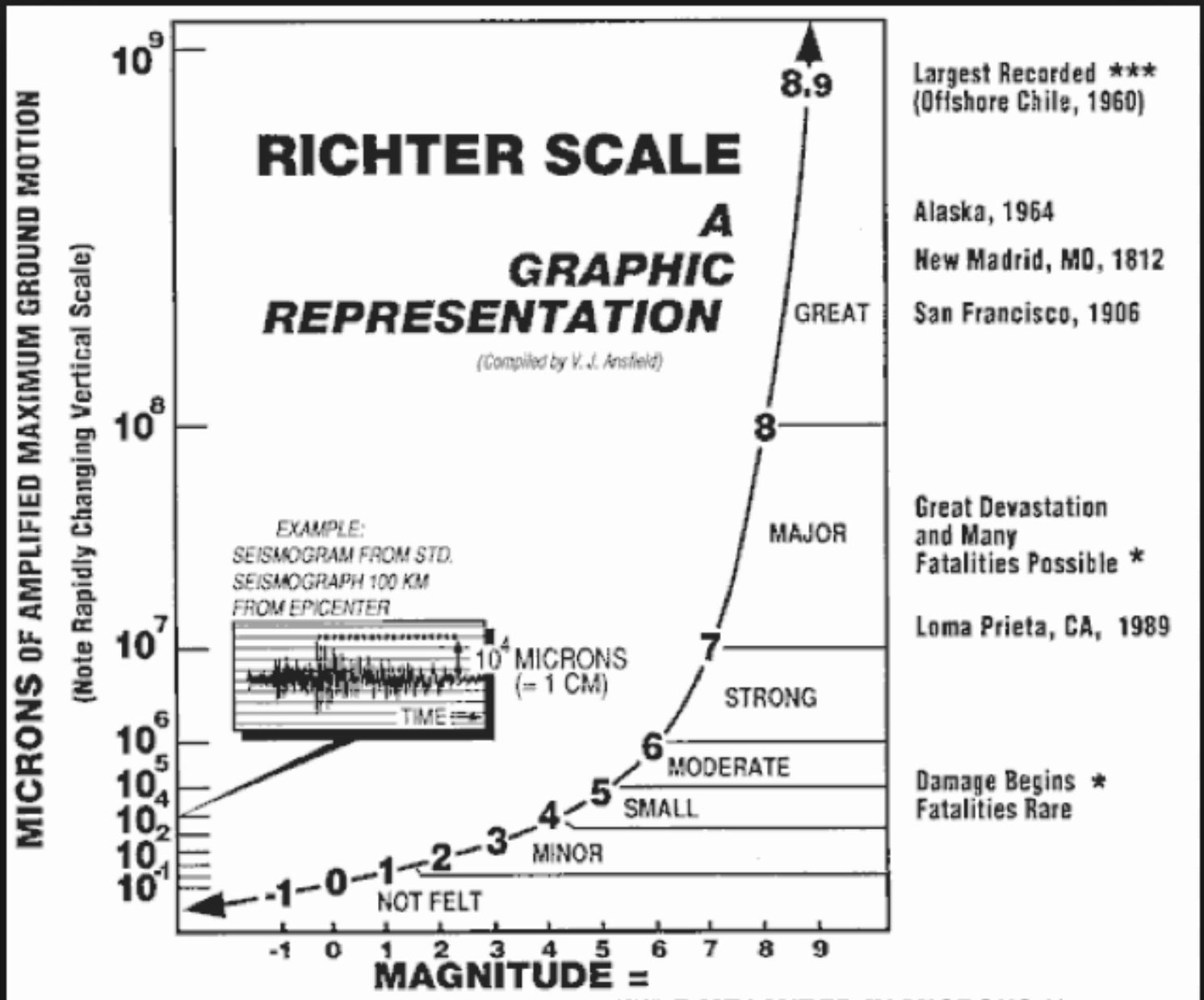

LOGARITHM (BASE 10) OF MAXIMUM AMPLITUDE MEASURED IN MICRONS **

* EFFECTS MAY VARY GREATLY DUE TO CONSTRUCTION PRACTICES, POPULATION DENSITY, SOIL DEPTH, FOCAL DEPTH, ETC.

** MICRON = A MILLIONTH OF A METER

*** EQUIVALENT TO A MOMENT MAGNITUDE OF 9.5

Escala de Richter	
Magnitud	**Efectos del terremoto**
menos de 3.5	Generalmente no se siente, pero se registra.
3.5 a 5.4	Se siente, pero sólo causa daños menores cerca de donde se produce.
5.5 a 6.0	Ocasiona daños ligeros a edificios mal construidos y otras estructuras en un radio de 10 km.
6.1 a 6.9	Puede ocasionar daños severos en áreas donde vive mucha gente.
7.0 a 7.9	Terremoto mayor. Causa graves daños a las comunidades en un radio de 100 km.
8.0 o más	Gran terremoto. Destrucción total de comunidades cercanas y daños severos en un radio de más de 1000 km de distancia.

MINISTERIO DE SALUD DIGESA

ESCALA SISMOLÓGICA DE RICHTER

Magnitud Richter	Equivalencia de la energía TNT	Referencias
–1,5	1 g	Rotura de una roca en una mesa de laboratorio
1,0	170 g	Pequeña explosión en un sitio de construcción
1,5	910 g	Bomba convencional de la II Guerra Mundial
2,0	6 kg	Explosión de un tanque de gas
2,5	29 kg	Bombardeo a la ciudad de Londres
3,0	181 kg	Explosión de una planta de gas
3,5	455 kg	Explosión de una mina
4,0	6 t	Bomba atómica de baja potencia
4,5	32 t	Tornado promedio
5,0	199 t	Terremoto de Albolote, Granada (España), 1956
5,5	500 t	Terremoto de Little Skull Mountain, Nevada (Estados Unidos),1992
6,0	1.270 t	Terremoto de Double Spring Flat, Nevada (Estados Unidos), 1994
6,5	31.550 t	Terremoto de Northridge, California (Estados Unidos), 1994
7,0	199.000 t	Terremoto de Hyogo-Ken Nanbu, Japón, 1995
7,5	**1.000.000 t**	**Terremoto de Landers, California, 1992, TERREMOTO EN PISCO, ICA, CHINCHA, LIMA Y CAÑETE, AGOSTO 2007**
8,0	6.270.000 t	Terremoto de México, México, 1985
8,5	31,55 millones de t	Terremoto de Anchorage, Alaska, 1964
9,2	220 millones de t	Terremoto del Océano Índico de 2004
9,6	260 millones de t	Terremoto de Valdivia, Chile, 1960
10,0	6.300 millones de t	Falla de tipo San Andrés
12,0	1 billón de t	Fractura de la Tierra por el centro Cantidad de energía solar recibida diariamente en la Tierra

Referencias: Hanks TC, Kanamori H (1979). «A moment magnitude scale». *Journal of Geophysical Research* 84 (B5): 2348-2350

FINAL

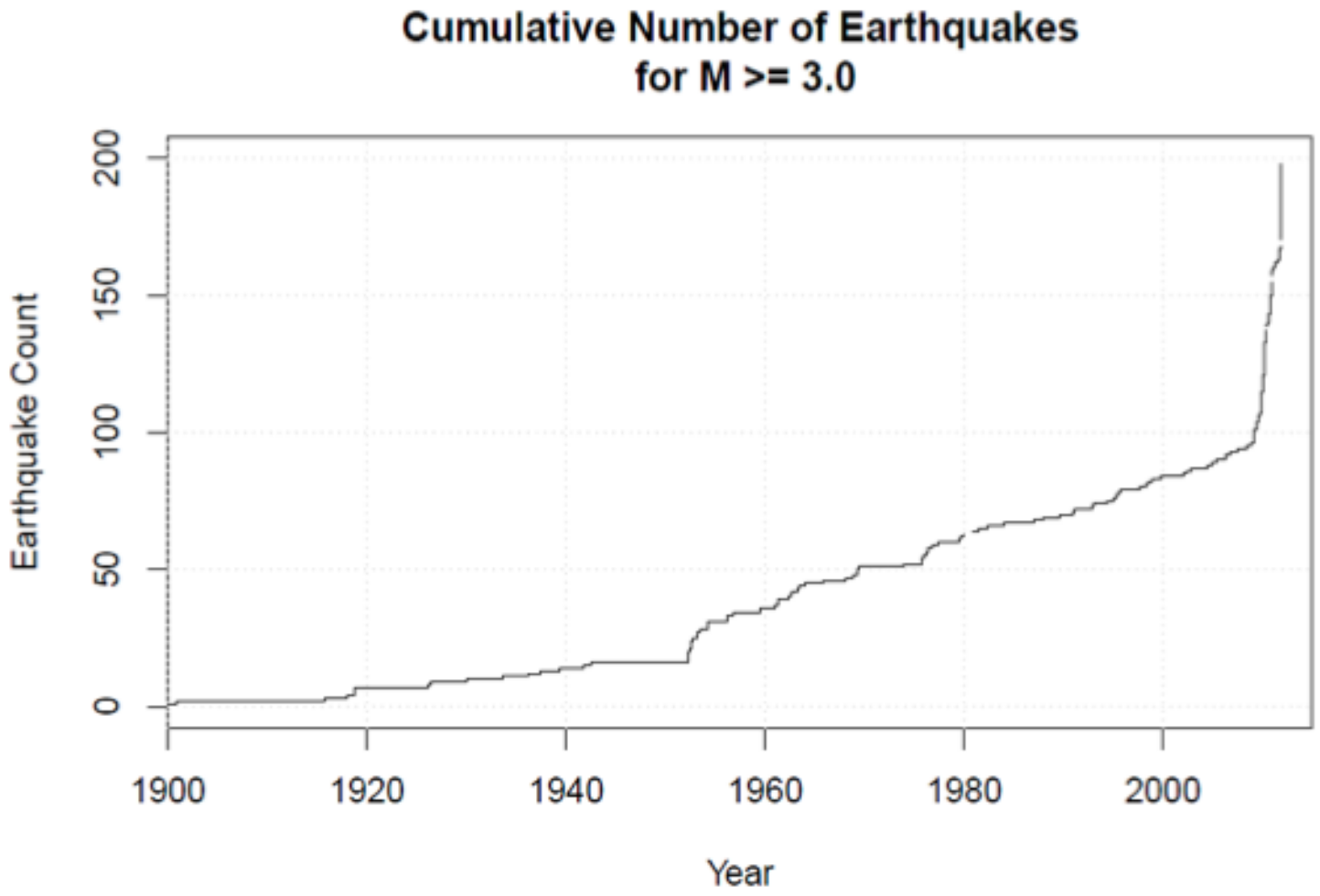

FIGURE 3.13 Graph showing the cumulative number of earthquakes **M** > 3.0 in the central Oklahoma region (34-37° North, 94-100° West) from 1900 to present day, showing a dramatic but as-yet unexplained increase in seismicity since 2009. SOURCE: Ellsworth et al. (2012).

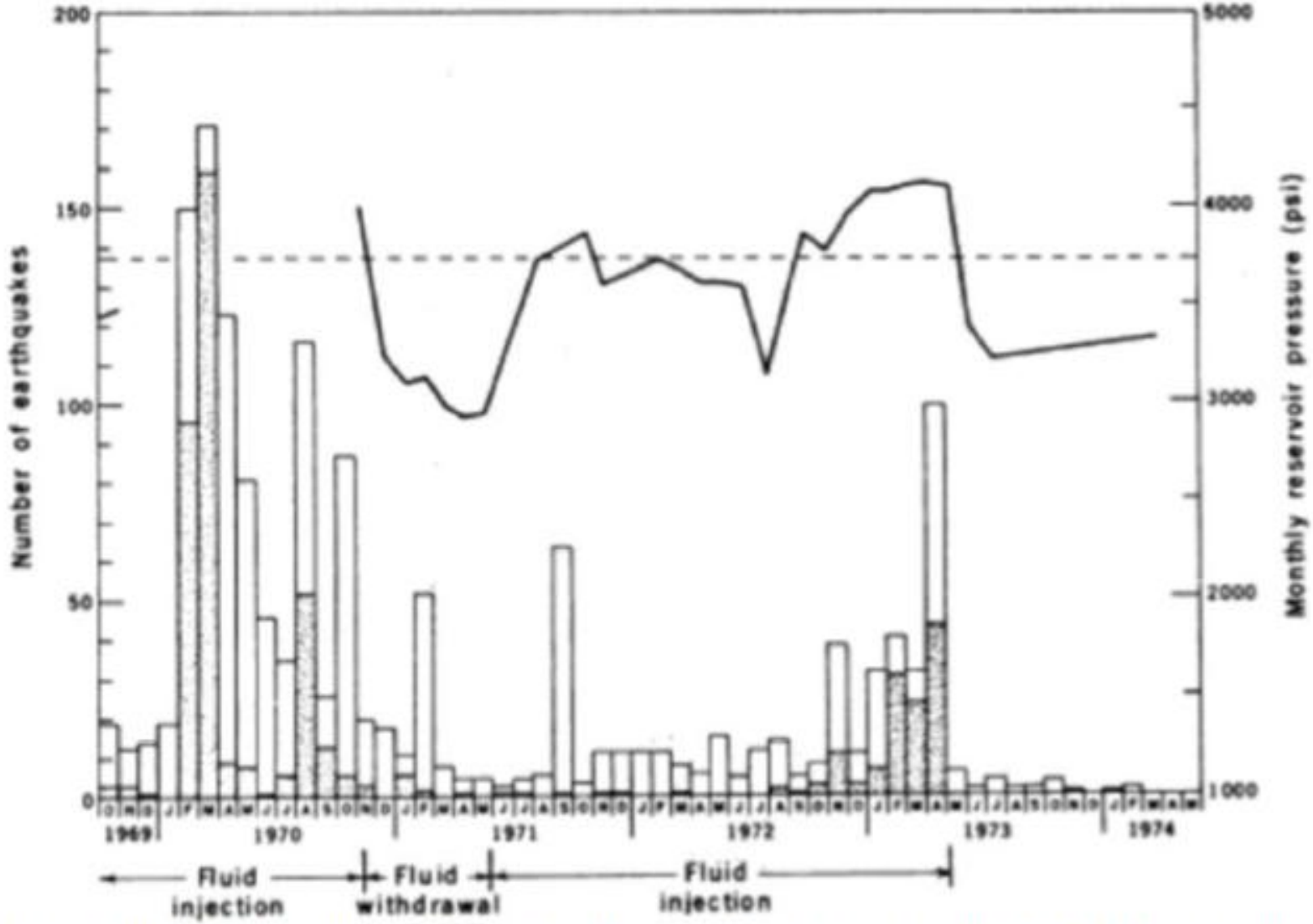

Figure 2 Frequency of seismic events at Rangely. Stippled bars are seismic events within 1 kilometer of the experimental wells. The clear bars represent all other events. Pressure history in well Fee 69 is shown by the heavy line and predicted critical pressure is designated by the dashed line. SOURCE: Raleigh et al. (1976).

OVERSIGHT, MONITORING, AND COORDINATION OF UNDERGROUND INJECTION ACTIVITIES FOR MITIGATING INDUCED SEISMICITY

Findings

1. Induced seismicity may be produced by a number of different energy technologies and may result from either injection or extraction of fluid. As such, responsibility for oversight of activities that can cause induced seismicity is dispersed among a number of federal and state agencies.
2. Recent, potentially induced seismic events in the United States have been addressed in a variety of manners involving local, state, and federal agencies, and research institutions. These agencies and research institutions may not have resources to address these unexpected events and more events could stress this ad hoc system.
3. Currently the Environmental Protection Agency (EPA) has primary regulatory responsibility for fluid injection under the Safe Drinking Water Act; however, this act does not address induced seismicity. EPA appears to be addressing the issue of induced seismicity through a current study in consultation with other federal and state agencies.
4. The USGS has the capability and expertise to address monitoring and research associated with induced seismic events. However, the scope of their mission within the seismic hazard assessment program is focused on large impact, natural earthquakes. Significant new resources would be required if the USGS mission is expanded to include comprehensive monitoring and research on induced seismicity.

Proposed Actions

1. A detailed methodology should be developed for quantitative, probabilistic hazard assessments of induced seismicity risk. The goals in developing the methodology would be to:
    - make assessments before operations begin in areas with a known history of felt seismicity;
    - update assessments in response to observed induced seismicity.
2. Data related to fluid injection (well locations coordinates, injection depths, injection volumes and pressures, time frames) should be collected by state and federal regulatory authorities in a common format and made accessible to the public (through a coordinating body such as the USGS).
3. In areas of high-density of structures and population, regulatory agencies should consider requiring that data to facilitate fault identification for hazard and risk analysis be collected and analyzed before energy operations are initiated.

BEST PRACTICES

Findings

1. The DOE Protocol for EGS, which lists seven sequential steps, provides a reasonable initial model for dealing with induced seismicity that can serve as a template for other energy technologies.
2. Based on this initial model, the committee has proposed two matrix-style protocols as examples to illustrate the manner in which these seven activities can ideally be undertaken concurrently (rather than only sequentially), while also illustrating how these activities should be adjusted as a project progresses from early planning through operations to completion.

Gap

No best practices protocol for addressing induced seismicity is generally in place for each of these technologies, with the exception of the protocol recently developed for EGS. The committee suggests that best practices protocols be adapted and tailored to each technology to allow continued energy technology development. Actions toward developing these protocols are outlined below.

Proposed Actions

1. A matrix-style "best practices" protocol should be developed in coordination with the permitting agency or agencies by experts in the field of each energy technology, including EOR, shale gas production, and carbon capture and sequestration.
2. The adoption and use by developers of such protocols is recommended in each case where there is a known or substantial probability of inducing seismicity at levels that could pose a concern to the public. In cases where induced seismicity becomes an issue at some stage in the project, the developer can adopt the protocol procedures needed to continue the project in a manner more satisfactory to the public.
3. Even with the adoption and use of a best practices protocol, induced seismicity of serious concern to public health and safety may occur. The regulatory body affiliated with the permitting of well(s) should include, as part of each project's operation permit, a mechanism

8000 millions persones.....

Table 3.3 Petroleum and Natural Gas Production in 2010

	Crude oil	Natural gas plant liquids (NGPL)	Other liquids	**Total crude oil, NGPL, and other liquids**		**Total dry natural gas**
United States	2.00 billion barrels	757 million barrels	391 million barrels	3.15 billion barrels	**501 million cubic meters**	**611 billion cubic meters**
World	27.0 billion barrels	3.08 billion barrels	754 million barrels	30.9 billion barrels	**4.91 billion cubic meters**	**3.17 trillion cubic meters**

NOTE: 1.00000 barrel = 0.15899 cubic meters
SOURCE: EIA 2010 International Energy Statistics (available at www.eia.gov/cfapps/ipdbproject/IEDIndex3.cfm).

per any

doi: 10.2110/sedred.2014.1
Volume 12, No. 1, March 2014

The SEDIMENTARY Record

A publication of SEPM Society for Sedimentary Geology
with the Sedimentary Geology Division of GSA

Cover graphic: Fly Ranch Geyser, Washoe County, Nevada. In the 1960's, geothermal fluids found a weak path around a well drilled earlier in 1916, and the Fly Ranch Geyser was born. Minerals deposited from these geothermal fluids have produced this magnificent formation and the fluids continue to flow until today. The water spouts to approximately 12 feet above ground level and the mineral mounds stand about 5 feet high.

SUBDUCTION EROSION AND ANDEAN MAGMATISM

Charles R. Stern

Department of Geological Sciences, University of Colorado, Boulder, CO, USA.
** Presenting Author's email: .....*

Subduction erosion occurs all along the western margin of South America. Rates of subduction erosion, which range up to >440 km3/km/my of crust subducted near the Chile Rise-Trench triple junction, vary both spatially and temporally as a function of convergence rates, subduction angle, and sediment supply to the trench, as well as the subduction of buoyant features such as seamount chains and oceanic spreading ridges which causes weakening of the forearc wedge. Revised estimates of long-term rates of subduction erosion appropriate for Peru and northern Chile (50-70 km^3/km/my since >150 Ma), and central (115 km^3/km/my since 30 Ma) and southernmost Chile (30-35 km^3/km/my since 15 Ma), are higher than previously thought. Subducted South American continental crust removed from the forearc wedge by subduction erosion is carried into the source region of Andean arc magmas and incorporated into these magmas by either dehydration of the subducted slab and the transport of their soluble components into the overlying mantle wedge source of arc basalts, and/or bulk melting of the subducted crust to produce adakites. A strong case can be made for the temporal and spatial correlation of distinctive crustal isotopic characteristics of Andean arc magmas and episodes or areas of enhanced subduction erosion. Nevertheless, overall most subducted continental crust (>90%) is transported deeper into the mantle and neither underplated below the forearc wedge nor incorporated in Andean arc magmas. The total current rate of return of South American continental crust into the deeper mantle is equal to or greater than the estimates of the rate at which the crust is being replaced by arc magmatic activity, indicating that currently the South American continental crust is probably slowly shrinking.

“Piton de la Fournaise” volcano (Reunion island) – August 2003 eruption

30 cm displacement **7 cm displacement**

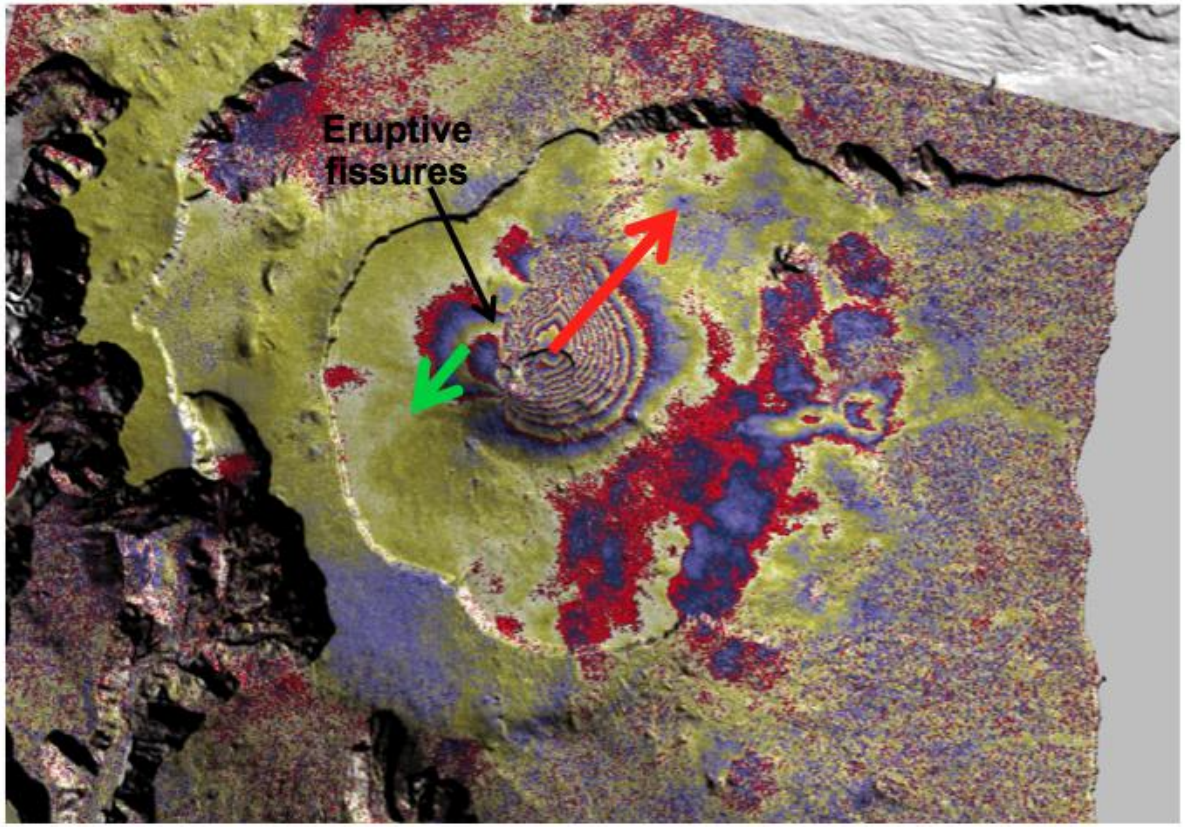

Courtesy:
- *Institut de Recherche pour le Développement (IRD), Clermont-Ferrand, France*
- *Université Blaise Pascal, Clermont-Ferrand, France*
- *Institut de Physique du Globe de Paris, Paris, France*
- *Université de la Réunion, Saint-Denis, France*

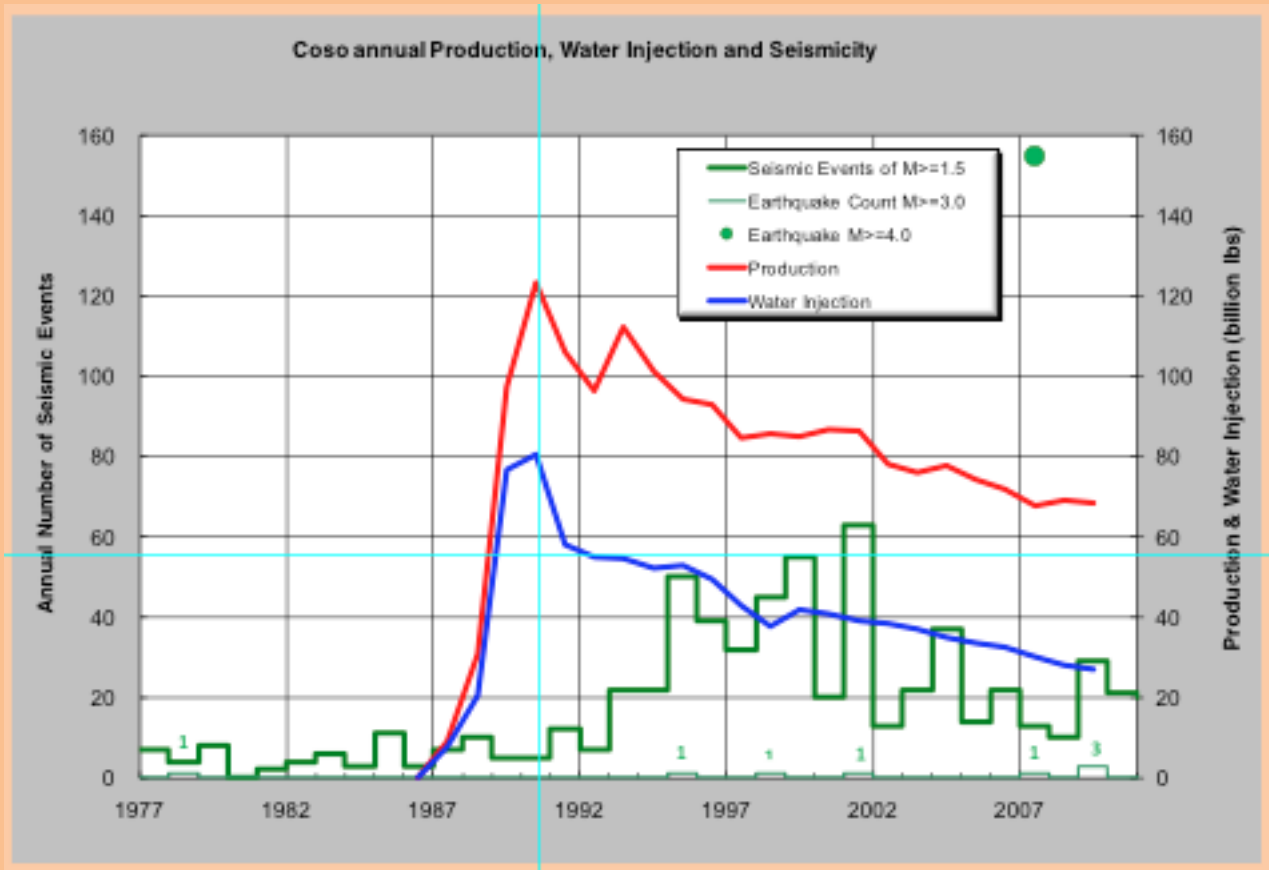

Figure 2 Annual Production, Water Injection and Seismicity at the Coso Geothermal Field. SOURCE: Generated by the study committee from available data.

Produint terratremols

Charles R. Stern

Department of Geological Sciences, University of Colorado, Boulder, CO, USA.
** Presenting Author's email: .....*

Subduction erosion occurs all along the western margin of South America. Rates of subduction erosion, which range up to >440 km3/km/my of crust subducted near the Chile Rise-Trench triple junction, vary both spatially and temporally as a function of convergence rates, subduction angle, and sediment supply to the trench, as well as the subduction of buoyant features such as seamount chains and oceanic spreading ridges which causes weakening of the forearc wedge. Revised estimates of long-term rates of subduction erosion appropriate for Peru and northern Chile (50-70 km^3/km/my since >150 Ma), and central (115 km^3/km/my since 30 Ma) and southernmost Chile (30-35 km^3/km/my since 15 Ma), are higher than previously thought. Subducted South American continental crust removed from the forearc wedge by subduction erosion is carried into the source region of Andean arc magmas and incorporated into these magmas by either dehydration of the subducted slab and the transport of their soluble components into the overlying mantle wedge source of arc basalts, and/or bulk melting of the subducted crust to produce adakites. A strong case can be made for the temporal and spatial correlation of distinctive crustal isotopic characteristics of Andean arc magmas and episodes or areas of enhanced subduction erosion. Nevertheless, overall most subducted continental crust (>90%) is transported deeper into the mantle and neither underplated below the

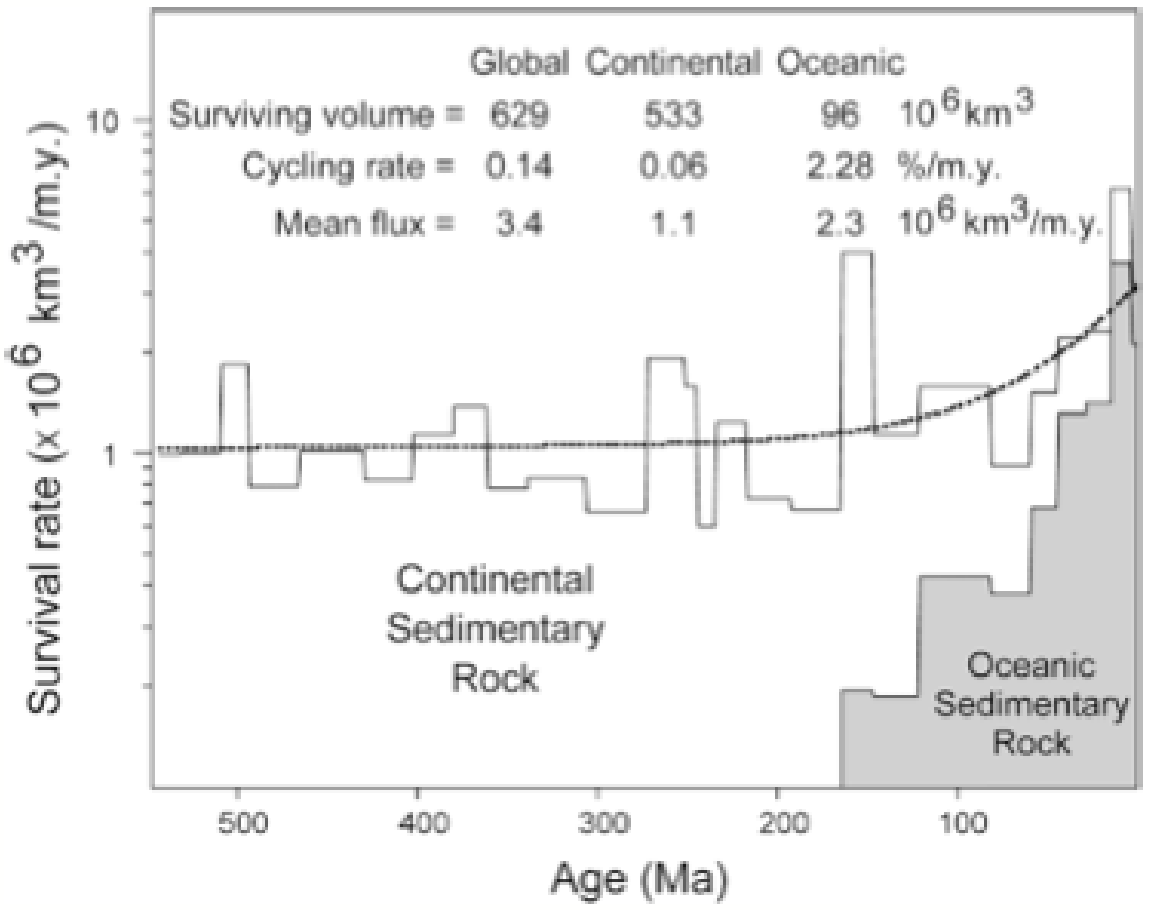

Figure 1. Data from Ronov (1983) on volumes of sediment of given age deposited on oceanic (shaded) and continental (unshaded) crust. Dashed line is best-fit model of decrease in global volume of sedimentary rock under assumptions that mean oceanic and continental sediment fluxes are 1.1 and 2.3 × 10^6 km^3/m.y., respectively (*y*-intercepts), and sediment destruction by subduction and erosion of 2.28%/m.y. and 0.06%/m.y., respectively (see text).

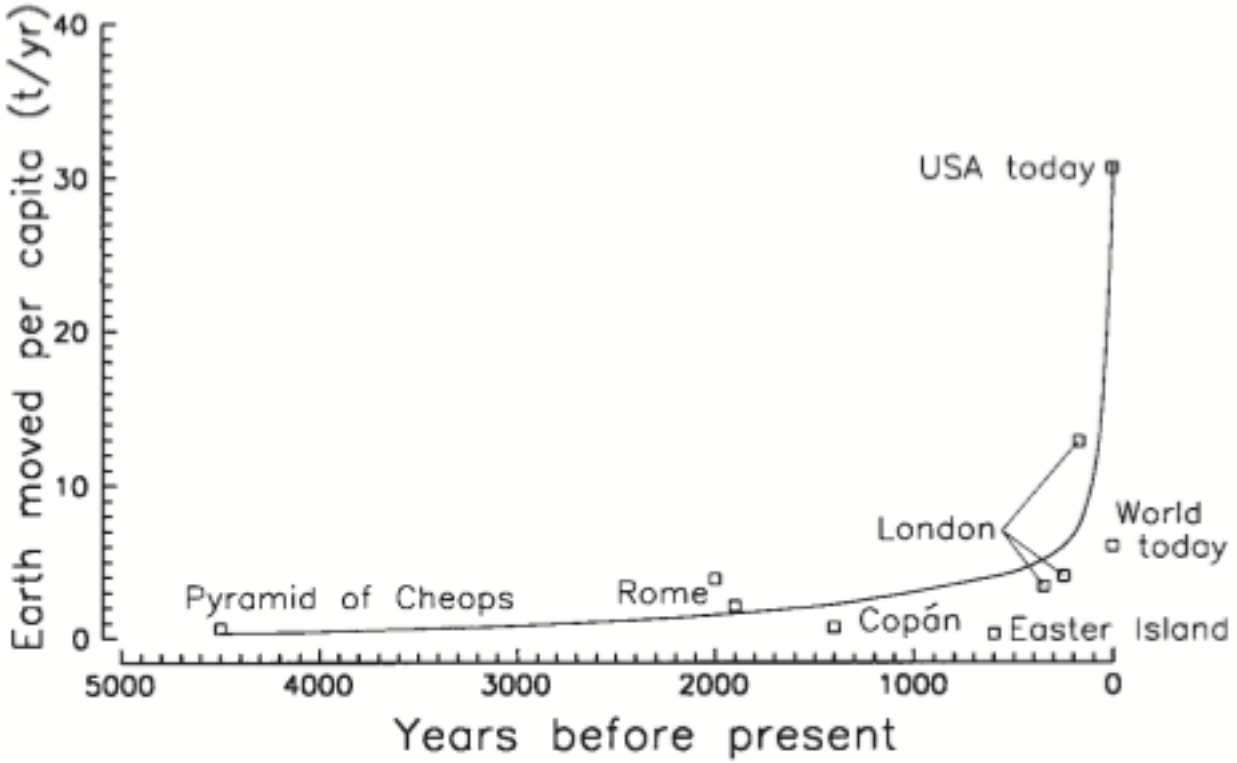

Figure 1. Estimates of amount of earth, including both soil and rock, moved per capita intentionally annually, by certain relatively advanced societies in the past; t is tons.

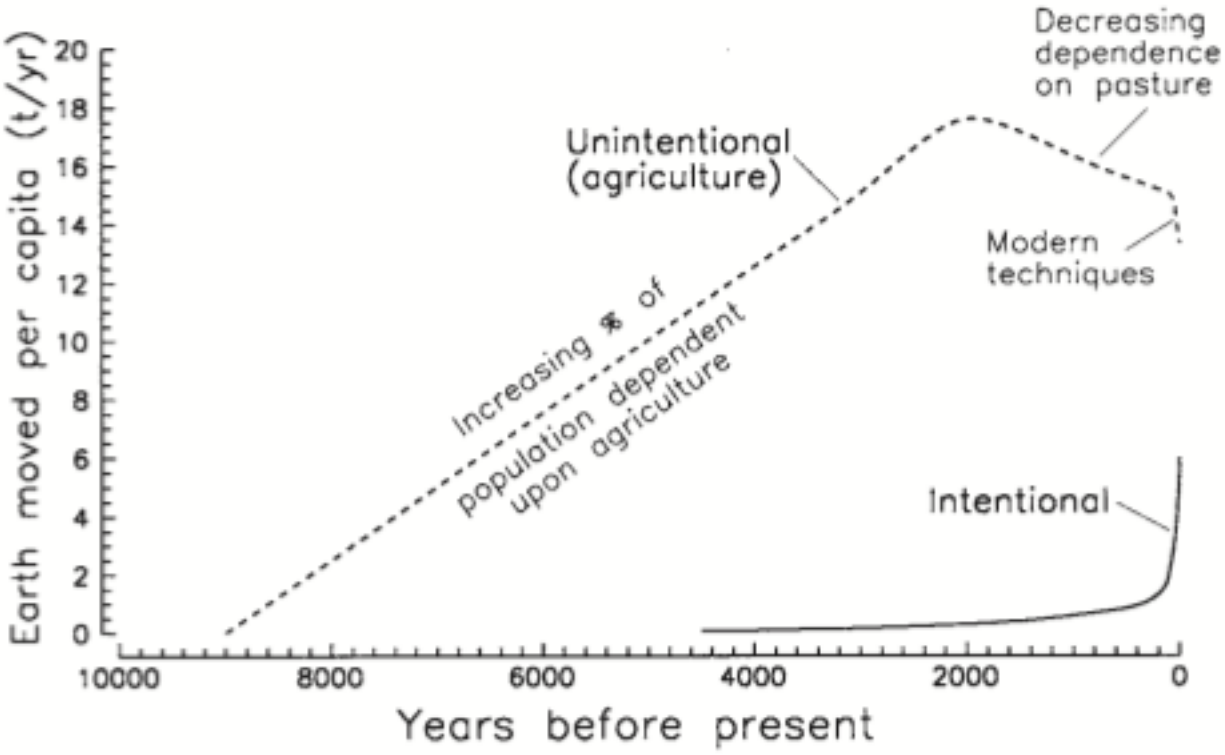

Figure 2. Estimates of the average amount of earth moved per capita at various times in the past, both intentionally as in house and road construction and mineral production (solid line) and unintentionally as in agriculture; t is tons.

Box 3.1
Geysers Annual Steam Production, Water Injection, and Observed Seismicity, 1965-2010

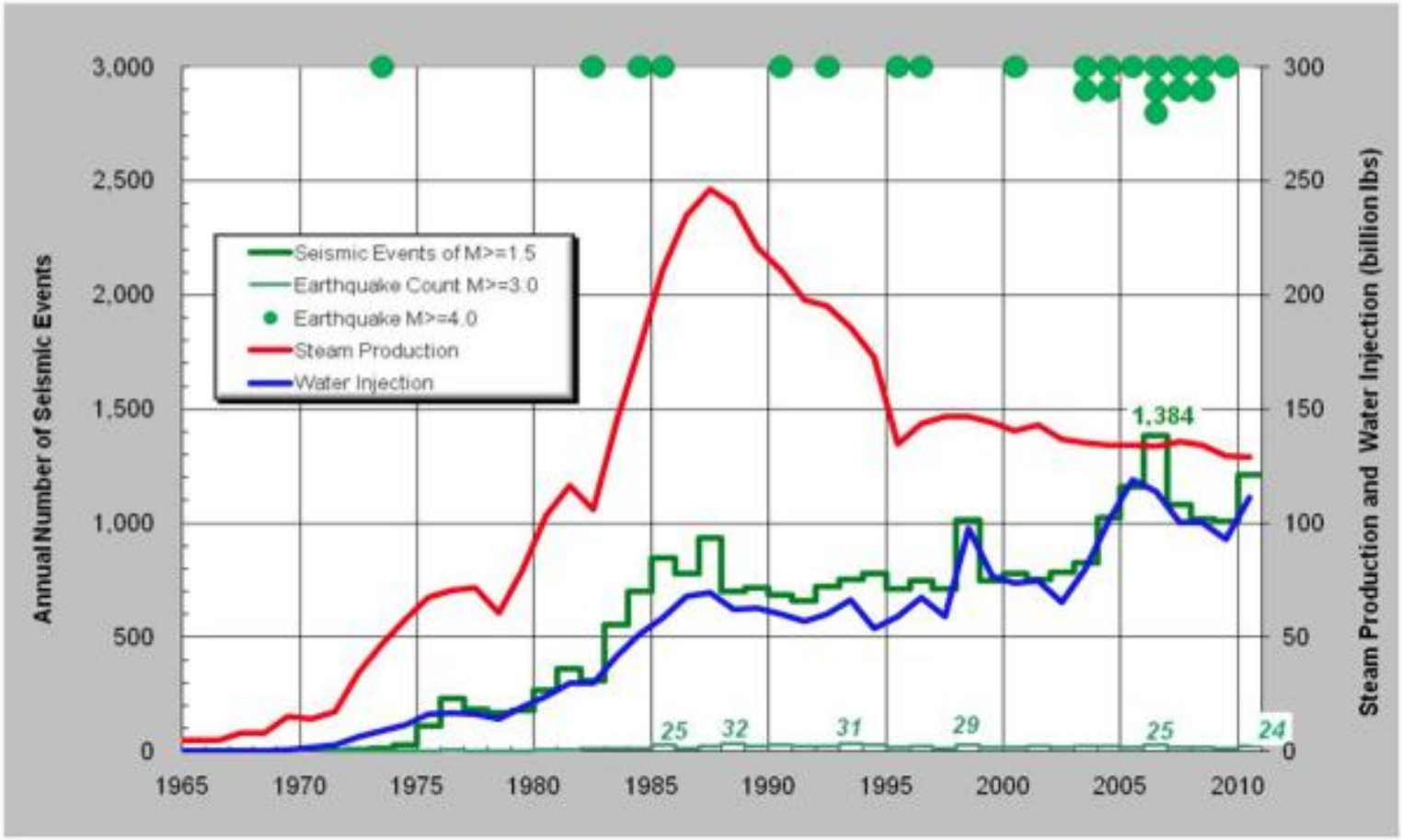

Figure The history of induced seismicity at The Geysers is shown in three forms. First, the number of recorded events of **M** 1.5* and greater is shown to have increased from almost none in the 1960s to 112 in 1975 and then to as many as 1,384 in 2006 (thick green line). Second, the annual number of earthquakes of **M** 3.0 and greater is shown along the bottom of the graph (pale green line). By 1985 25

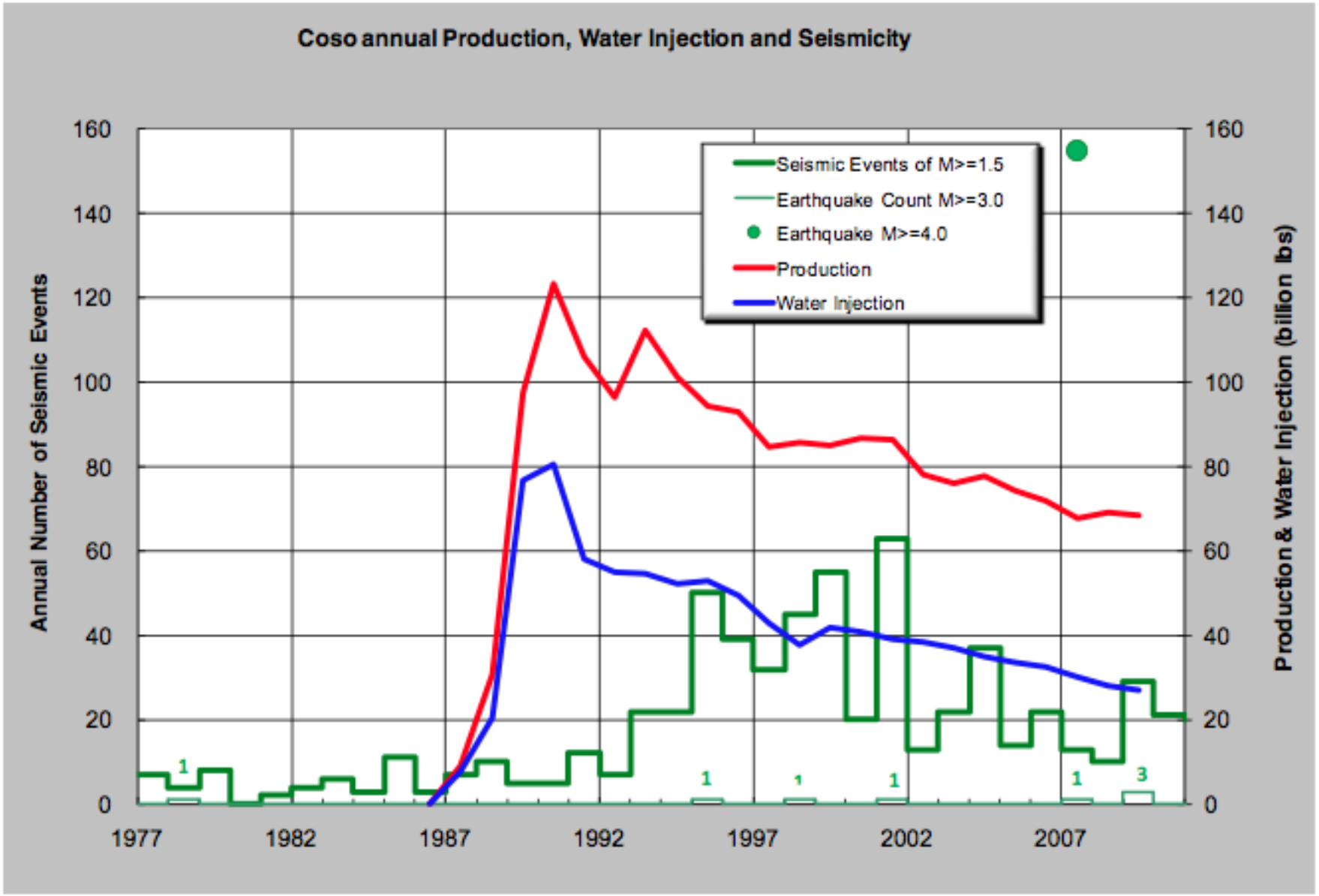

Figure 2 Annual Production, Water Injection and Seismicity at the Coso Geothermal Field. SOURCE: Generated by the study committee from available data.

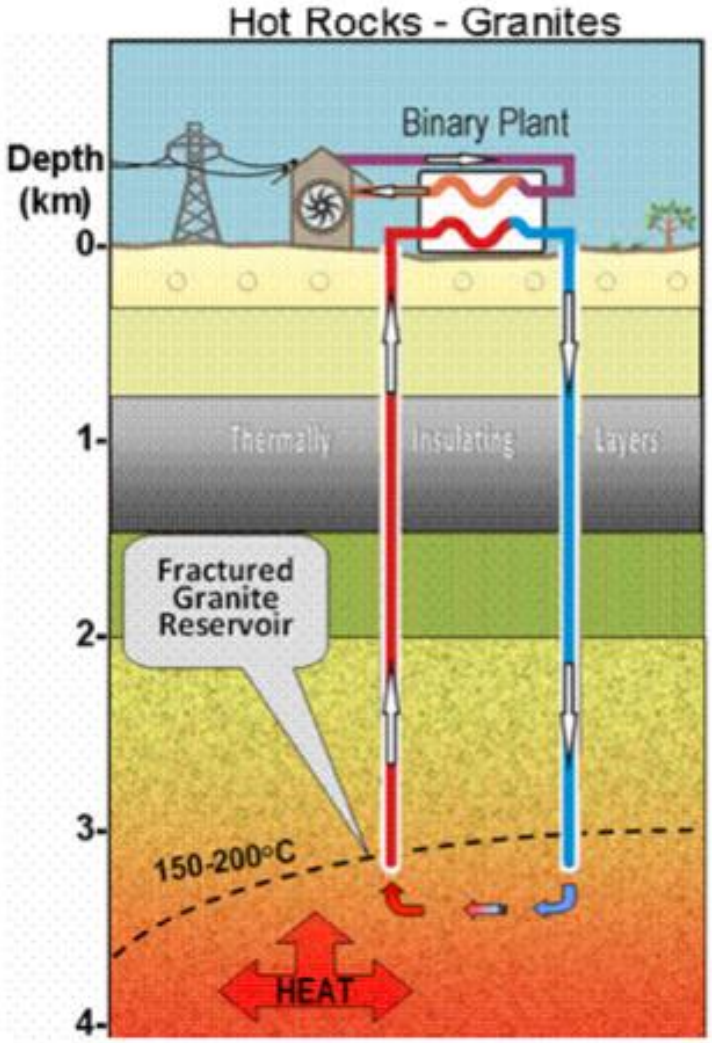

Figure 3.7 Schematic of an EGS development with an injection-production well pair and a power plant. The injection well (blue) is accompanied by a second (production) well (red) that is drilled to intersect the fractures generated by the injection well at a depth and appropriate lateral distance from the injection well. The distance allows the injected water to be sufficiently heated by the surrounding rock as it is circulated to the production well and pumped to the surface. Once at the surface the hot water can be flashed to steam or used to heat a secondary fluid that can be used in a binary cycle process. SOURCE: Courtesy of Clean Energy Australia Pty Ltd.

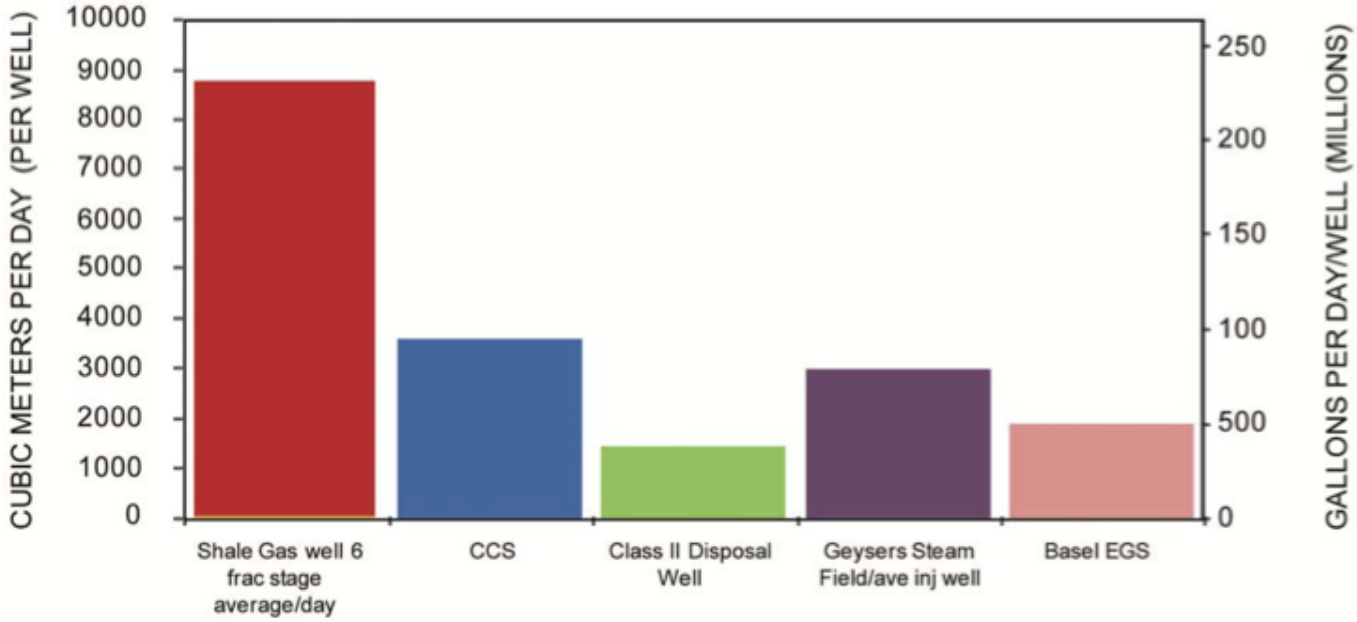
CUBIC METERS PER DAY (PER WELL)
10000
9000
8000
7000
6000
5000
4000
3000
2000
1000
0
250
200
150
100
500
0
GALLONS PER DAY/WELL (MILLIONS)
Shale Gas well 6 frac stage average/day
CCS
Class II Disposal Well
Geysers Steam Field/ave inj well
Basel EGS

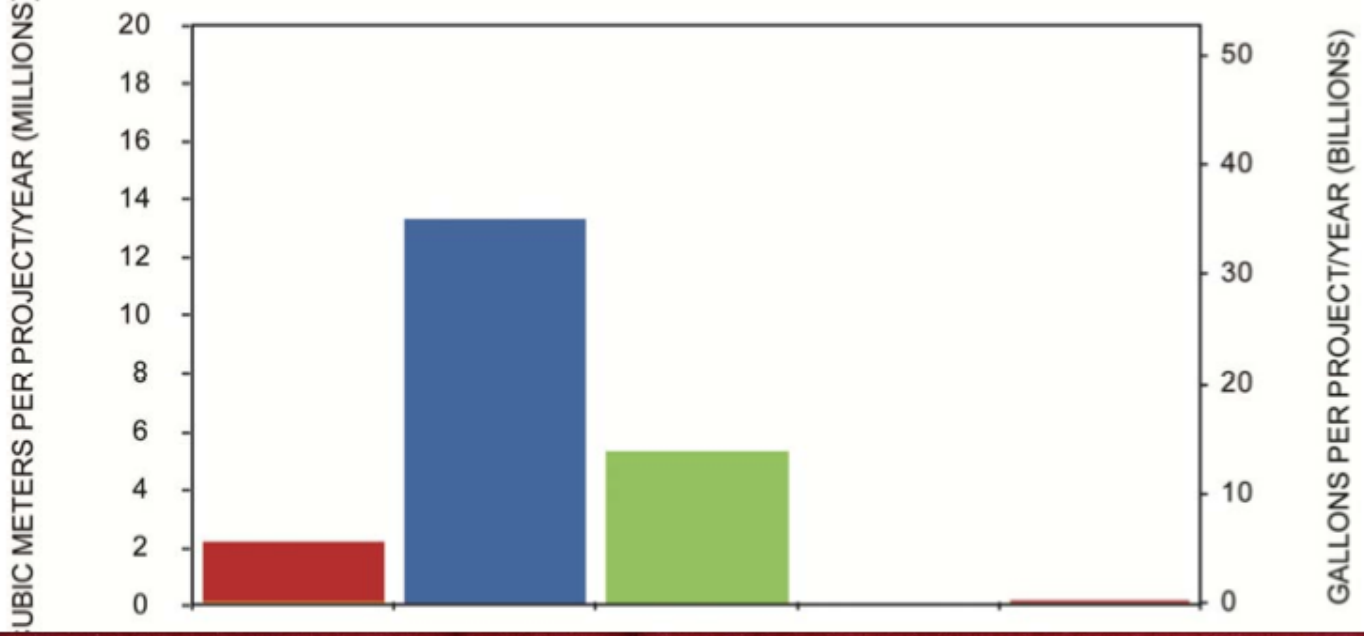
UBIC METERS PER PROJECT/YEAR (MILLIONS)
20
18
16
14
12
10
8
6
4
2
0
50
40
30
20
10
0
GALLONS PER PROJECT/YEAR (BILLIONS)

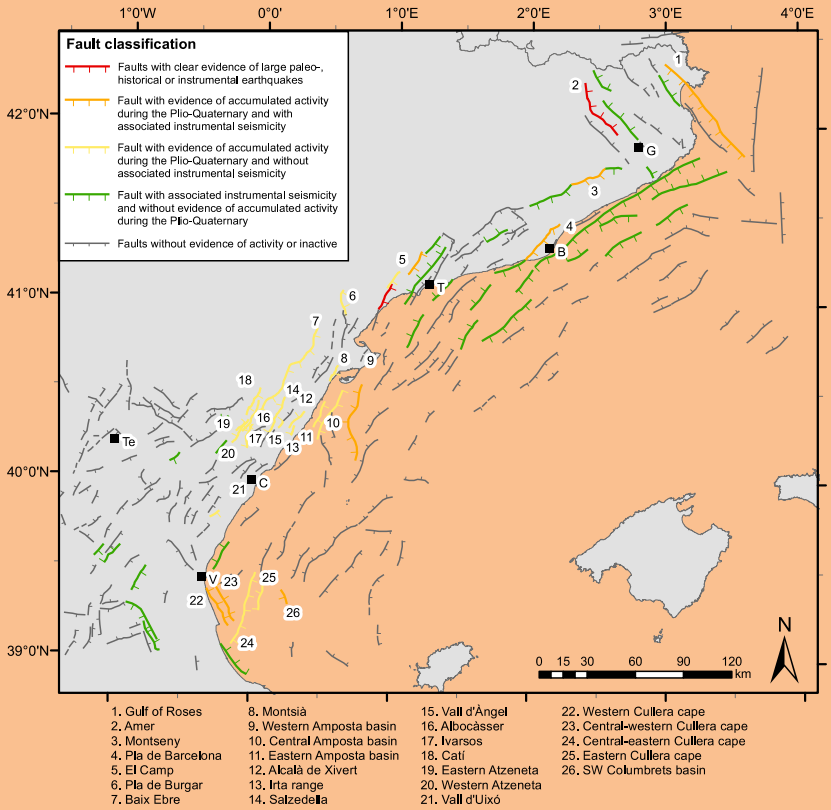

Fig. 8.- Map (modified from Perea *et al.*, 2006) showing the location of the faults corresponding to each of the different types of active faults (Fig. 7): a) faults with clear evidence of large paleo-, historic or instrumental earthquakes (red lines); b) faults with evidence of accumulated activity during the Plio-Quaternary and with associated instrumental seismicity (orange lines); c) faults with evidence of accumulated activity during the Plio-Quaternary and without associated instrumental seismicity (yellow lines); d) faults with associated instrumental seismicity and without evidence of accumulated activity during the Plio-Quaternary (green lines), and e) faults without evidence of activity or inactive faults (gray lines). B: Barcelona; C: Castelló; G: Girona; T: Tarragona; Te: Teruel; V: València. The seismic parameters of the numbered faults and their description are given in table 1 and in the text, respectably.

Fig. 8.- Mapa (modificado de Perea *et al.*, 2006) donde se muestra la localización de las fallas correspondientes a los distintos tipos de fallas activas (figura 7): a) fallas con claras evidencias de paleoterremotos o terremotos históricos o instrumentales (líneas rojas); b) fallas con evidencias de actividad acumulada durante el Plio-cuaternario y con asociación de terremotos instrumentales (líneas naranjas); c) fallas con evidencias de actividad acumulada durante el Plio-cuaternario y sin asociación de terremotos instrumentales (líneas amarillas); d) fallas con asociación de terremotos instrumentales y sin evidencias de actividad acumulada durante el Plio-cuaternario (líneas verdes); y e) fallas sin evidencias de actividad o inactivas (líneas grises). B: Barcelona; C: Castellón; G: Gerona; T: Tarragona; Te: Teruel; V: Valencia. Los parámetros sísmicos de las fallas y su descripción se encuentran en la tabla 1 y en el texto respectivamente..

3.3. Evaluation of the seismic parameters of active faults

In order to include the active faults in time dependent seismic hazard studies, it is necessary to have knowledge of the parameters that describe the seismic cycle of each fault in addition to information about geometry and kinematics. These parameters give us an idea of how tectonic stress is accumulated and released, i.e. the size and frequency of the seismic events. As a simplification, it is generally assumed that large earthquakes produced by

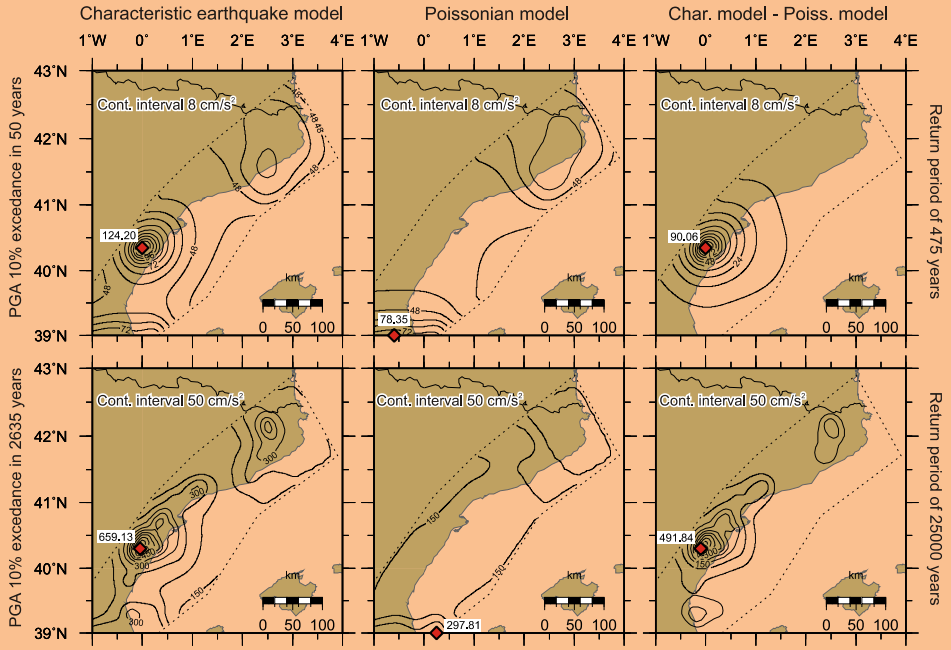

Fig. 10. Maps showing the PGA distribution (modified from Perea, 2006 and Perea and Atakan, 2007) corresponding to a model considering faults as time dependent sources (characteristic earthquake model column), a model without considering faults (poissonian model column) and the difference between both models (third column) for 10% of probability of exceedance in 50 (upper row) and 2634 (lower row) years (corresponding to return periods of 475 and 25000 years respectively). The map corresponding to the difference shows the variations of PGA when faults are introduced into the hazard computations as time dependent sources. Note the variations obtained when faults are used. Diamonds indicate the location of the highest PGA and the corresponding number indicates its value. The contour interval is indicated in each map. The dotted line bounds the study zone.

Fig. 10.- Mapa que muestra la distribución del PGA (aceleración pico del terreno) (modificado de Perea, 2006 y Perea y Atakan, 2007) correspondiente a un modelo que considera las fallas como fuentes dependientes del tiempo (columna del modelo de terremoto característico), a un modelo sin considerar las fallas (columna del modelo poisoniano) y a la diferencia entre ambos modelos (tercera columna), para un 10% de probabilidad de excedencia en 50 (fila superior) y en 2634 (columna inferior) años (correspondientes a periodos de retorno de 475 y 25000 años, respectivamente). El mapa correspondiente a la diferencia muestra la variación del PGA causadas por la introducción de las fallas como fuentes dependientes del tiempo en los cálculos de la peligrosidad. Nótese las variaciones que se obtienen cuando se utilizan las fallas. Los diamantes indican la localización de los mayores PGA y el número correspondiente indica su valor. El intervalo entre las isolíneas se indica en cada mapa. La línea de puntos limita la zona de estudio.

lumbrets basin is situated to the NE of the Cullera Cape. Towards the south of the basin, the seismic reflection profile SSP-7 (seismic survey SSP conducted by WESTERN in 1974; in Roca, 1992) shows some faults that displace the base of the Plio-Quaternary unit and one of them offsets reflectors close to the surface, suggesting that it is currently active. This fault trends NW-SE, dips to the NE and is 10 km long. It offsets the base of the Plio-Quaternary unit 0.07 s TWTT, which corresponds to 55 m, assuming that 1500 m/s is the propagation speed of the seismic waves. Thus, the slip rate of the fault varies between 0.01 and 0.03 mm/year (Perea, 2006). In addition, this fault accounts for some of the instrumental seismicity in the vicinity.

4. Final remarks

Studies in active tectonics and paleoseismology have helped us to improve our understanding of the active faults in the northwestern margin of the València trough. This has resulted in the mapping of the active faults and has enabled us to calculate the parameters that describe

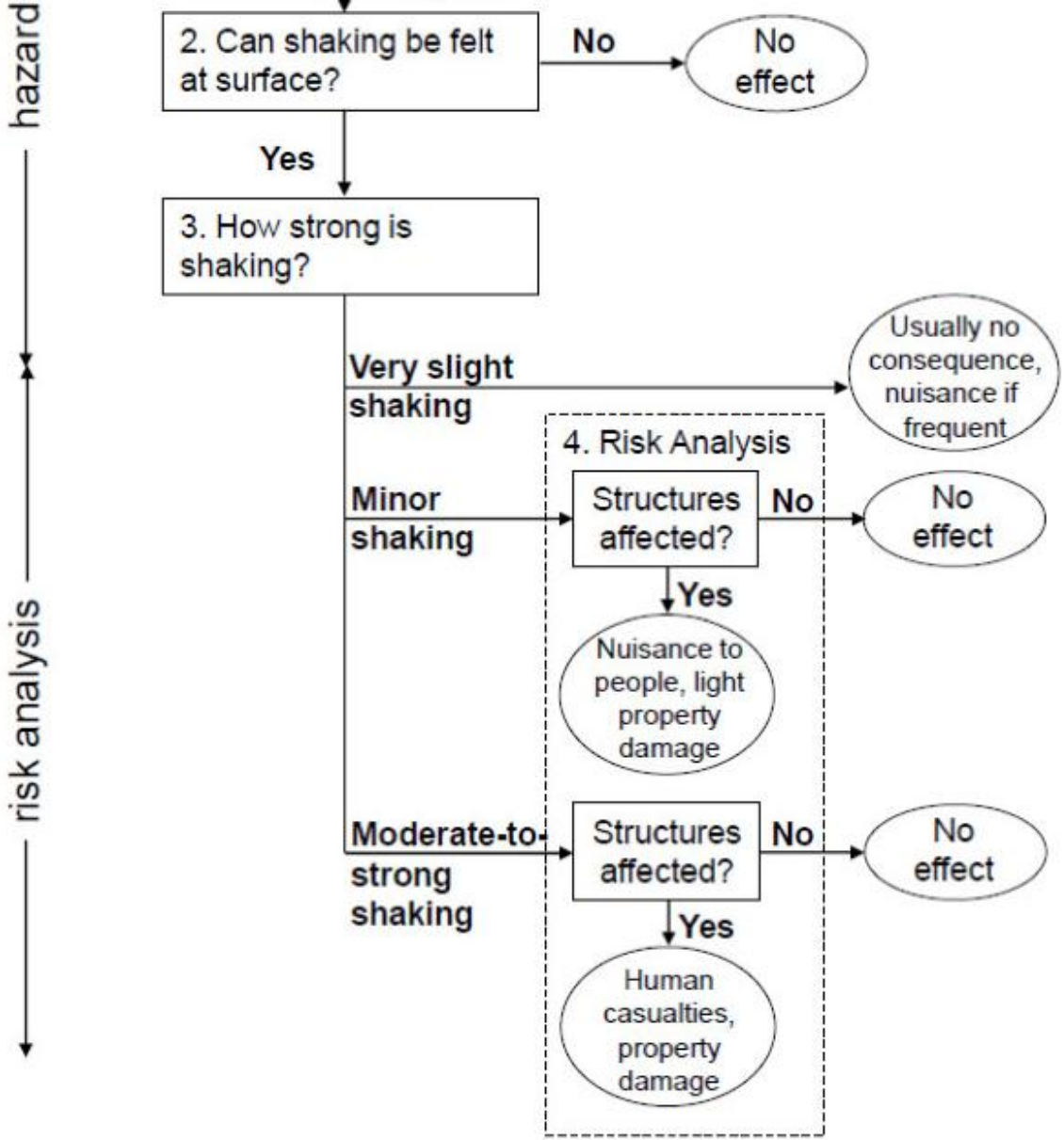

Figure 5.1 Evaluations needed for hazard analysis and risk analysis associated with induced seismicity for one well.

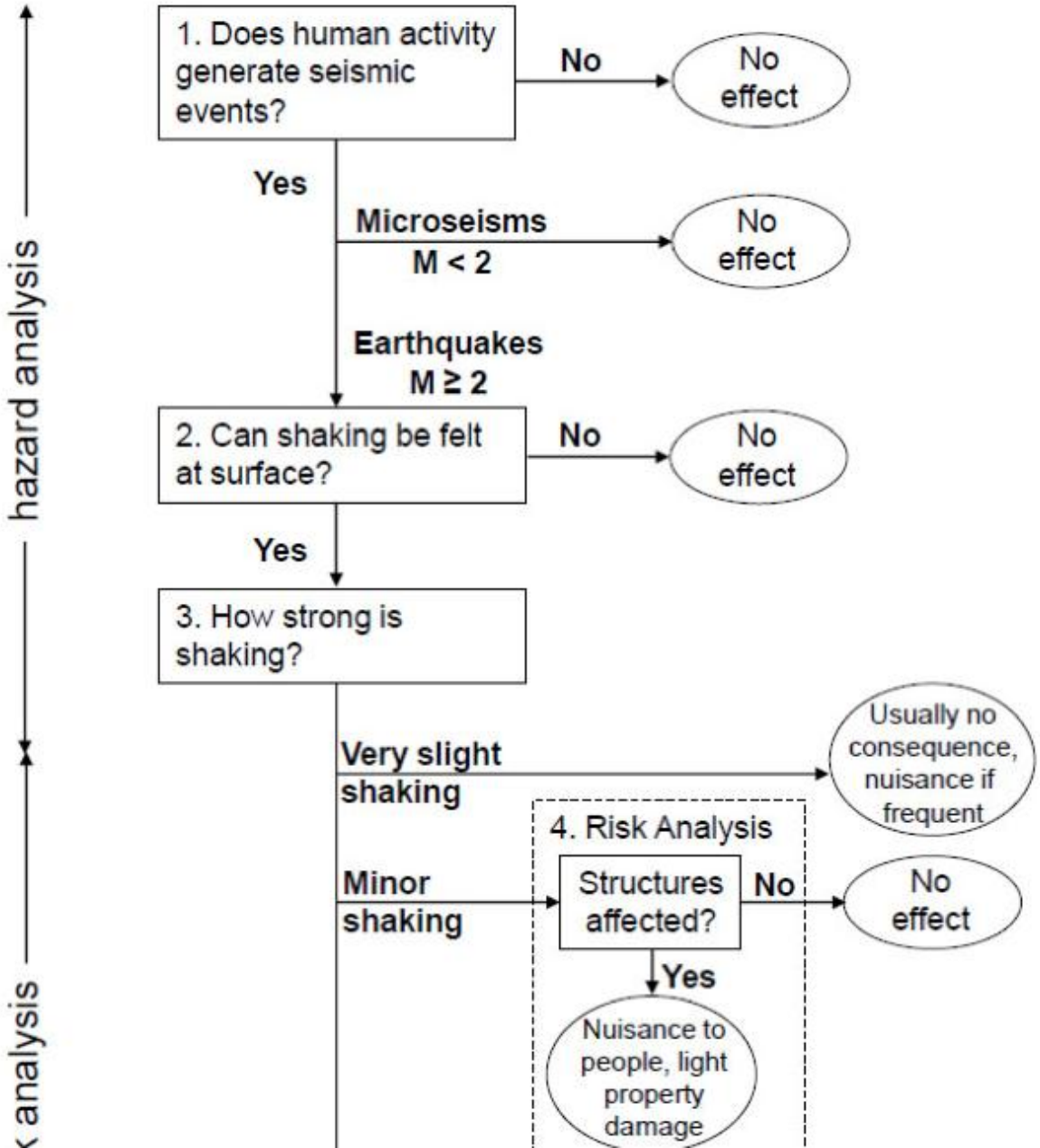
hazard analysis
risk analysis
1. Does human activity generate seismic events?
No
No effect
Yes
Microseisms
M < 2
No effect
Earthquakes
M ≥ 2
2. Can shaking be felt at surface?
No
No effect
Yes
3. How strong is shaking?
Very slight shaking
Usually no consequence, nuisance if frequent
4. Risk Analysis
Minor shaking
Structures affected?
No
No effect
Yes
Nuisance to people, light property damage

Science 9 April 2010:
Vol. 328 no. 5975 pp. 181–182
DOI: 10.1126/science.1189197

PERSPECTIVE

GEOPHYSICS

Central Chile Finally Breaks

Raul Madariaga[1], Marianne Métois[1], Christophe Vigny[1] and Jaime Campos[2]

+ Author Affiliations

E-mail: madariag@geologie.ens.fr

Chile is the site of some of the largest earthquakes in the world: On average, a magnitude 8 earthquake occurs there every 10 years or so. These earthquakes take place in the subduction zone, either as interplate ruptures at the interface between the South American and Nazca plates or as intraplate events within the subducted Nazca plate. A few times in every century, massive plate-interface earthquakes break several hundred kilometers in a single shock. This is what happened on 27 February 2010, when a major earthquake (magnitude 8.8) occurred in the Maule and Biobío regions in central Chile (see the first figure). This region had last experienced a major subduction earthquake in 1835, when Darwin (*1*) visited the area as part of his voyage on the Beagle. His description of the earthquake inspired many seismologists and historians of Chilean earthquakes (*2*, *3*).

Read the Full Text

Miercoles, 02 de abril de 2014 | 11:19 pm

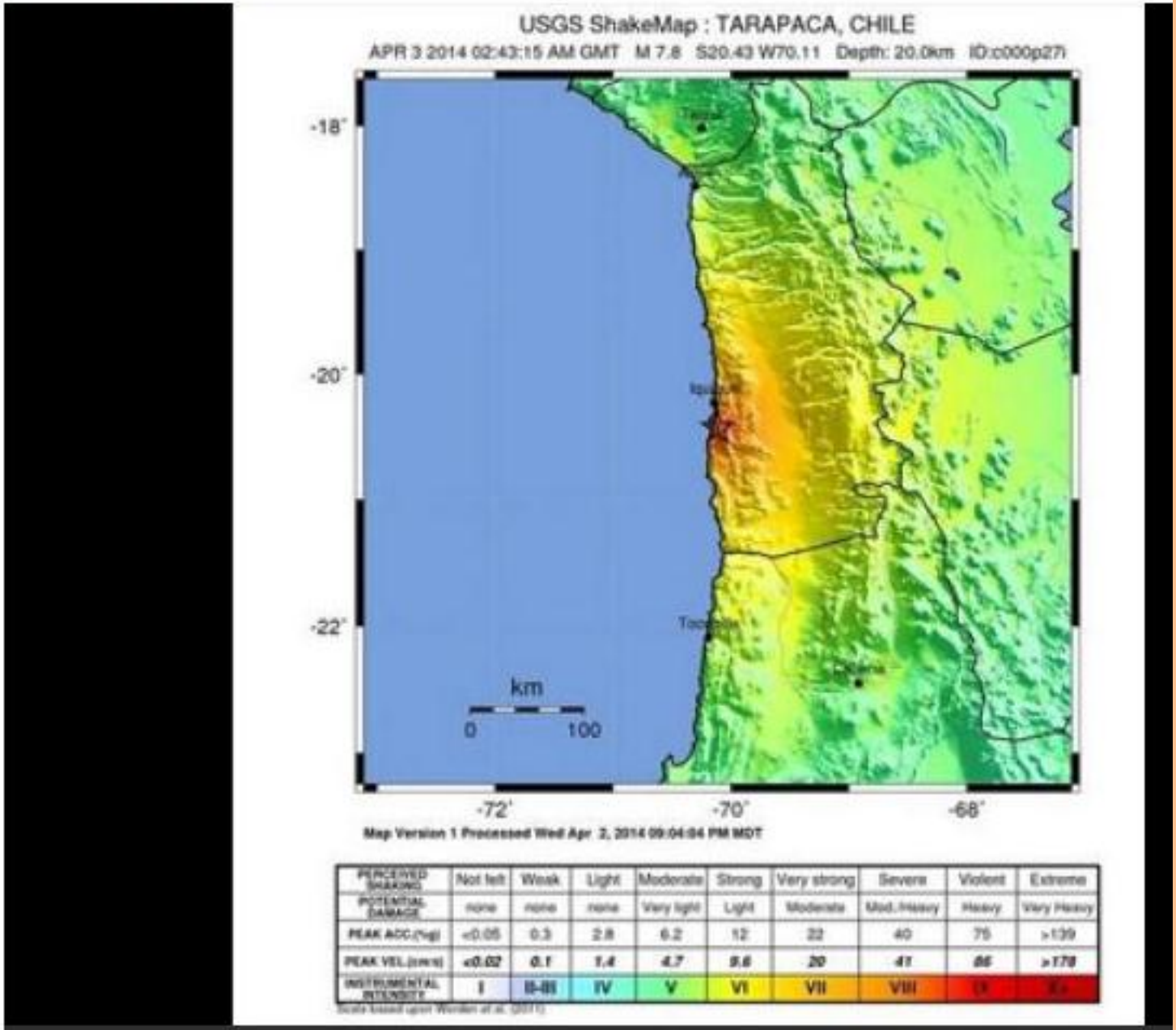

Terremoto en Chile: se eleva a seis cifra de muerto. (Fotos: EFE/Reuters)

Sismologie à Normal sup'

The 27/02/2010 Mw 8.8 Maule earthquake

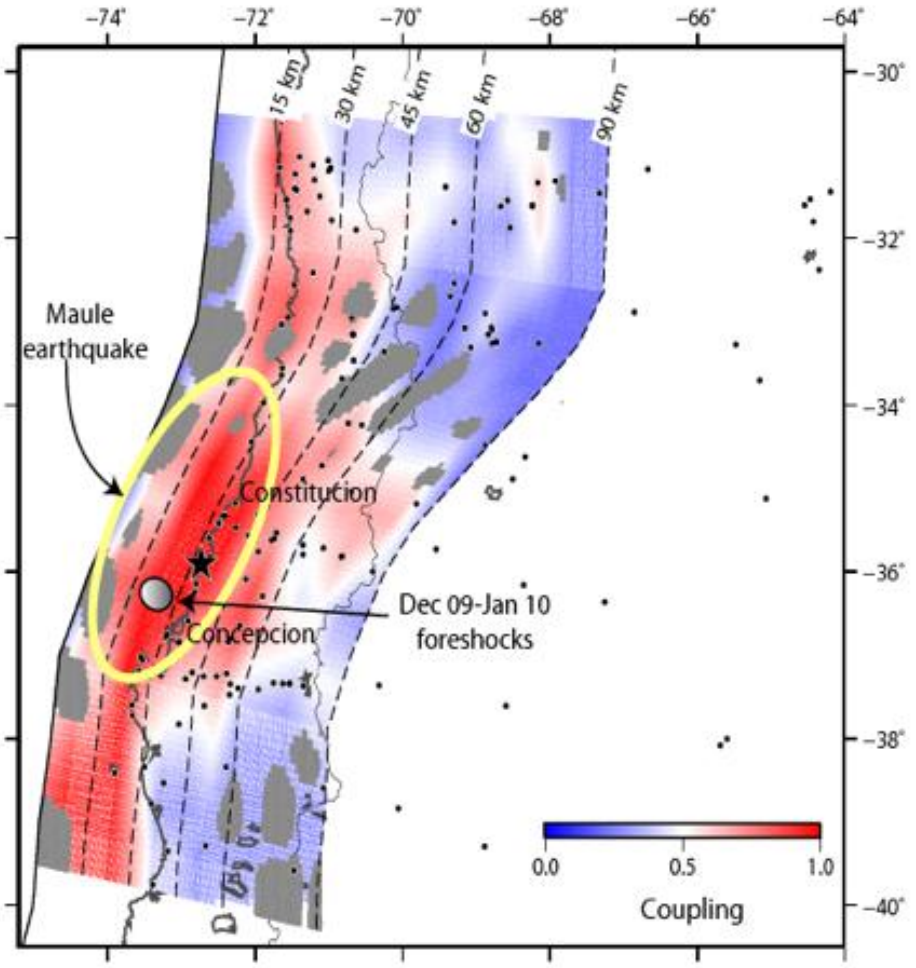

DISCUSSION

Geothermal, enhanced geothermal, oil and gas, unconventional oil and gas, and CCS technologies all involve fluid withdrawal and/or injection thereby providing the potential to induce seismic events. The rates, volumes, pressure, and duration of the injection varies with the technology as do the potential sizes of the earthquakes, the mechanisms to which the earthquakes are attributed (Table 3.4), and the possible risk and hazards of the induced events.

Induced seismicity is commonly characterized by large numbers of small earthquakes that persist during, and in some cases significantly after, fluid injection or removal. At several sites of seismicity caused by or likely related to energy technologies, calculations based on the measured injection pressure and the measured or the inferred state of stress in the Earth's crust suggest that the theoretical threshold for frictional sliding along favorably oriented preexisting fractures was exceeded (see also Chapter 2).

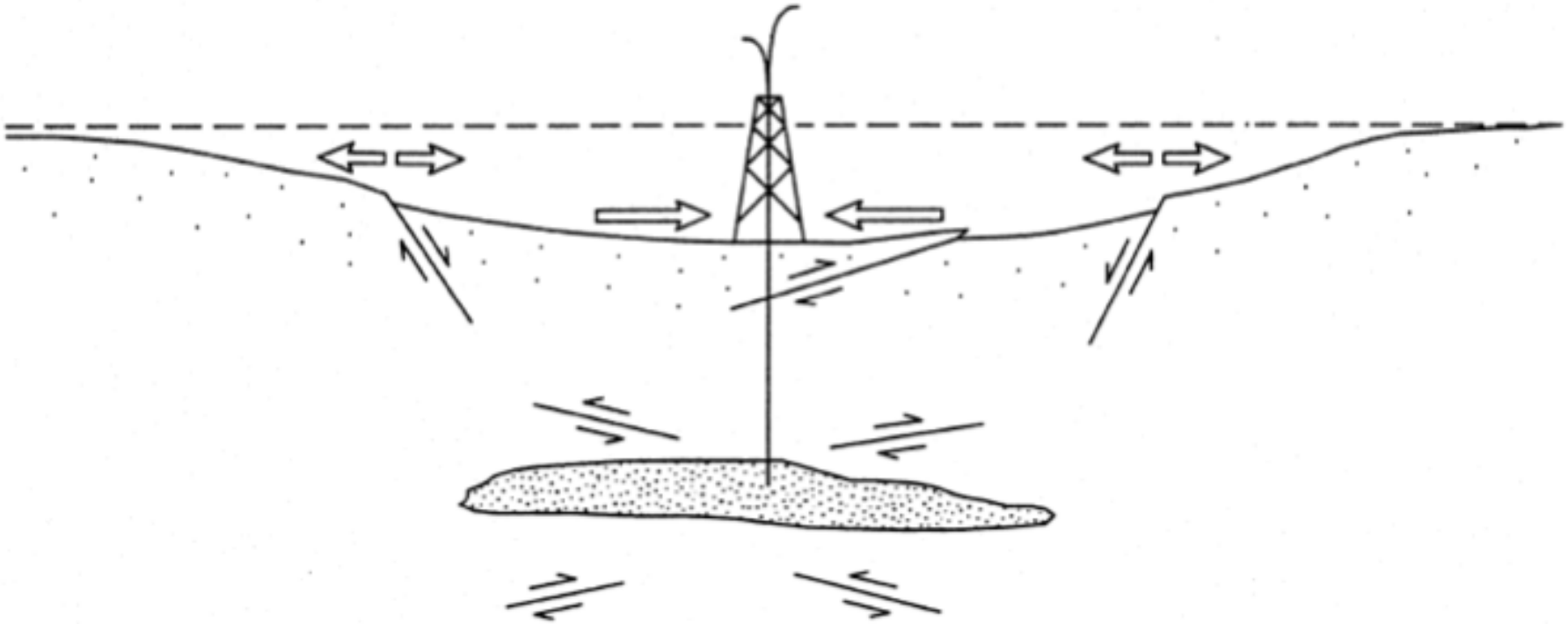

Figure 2.2 Observed faulting suggested to be associated with fluid withdrawal. Open arrows denote horizontal strain. In this interpretation, normal faults develop on the flanks of a field when the oil reservoir is located in a region of crustal extension. Reverse faults may develop above and below the reservoir if the reservoir is located in a region undergoing compression. Adapted after Segall (1989).

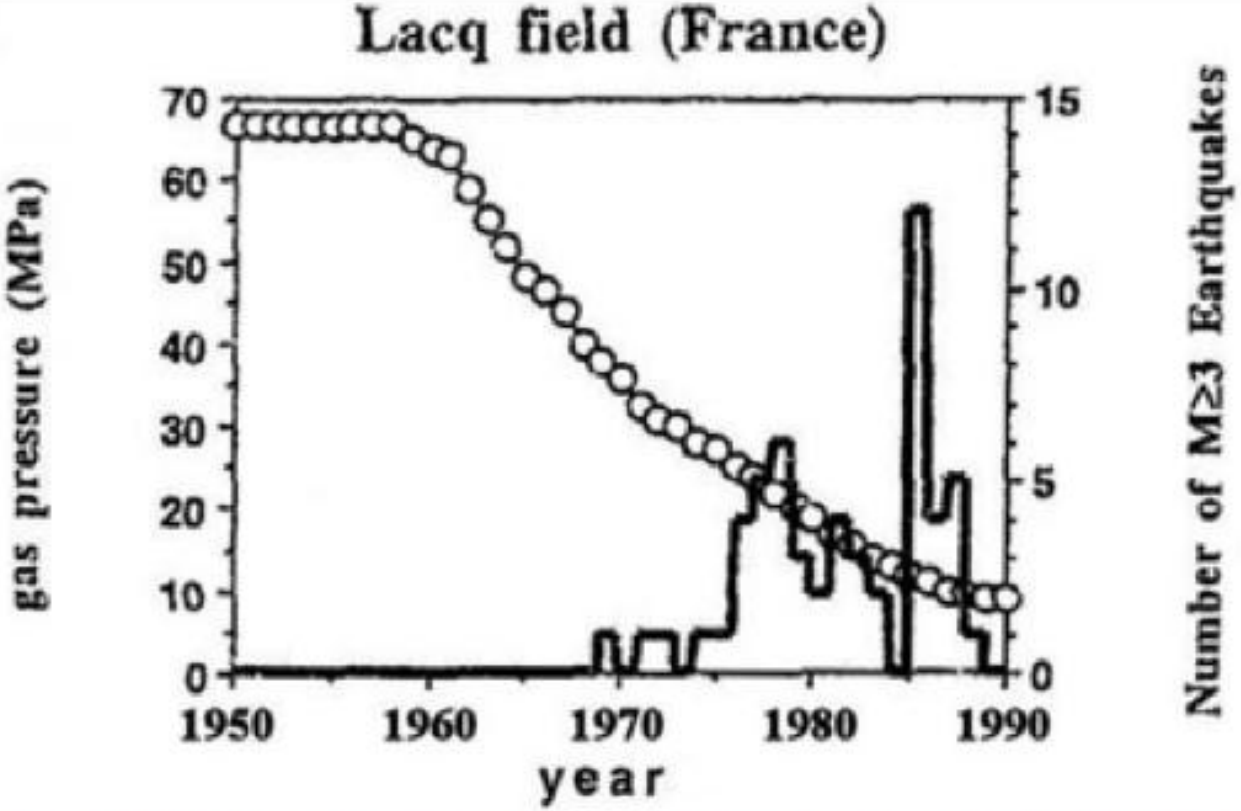

Figure 2 Decline of the pore pressure due to production at the Lacq gas reservoir and number of recorded earthquakes with magnitude **M** ≥ 3, with time Gas pressure (in MPa; 1 MPa is equal to 10 bars) (circles, left scale) and number of **M**>3 earthquakes per year (solid line, right scale). The number of earthquakes increased with decreasing pressure. SOURCE: Segall (1989).

SOURCES: Segall (1989), Segall et al. (1994), Segall and Fitzgerald (1998), Grasso and Wittlinger (1990), Grasso (1992)

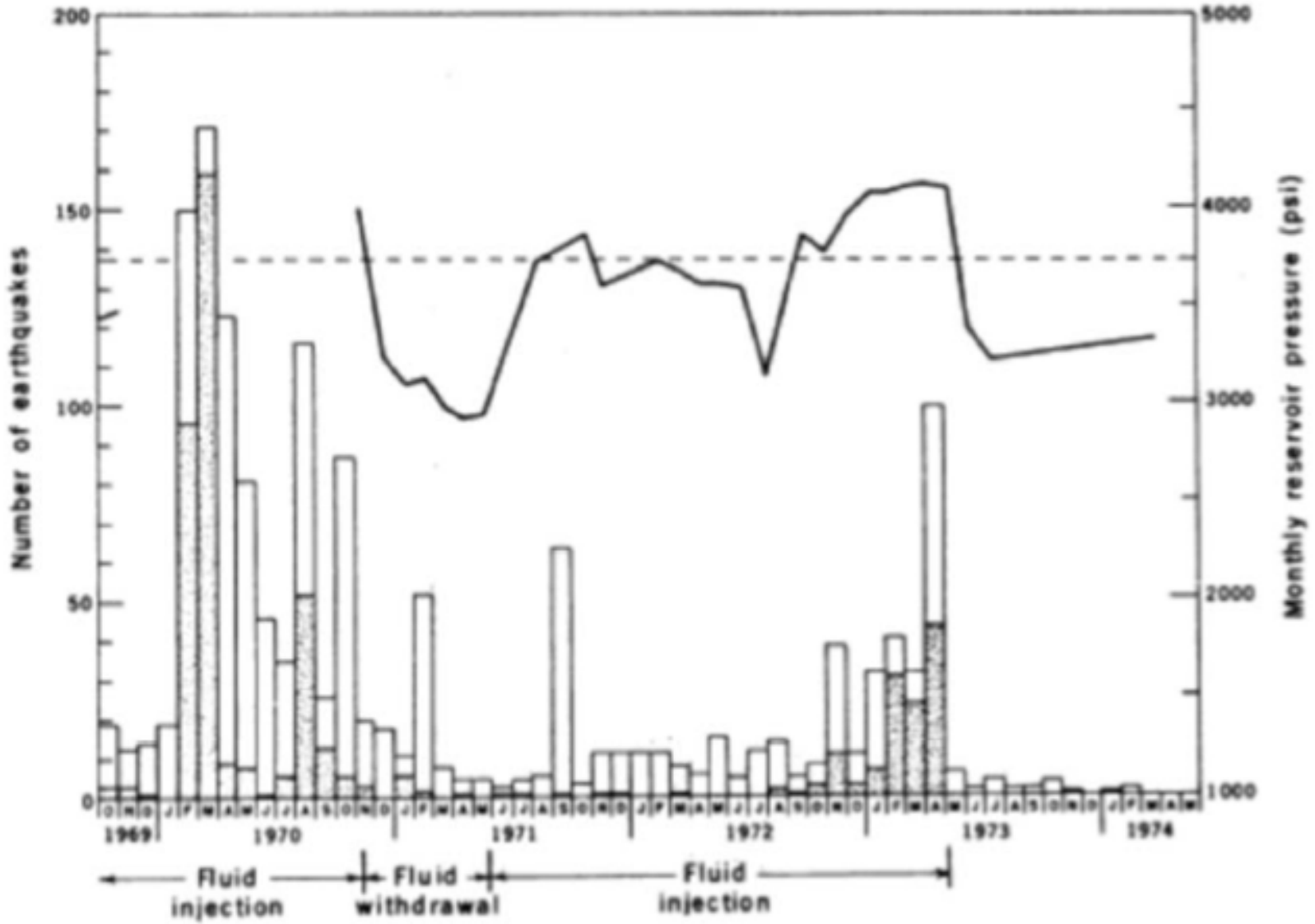

Figure 2 Frequency of seismic events at Rangely. Stippled bars are seismic events within 1 kilometer of the experimental wells. The clear bars represent all other events. Pressure history in well Fee 69 is shown by the heavy line and predicted critical pressure is designated by the dashed line. SOURCE: Raleigh et al. (1976).

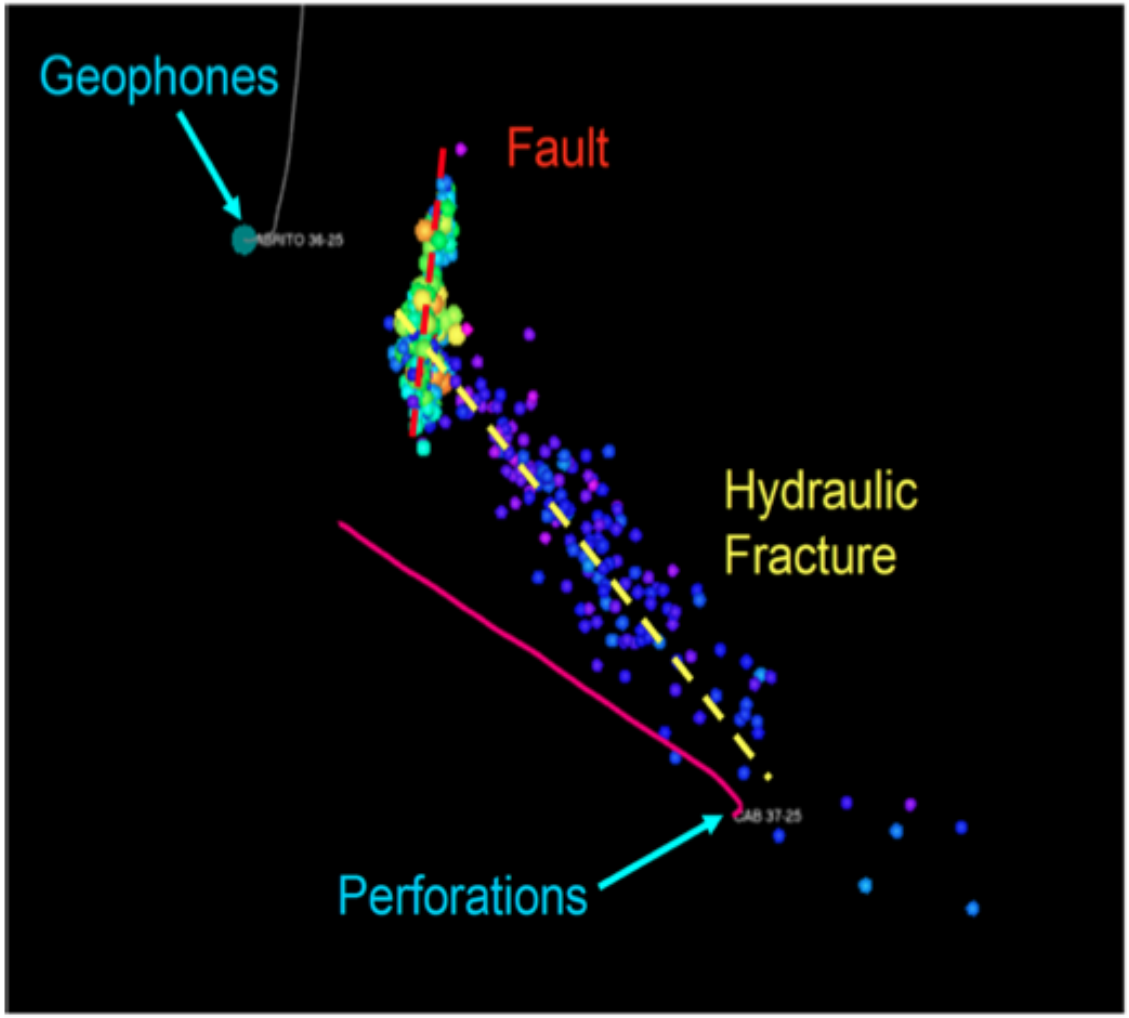

Figure E.2 Example of a reactivated fault during hydraulic fracturing. The figure is map view of a microseismicity (colored spheres which are colored and by magnitude, cool colors are small events) during a hydraulic fracture treatment. The fracturing well is shown by the pink line and is deviated away from a central well head location and extends vertically through the reservoir section, the injection location is labeled 'perforations'. The data was recorded and analyzed using borehole receivers (marked Geophones). The blue dots show the growth of the hydraulic fracture to the NW, then intersecting and reactivating a small fault in the reservoir, shown by change in fracture orientation and larger magnitude events (yellow dots). SOURCE: From Maxwell et al. (2008).

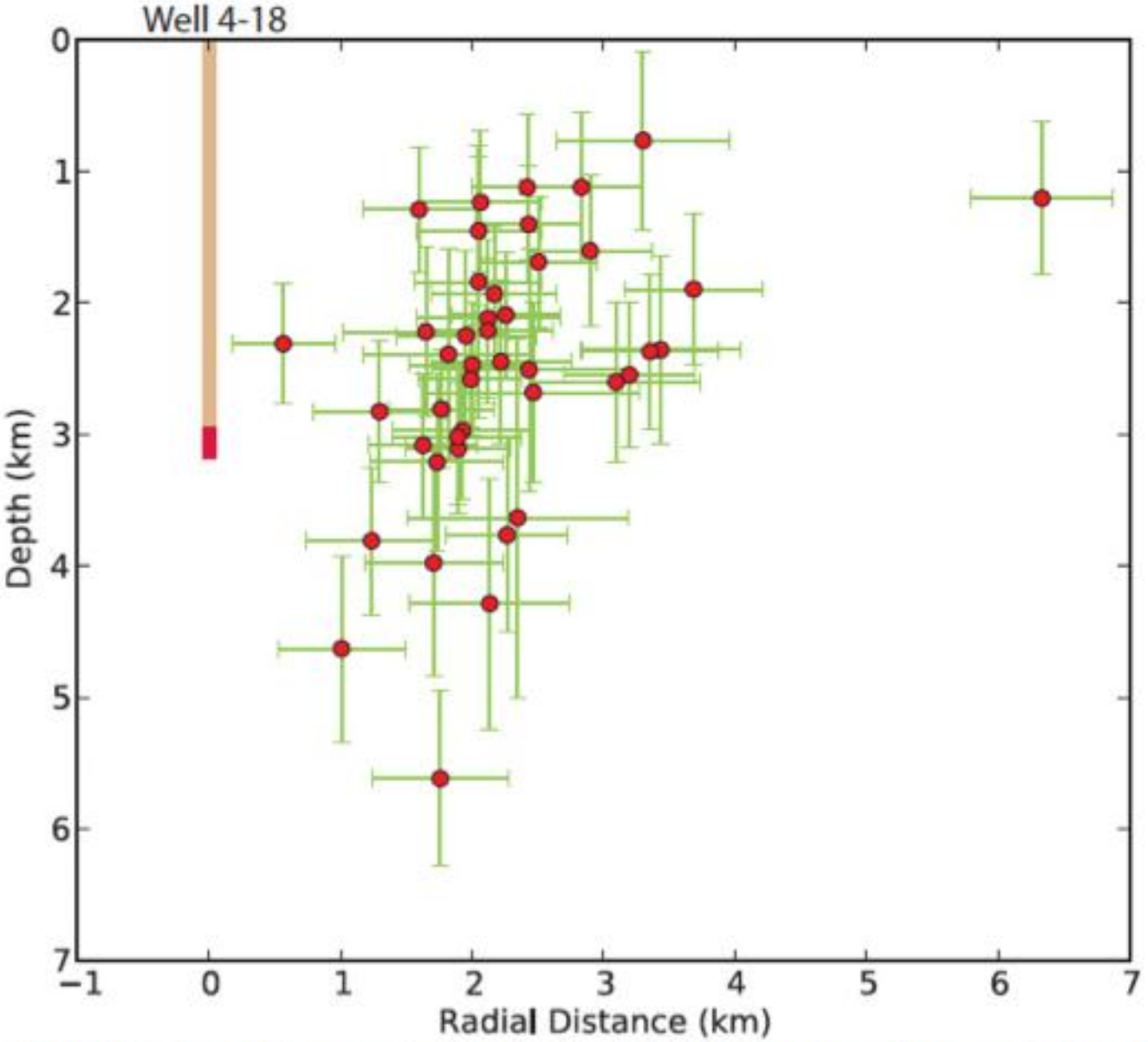

Figure J.3 Depth distribution of hypocenters and uncertainty estimates with respect to the fracture well 4.18. SOURCE: Holland (2011).

CONCLUDING REMARKS

Human activity, including injection and extraction of fluids from the Earth, can induce seismic events. While the vast majority of these events have intensities below that which can be felt by people living directly at the site of fluid injection or extraction, there is potential to produce significant seismic events that can be felt and cause damage and public concern. Examination of known examples of induced seismicity can aid in determining what the risks are for energy technologies. These examples also provide data on the types of research required to better constrain induced seismicity risks and to develop options for best practices to define and alleviate risks from energy-related induced seismicity. These issues are explored in the remaining chapters of this report.

DOI: 10.1126/science.1189197

- Perspective

Geophysics

Central Chile Finally Breaks

1. Raul Madariaga1,
2. Marianne Métois1,
3. Christophe Vigny1 and
4. Jaime Campos2

+ Author Affiliations

1. [1]*Laboratoire de Géologie et LIA Montessus de Ballore, CNRS and Ecole Normale Supérieure, 75231 Paris Cedex 05, France.*
2. [2]*LIA Montessus de Ballore, Departamento de Geofisica, FCFM, Universidad de Chile, Santiago, Chile.*

1. E-mail: madariag@geologie.ens.fr

Summary

Chile is the site of some of the largest earthquakes in the world: On average, a magnitude 8 earthquake occurs there every 10 years or so. These earthquakes take place in the subduction zone, either as interplate ruptures at the interface between the South American and Nazca plates or as intraplate events within the subducted Nazca plate. A few times in every century, massive plate-interface earthquakes break several hundred kilometers in a single shock. This is what happened on 27 February 2010, when a major earthquake (magnitude 8.8) occurred in the Maule and Biobío regions in central Chile (see the first figure). This region had last experienced a major subduction earthquake in 1835, when Darwin (*1*) visited the area as part of his voyage on the Beagle. His description of the earthquake inspired many seismologists and historians of Chilean earthquakes (*2*, *3*).

Read the Full Text

Observations of Induced Seismicity

Site/City/State	Country	Max Magnitude	Technology type (causing induced seismicity)	Reference
Akmaar	Netherlands	3.5	Oil and gas extraction	Giardini (2011)
Akosombo	Ghana	5.3	Surface water reservoir	Guha (2000)
Apollo Hendrick Field, Texas	USA	2	Secondary recovery	Doser et al. (1992)
Ashtabula, Ohio	USA	3.6	Waste water injection	Armbruster et al. (1987)
Assen	Netherlands	2.8	Oil and gas extraction	Grasso (1992)
Aswan	Egypt	5.6	Surface water reservoir	Guha (2000)
Attica, New York	USA	5.2	Other	Nicholson and Wesson (1992)
Bad Urach	Germany	1.8	Geothermal	Evans et al. (2012)
Bajina Basta	Yugoslavia	4.8	Surface water reservoir	Guha (2000)
Barsa-Gelmes-Wishka Oilfield	Turkmenistan	6	Secondary recovery	Kouznetsov et al. (1994)
Basel	Switzerland	3.4	Geothermal	Giardini (2011)
Belchalow	Poland	4.6	Other	Giardini (2011)
Benmore	New Zealand	5	Surface water reservoir	Guha (2000)
Bergermeer Field	Netherlands	3.5	Oil and gas extraction	van Eck et al. (2006)
Berlin	El Salvador	4.4	Geothermal	Bommer et al. (2006)
Bhatsa	India	4.8	Surface water reservoir	Guha (2000)
Blackpool	UK	2.3	Hydraulic fracturing	de Pater and Baisch (2011)
Cajuru, Brazil	Brazil	4.7	Surface water reservoir	Guha (2000)
Camarillas, Spain	Spain	4.1	Surface water reservoir	Guha (2000)
Canelles, Spain	Spain	4.7	Surface water reservoir	Guha (2000)
Catoosa, Oklahoma[1]	USA	4.7	Oil and gas extraction	Nicholson and Wesson (1992)
Cesano	Italy	2	Geothermal	Evans et al. (2012)
Charvak	Uzbekistan	4	Surface water reservoir	Guha (2000)
Clark Hill	USA	4.3	Surface water reservoir	Guha (2000)

Ramon Carbonell [ramon.carbonell@gmail.com] de part de Ramo...

Accions

Per a: PEDRO BUSQUETS BUEZO; Pere Busquets [pere.busquets@ub.es]

dimarts, 1 / abril / 2014 11:26

- Has contestat el 01/04/2014 16:52.

Sobre el que hem parlat

INSAR

http://volcanoes.usgs.gov/activity/methods/insar/
http://www.sciencemag.org/content/328/5975/181.summary

Ramon

--
Ramon Carbonell

Prof. of Research
Dept. Structure & Dynamics of the Earth
CSIC-Institut de Ciències de la Terra Jaume Almera
LLuís Solé i Sabarís s/n — Tel: +34934095410
08028 Barcelona, Spain. — Fax: +34934110012
http://www.ictja.csic.es/edt/ — Cell: +34660572489
eMails: ramon.carbonell@csic.es — ramon.carbonell@gmail.com

Table 5.1 Probability of Damage Increases with Number of Wells

Total number of wells (N)	$[P_M]_{N\ wells}$	Expected number of wells causing moderate+ damage
1	1%	0
5	5%	0
10	10%	0
100	63%	1
1000	99.9%	10

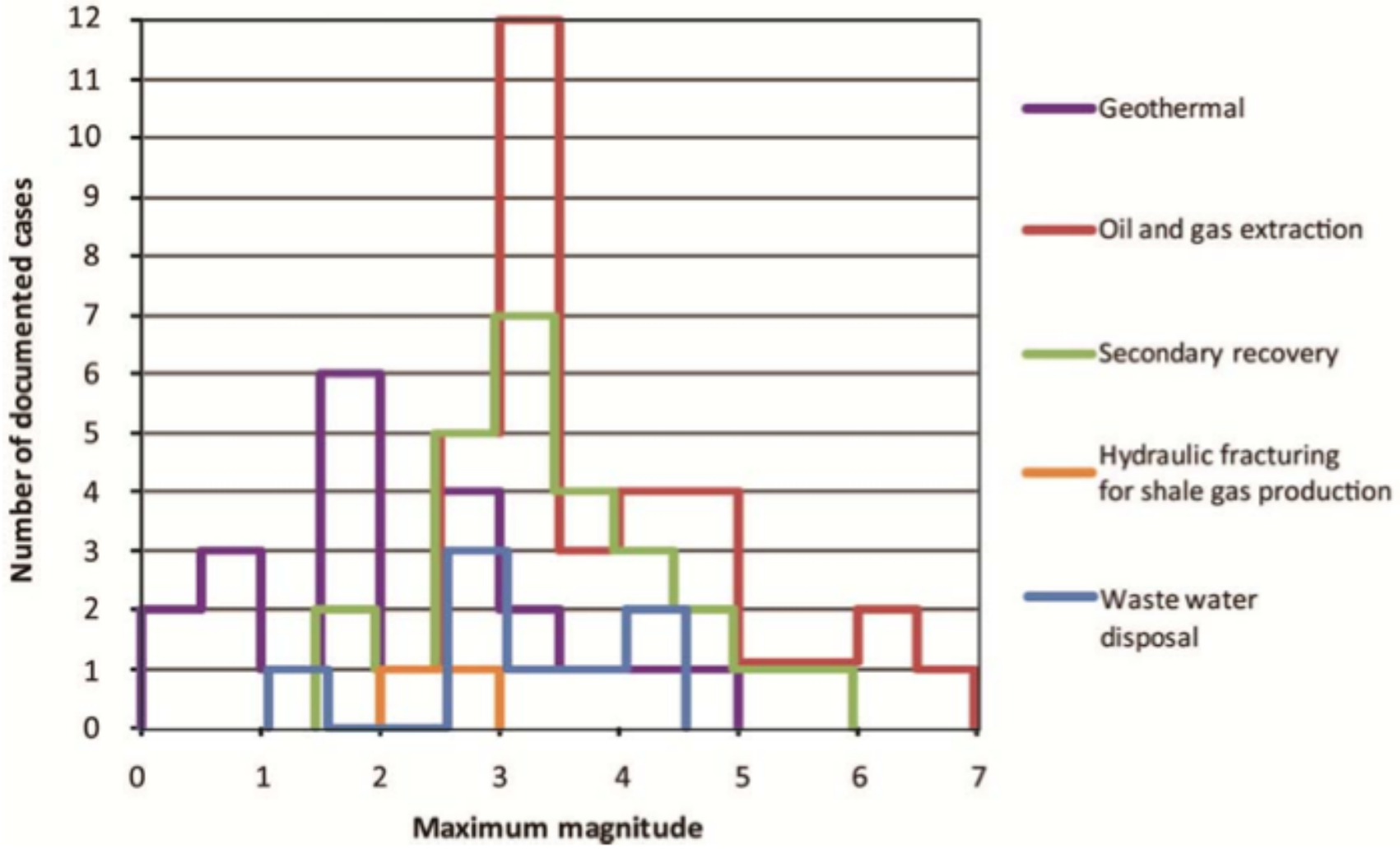

Figure 3.15 Histograms of maximum magnitudes documented in technical literature caused by or likely related to subsurface energy production globally. Note: Many gas and oil fields undergo extraction of hydrocarbons along with injection of water for secondary recovery, but if the reported total volume of extracted fluids exceeds that of injection, the site is categorized as extraction. Some cases of induced seismicity in the list above do not have reported magnitudes associated with earthquakes, and those cases are not included in the counts used to develop this figure. No induced seismic events have been recognized related to existing CCS projects. SOURCE: See Appendix C.

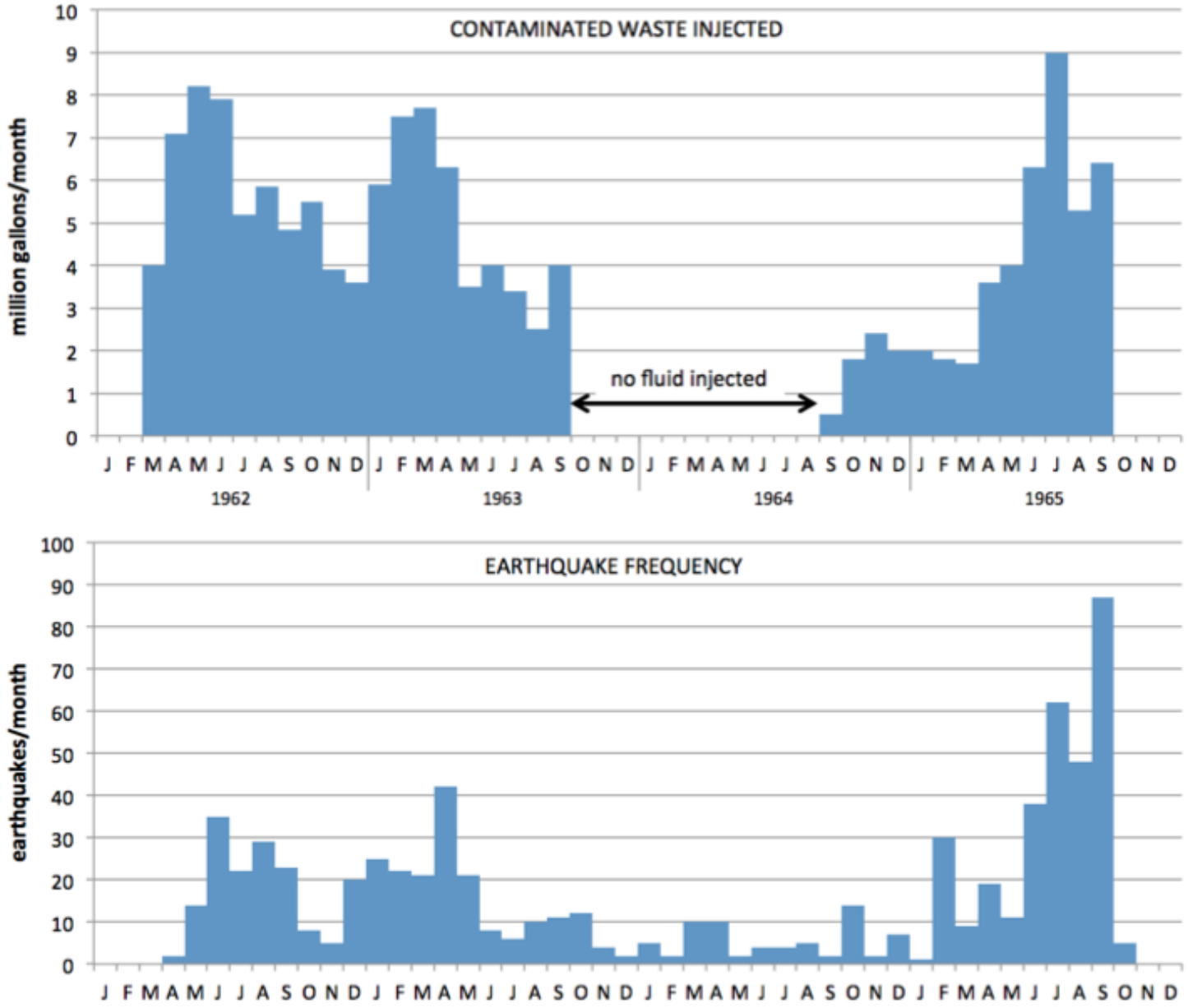

Figure Histograms showing relation between volume of waste injected into the Rocky Mountain Arsenal well and earthquake frequency. SOURCES: Adapted from Evans (1966); Healy et al. (1968); McClain (1970); Hsieh and Bredehoeft (1981).

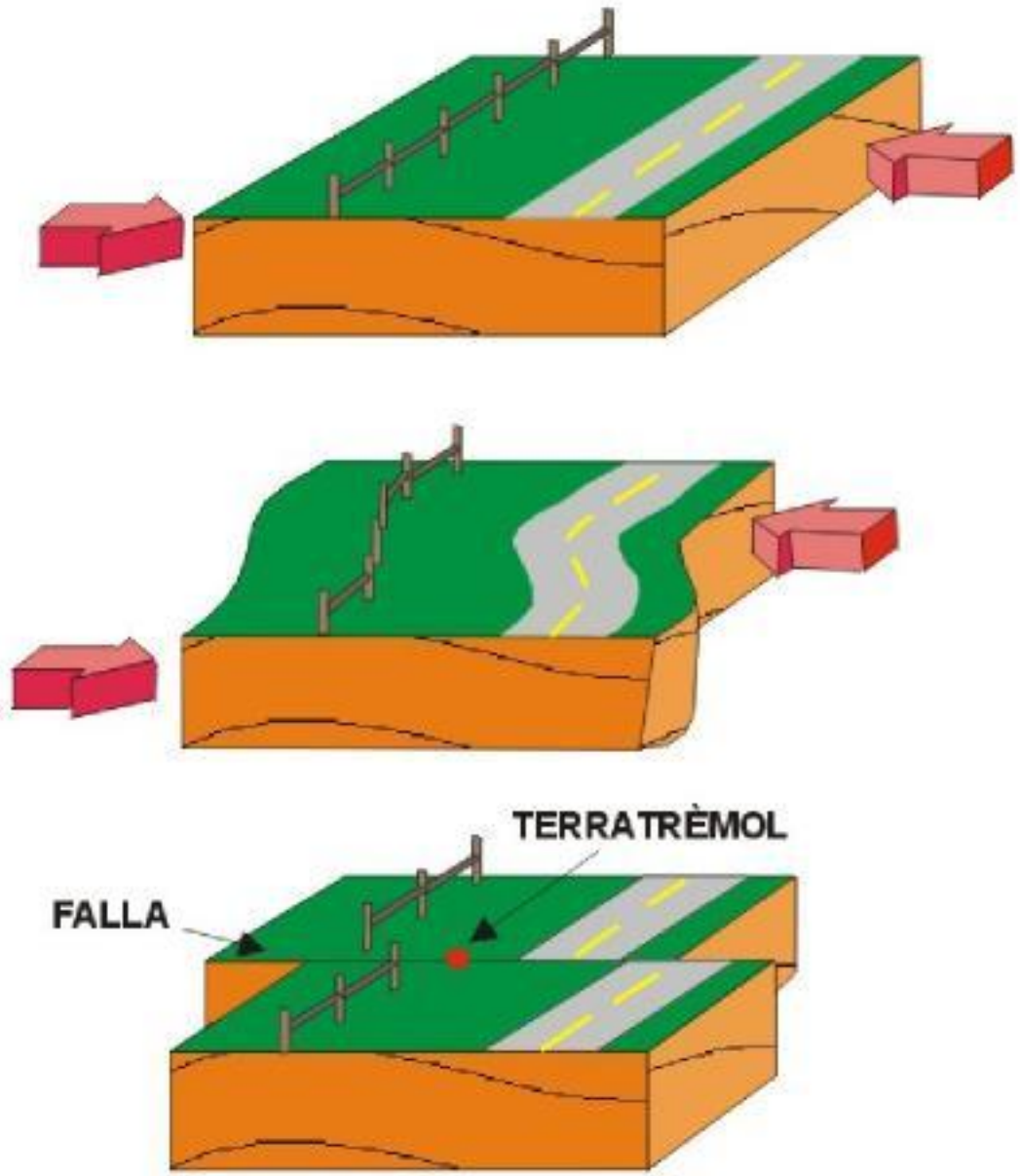
TERRATRÈMOL
FALLA

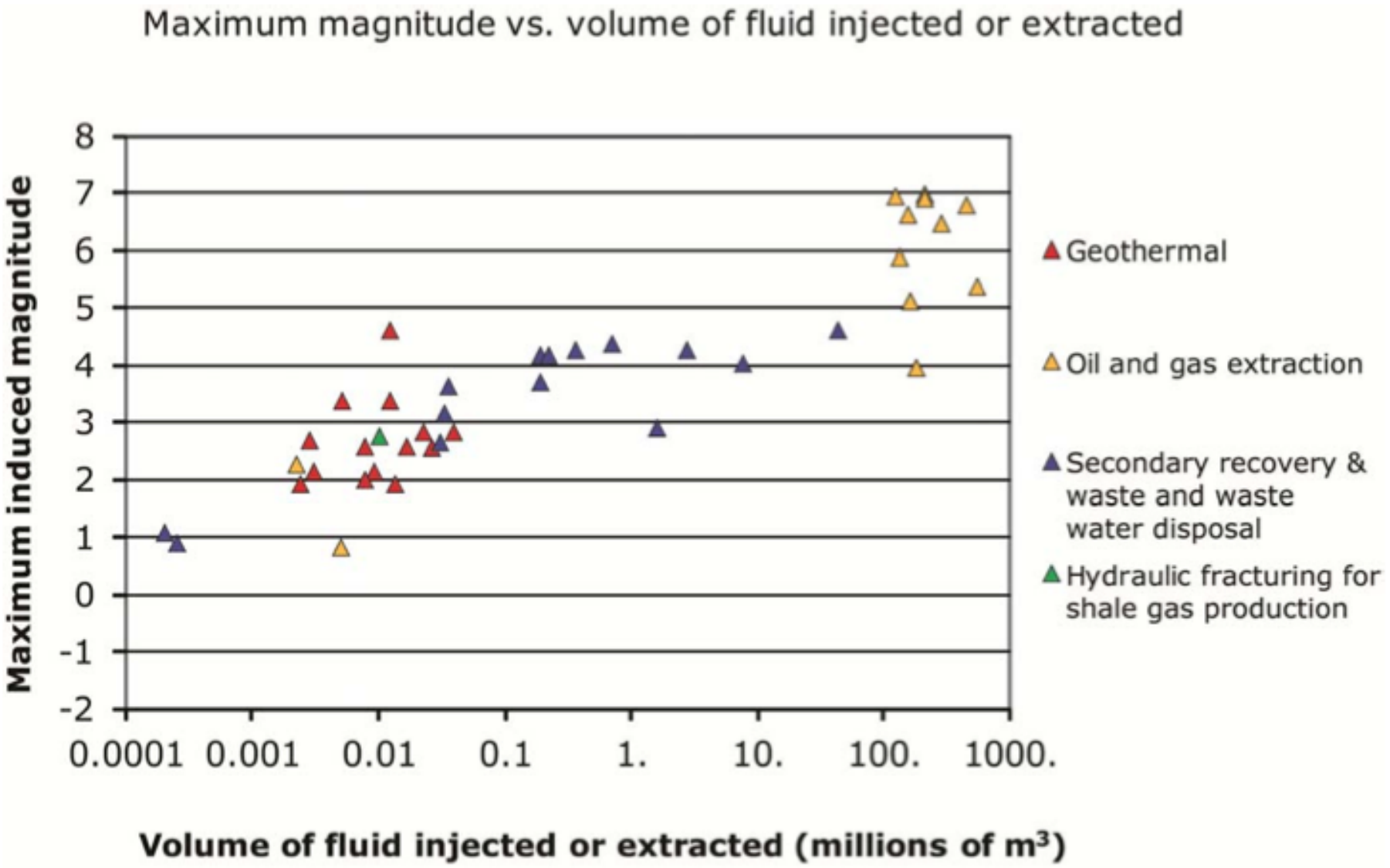
Maximum magnitude vs. volume of fluid injected or extracted
Maximum induced magnitude
8
7
6
5
4
3
2
1
0
-1
-2
0.0001
0.001
0.01
0.1
1.
10.
100.
1000.
Volume of fluid injected or extracted (millions of m³)
Geothermal
Oil and gas extraction
Secondary recovery & waste and waste water disposal
Hydraulic fracturing for shale gas production

Los tuneles del AVE en Pajares

- Los resultados obtenidos en este tra- bajo permiten plantear que el efecto dren, originado por la construcción de los Túneles de base de Pajares, ha causado el abati- miento general del nivel freático que afec- taría al endokarst de las calizas de Láncara y generaría con ello la aparición de estruc- turas de colapso en los sedimentos supra- yacentes poco tiempo después de perfo- rarse el túnel. El proceso sigue activo y se prevé que continúe progresando debido, entre otros factores, a la acción erosiva que ejerce el flujo superficial del arroyo al infil- trarse hacia su nuevo nivel de base.

Ejemplo: Explotación geotérmica de Olkaria, Kenia.

Avance de la nube de micro-eventos con el tiempo en el entorno de un sondeo hidráulico de inyección

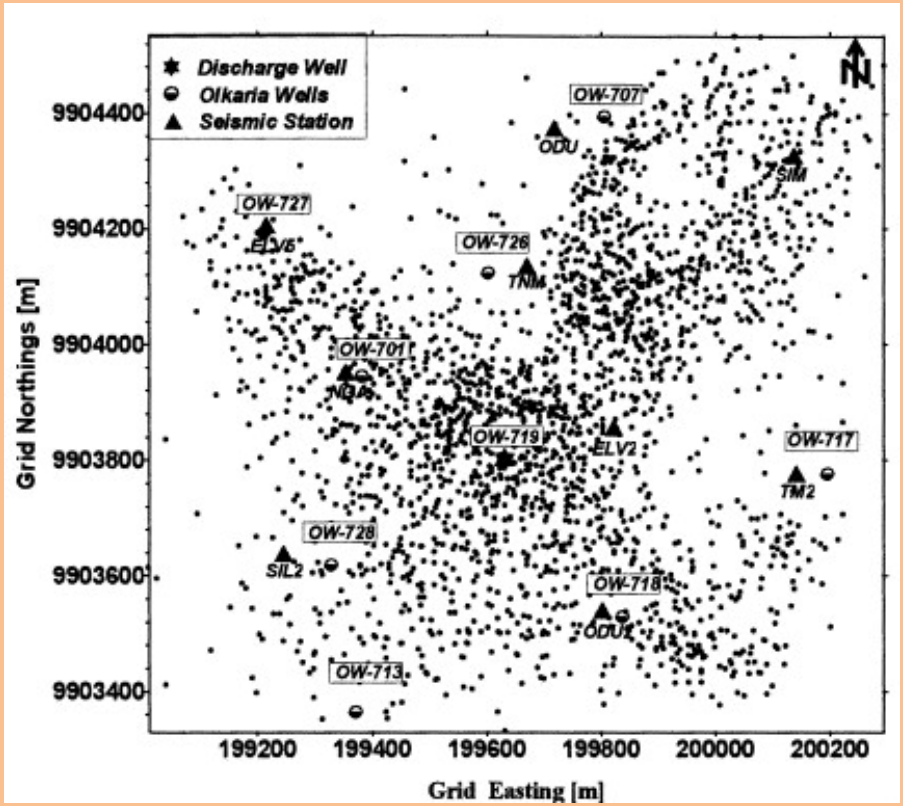

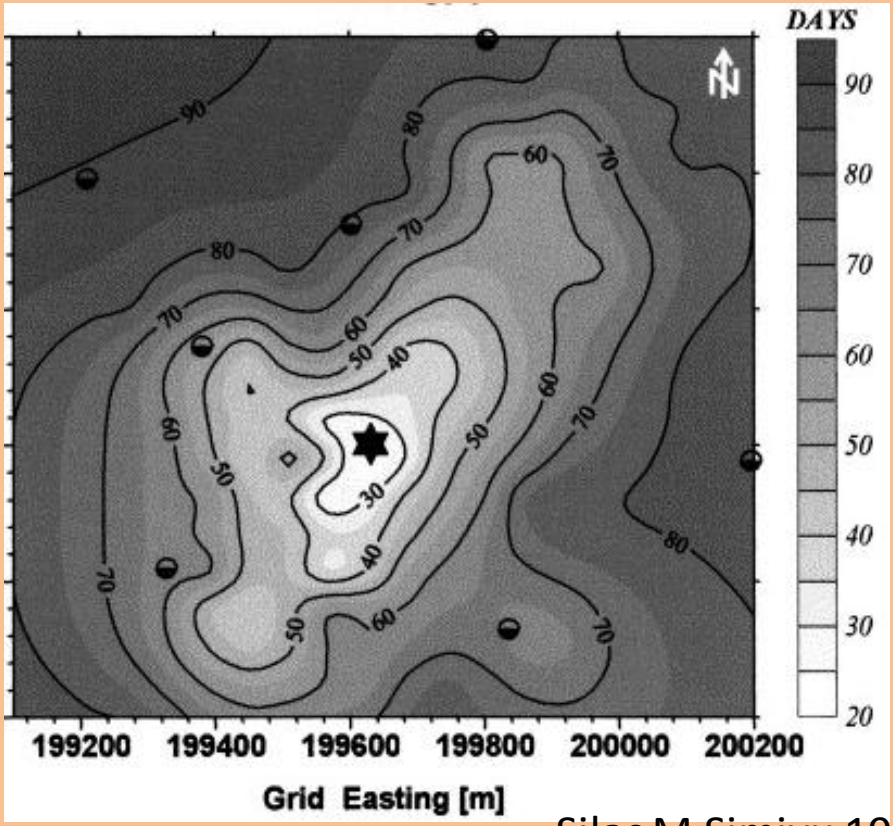

Silas M Simiyu 1999

Terratremols

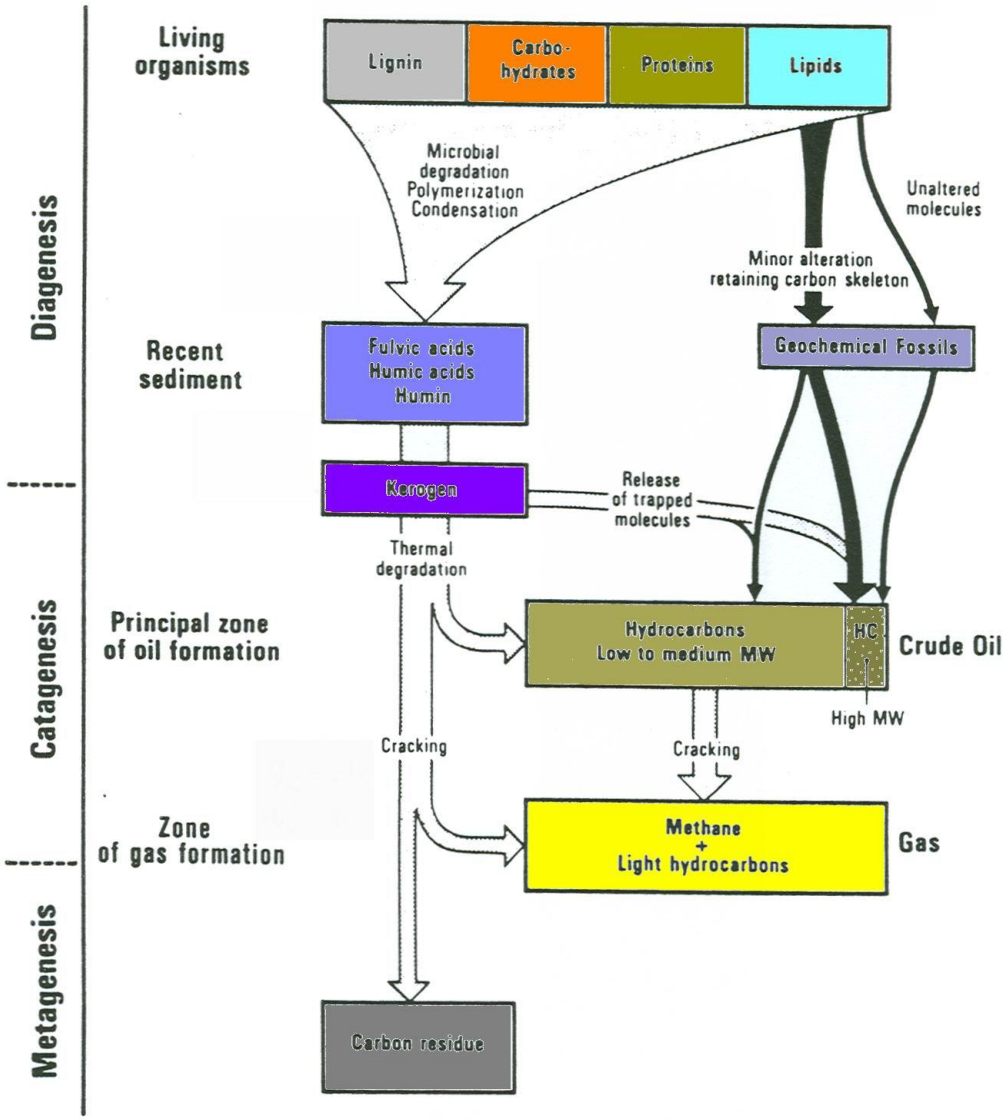

Fig. II.3.1. Sources of hydrocarbons in geological situations, with regard to the evolution of organic matter. Geochemical fossils represent a first source of hydrocarbons in the subsurface *(black solid arrows)*. Degradation of kerogen represents a second source of hydrocarbons *(grey dotted arrows)*

Terratremols

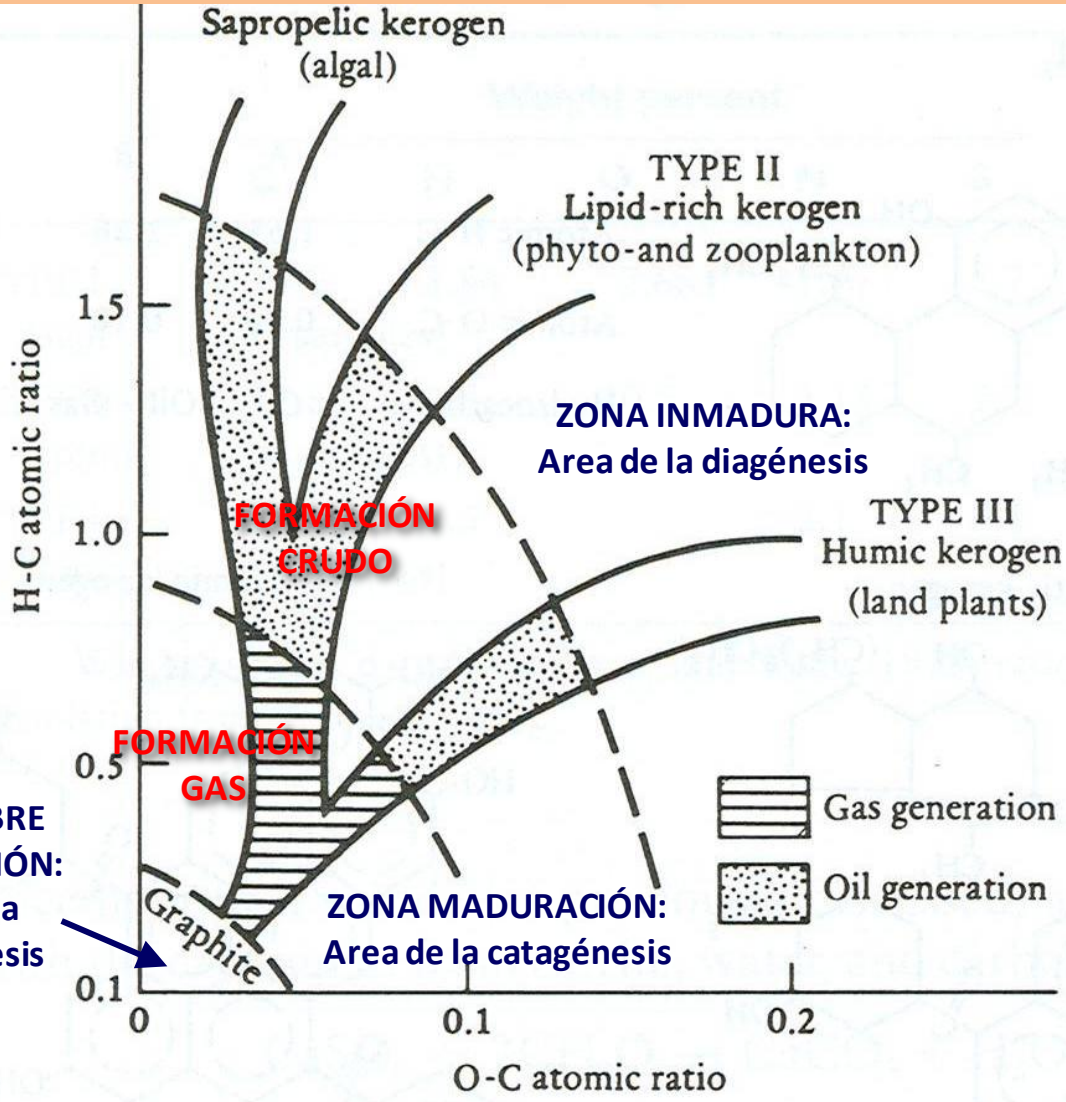

FIGURE 5.13 Graph showing the maturation paths of the three different types of kerogen.

Terratremols

6.5. El concepto de "ventana del petróleo".

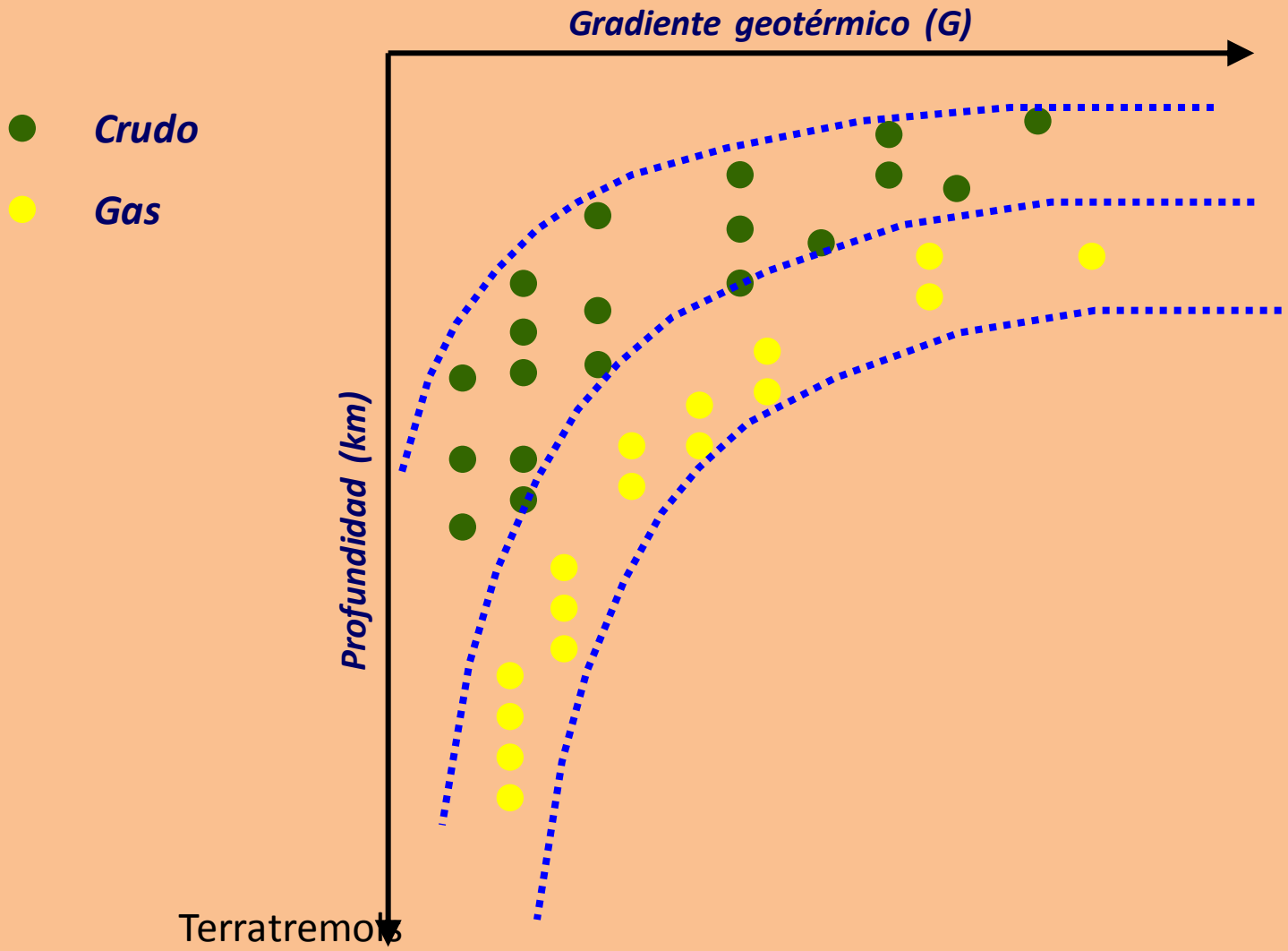

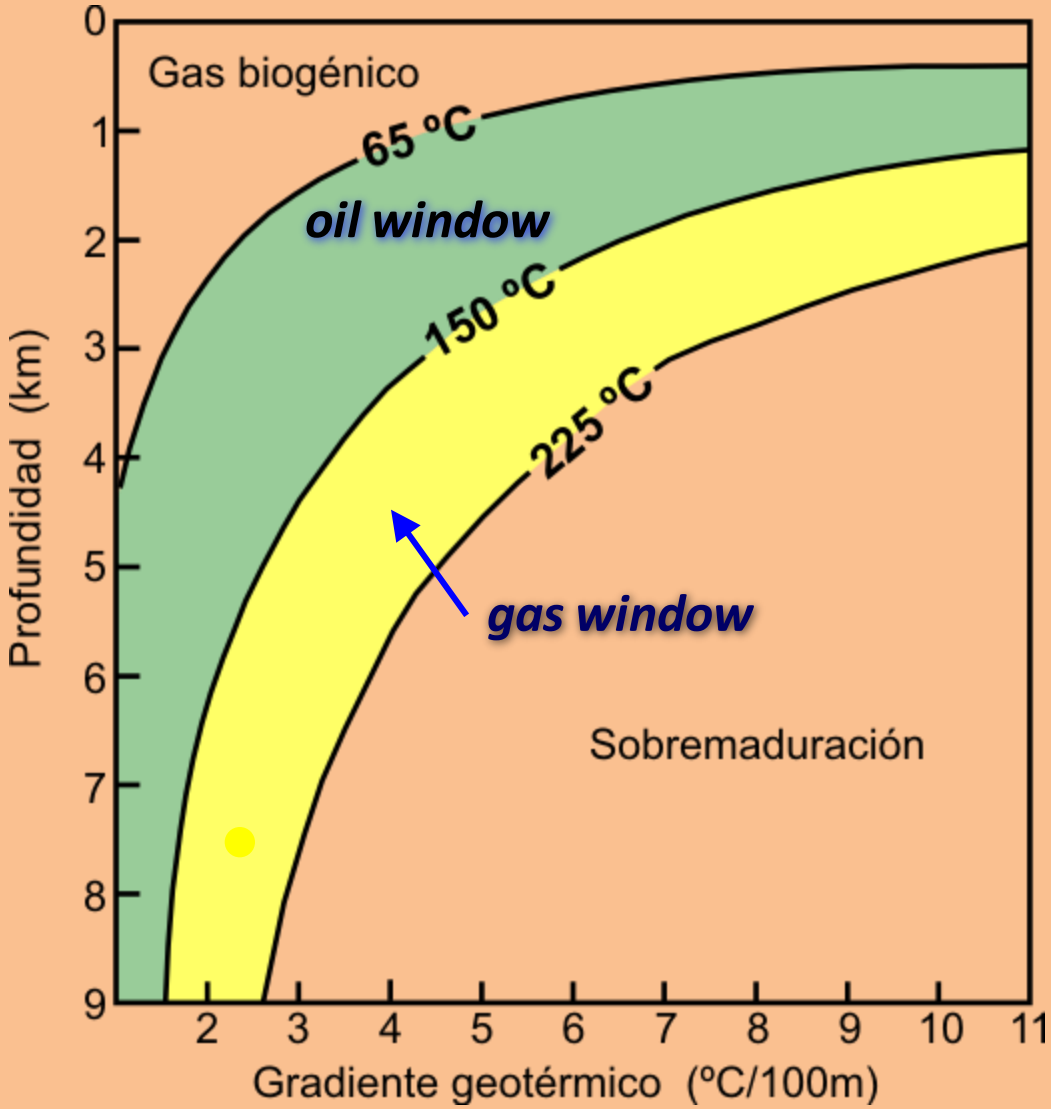
Gas biogénico
65 °C
oil window
150 °C
225 °C
gas window
Sobremaduración
Profundidad (km)
0
1
2
3
4
5
6
7
8
9
2
3
4
5
6
7
8
9
10
11
Gradiente geotérmico (ºC/100m)

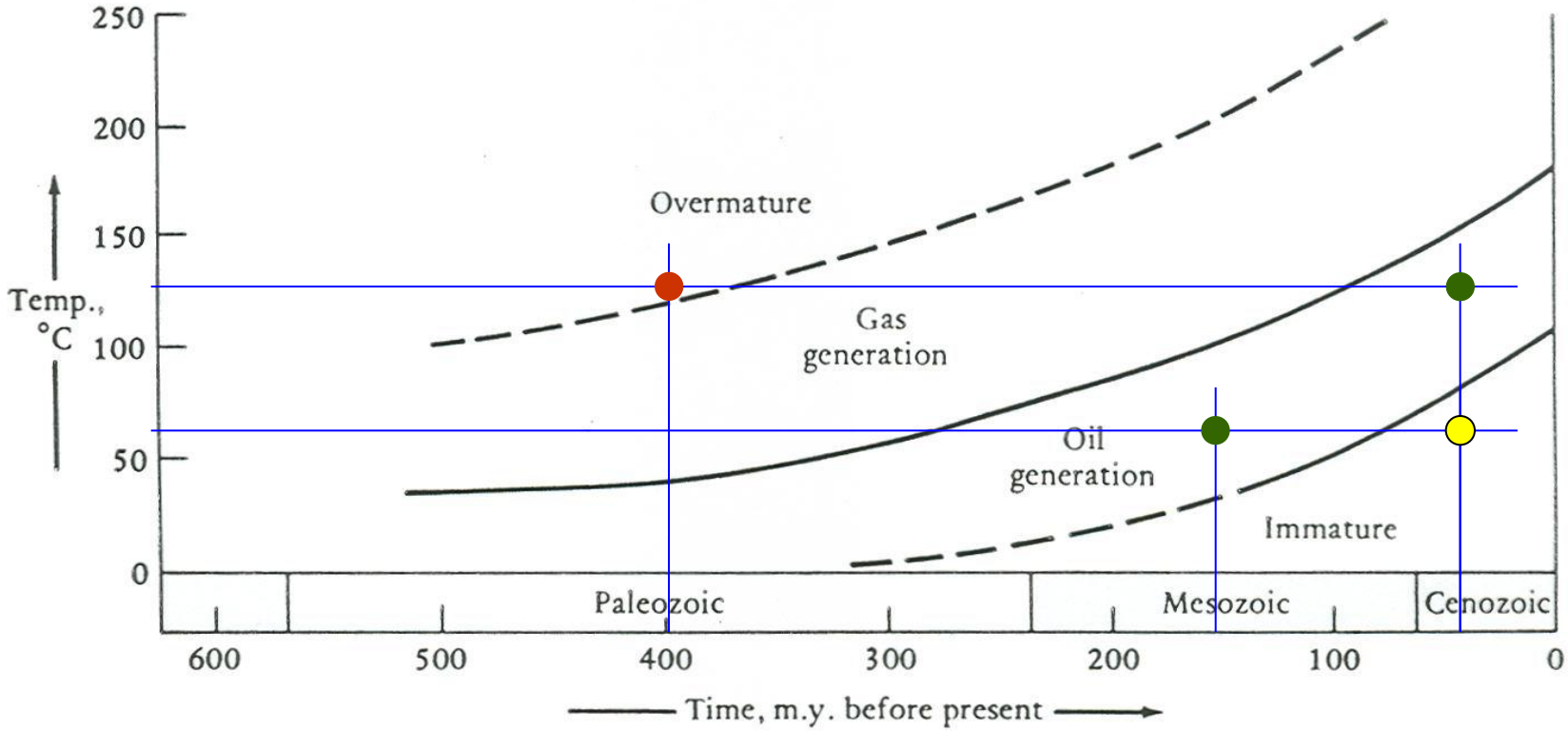

FIGURE 5.12 *Graph of temperature against time of oil and gas formation. For the problems of interpreting this figure, see text. (After Connan, 1974; Erdman, 1975; and Cornelius, 1975.)*

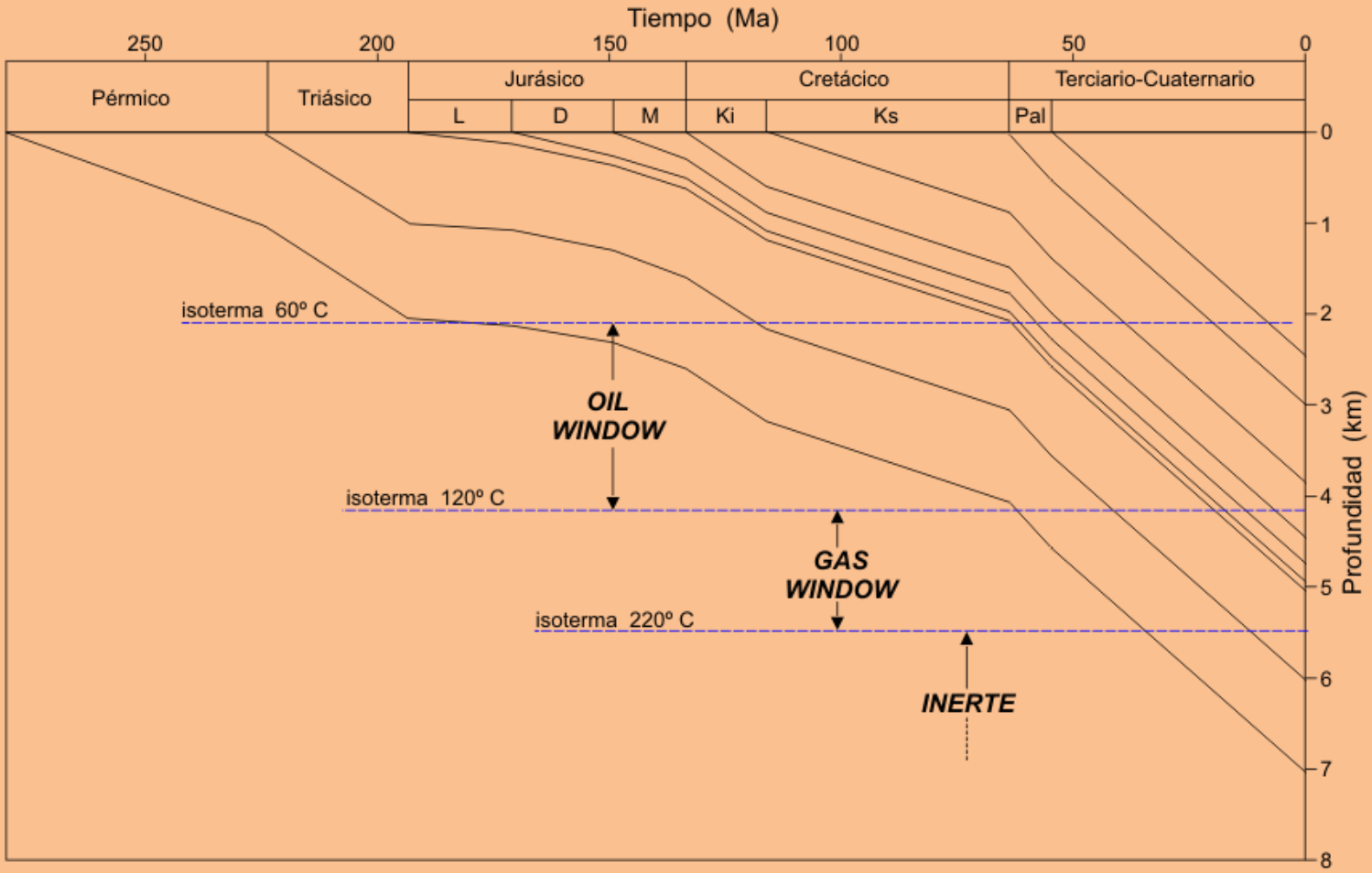
Tiempo (Ma)
250
200
150
100
50
0
Pérmico
Triásico
Jurásico
L
D
M
Cretácico
Ki
Ks
Terciario-Cuaternario
Pal
isoterma 60º C
OIL WINDOW
isoterma 120º C
GAS WINDOW
isoterma 220º C
INERTE
Profundidad (km)
0
1
2
3
4
5
6
7
8

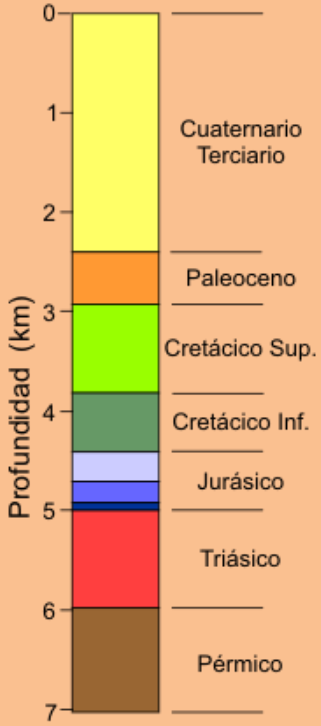
Profundidad (km)
0
1
2
3
4
5
6
7
Cuaternario
Terciario
Paleoceno
Cretácico Sup.
Cretácico Inf.
Jurásico
Triásico
Pérmico

<0 G$0'"- : #2$H#*- 3*. B#*; $2. B*/%I J*) $8&

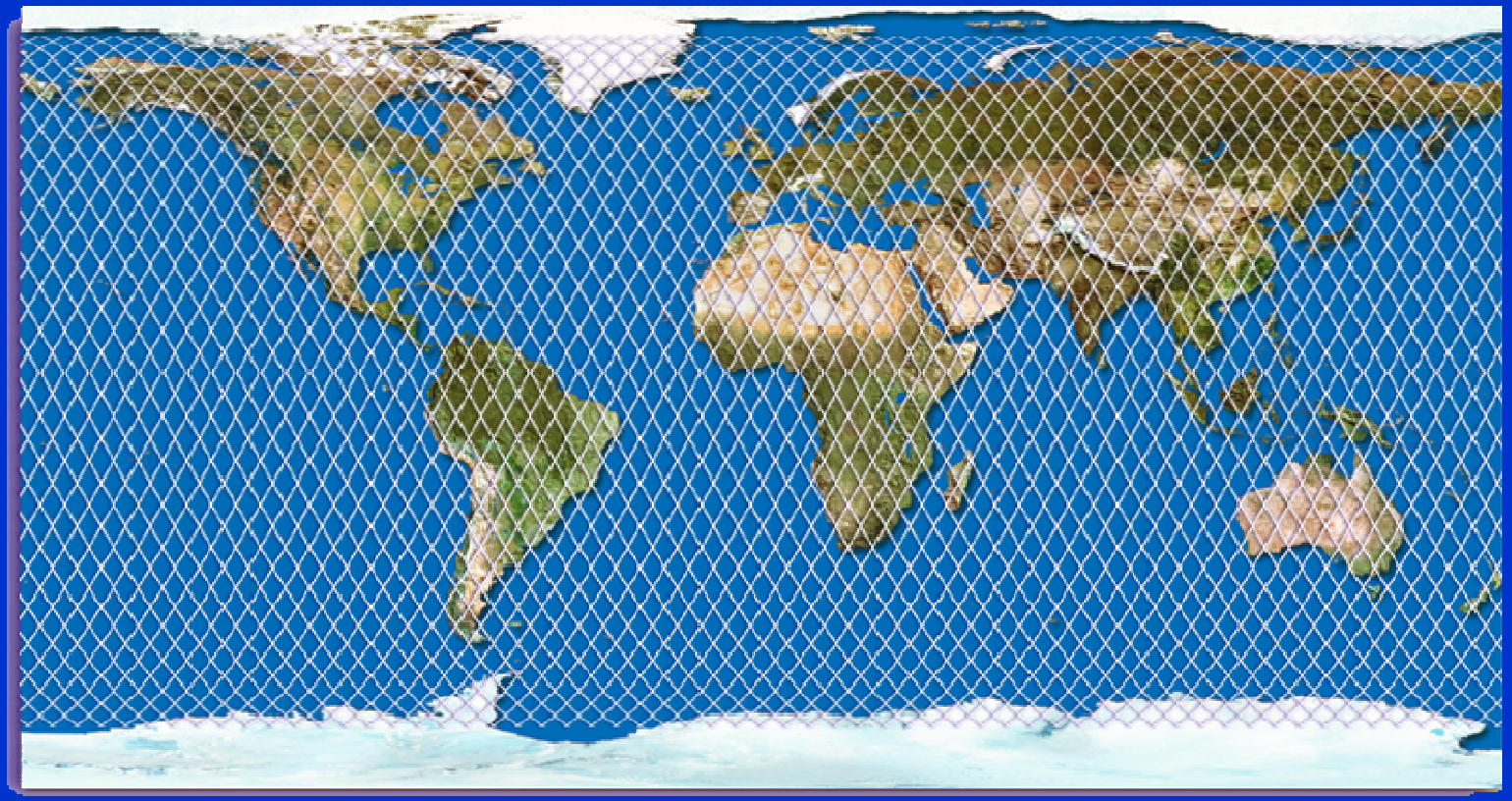

P4"#5/4 4A33'5%$

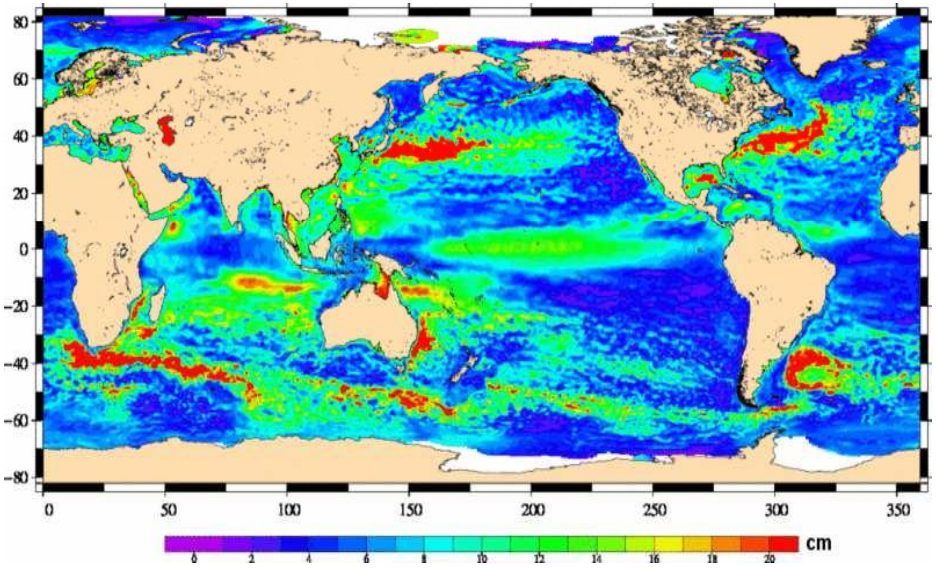

@#30"*$4#6' ' 4"#5 4/34A6#% 5

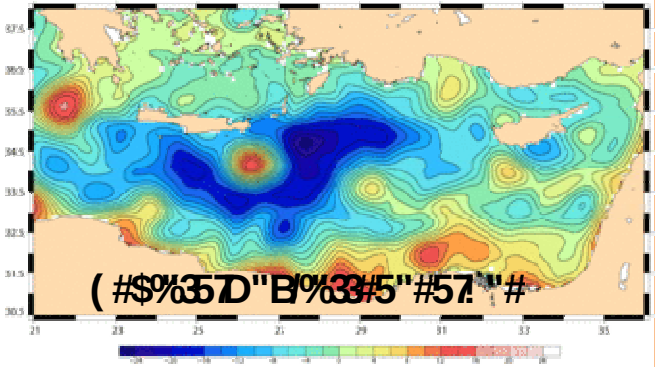

(#$%35D"B!%33#5"#57!"#

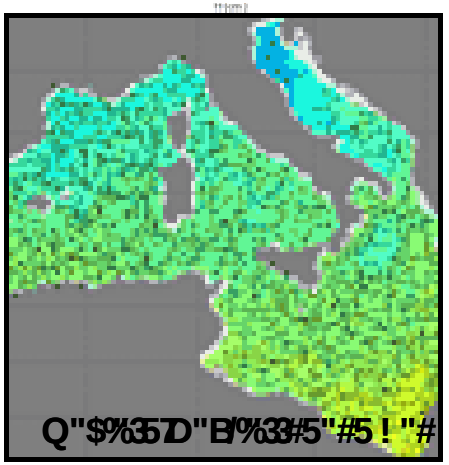

Q"$%35D"B!%33#5"#5!"#

3 4(%)$56")*60( )"67%)4/1

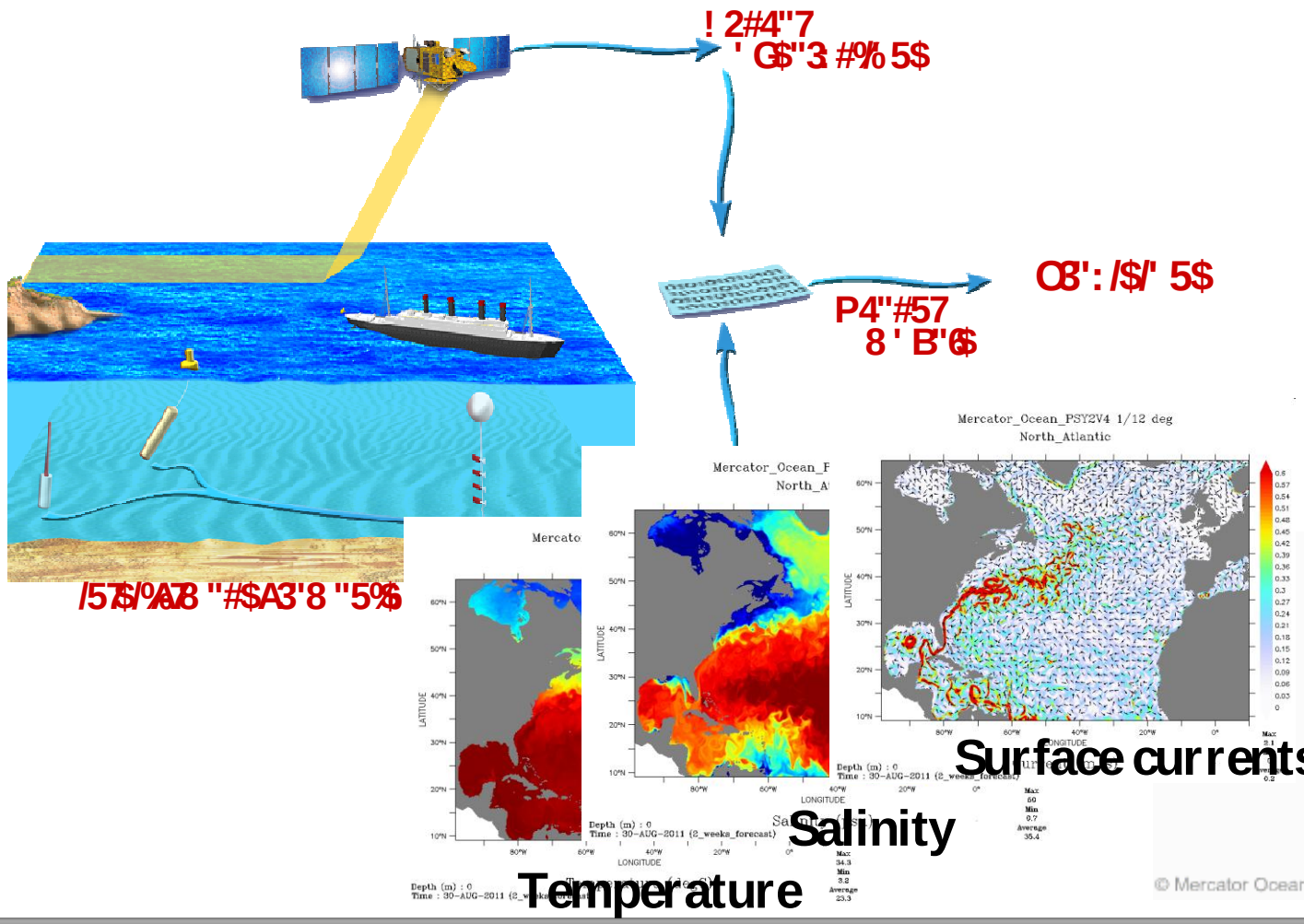
! 2#4"7
' G$"3 #% 5$
O8': /$/' 5$
P4"#57
8 ' B'6$
/57$/%A8 "#$A3'8 "5%6
Mercator_Ocean_PSY2V4 1/12 deg
North_Atlantic
Surface currents
Salinity
Temperature
© Mercator Ocean

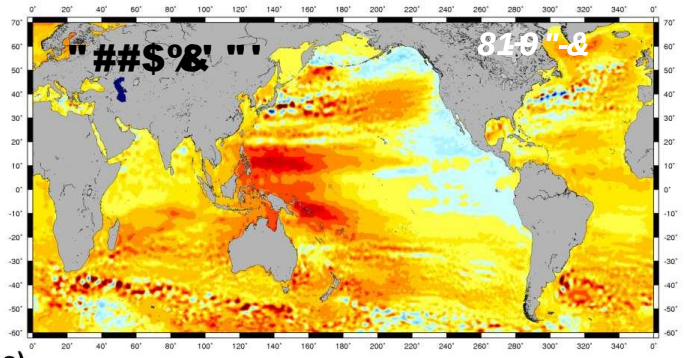
a)

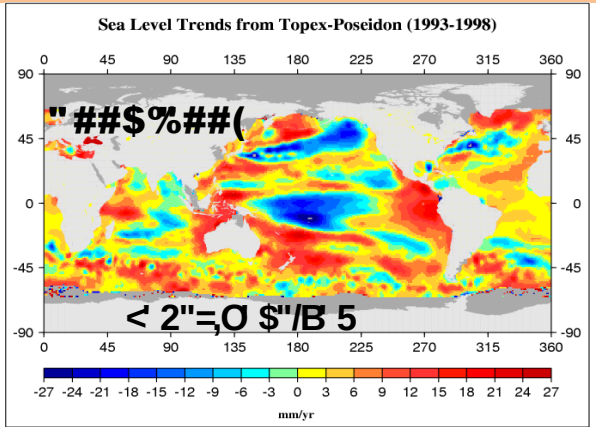
Sea Level Trends from Topex-Poseidon (1993-1998)
mm/yr

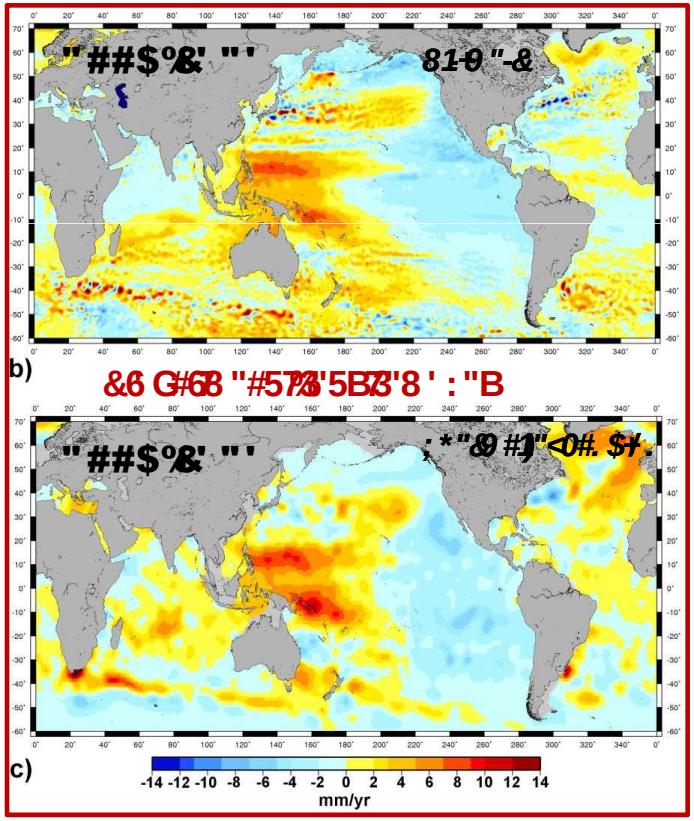
b)
c)
mm/yr

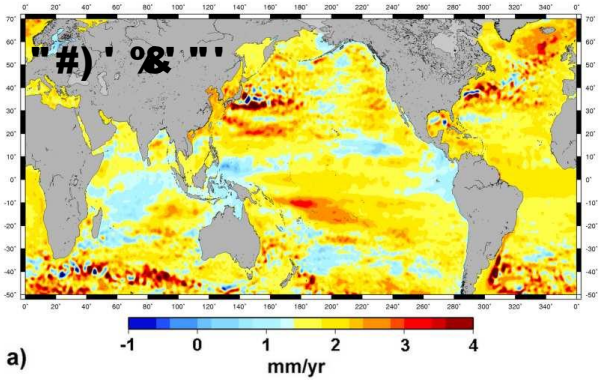
a)
mm/yr

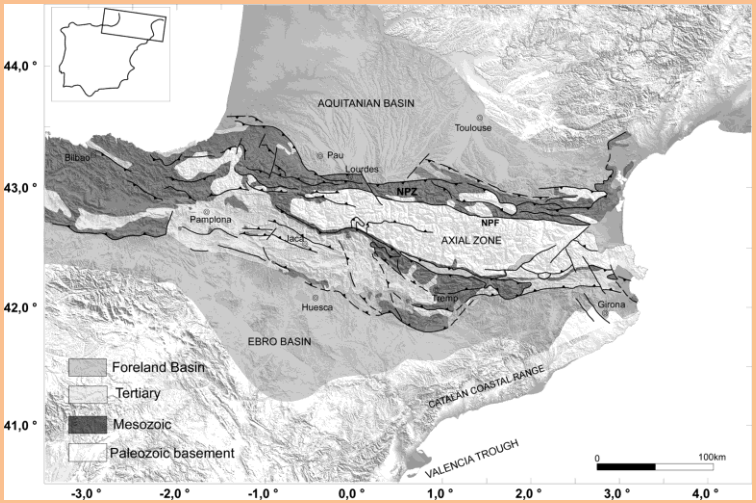

Figure 1. Geologic map of the Pyrenees. NPF, North Pyrenean Fault; NPZ, North Pyrenean Zone. The inset shows the location of the study area within the Iberian Peninsula. Figure modified from Teixell (1996).

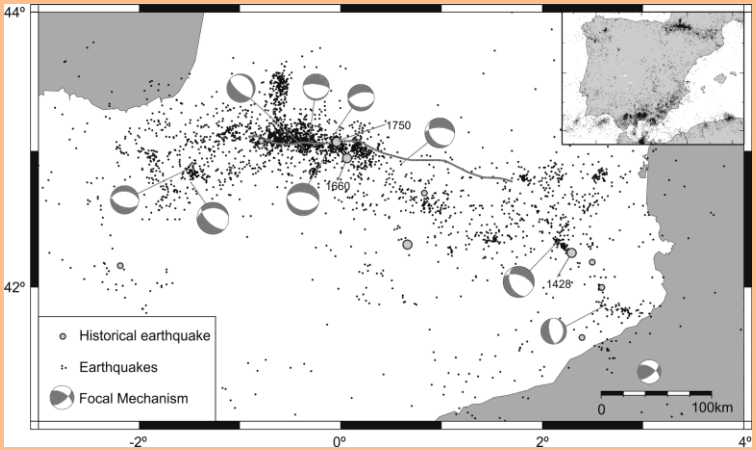

Figure 2. Seismicity map of the Pyrenees and the entire Iberian Peninsula (the inset) during the 1973–2011 time period. Earthquakes with $M > 2$ were chosen from the USGS/NEIC catalogue (http://neic.usgs.gov). Grey dots depict historical earthquakes of MSK $\geq$VIII (Olivera *et al.* 2006; Souriau & Pauchet 1998). Focal mechanisms (1984–2008) are from Stich *et al.* (2006, 2010). Grey line depicts the North Pyrenean Fault (NPF).

and the Valencia Trough (Banda & Santanach 1992; Roca *et al.* 1999; Fig. 1). The earthquakes are generally shallow, not exceeding 20 km depth, which suggests an average thickness for the seismogenic crust of ∼15 km (Perea 2009).

The focal mechanisms displayed in Fig. 2 were obtained by Stich *et al.* (2006, 2010) using moment tensor inversion for regional earthquakes higher than M_w3.5 from 1986 to 2008. They calculated 10 focal mechanisms, with eight events falling within the region of our study and two in the CCR. All of the Pyrenees earthquakes indicate normal faulting with approximately NNE–SSW oriented tension axes, roughly perpendicular to the trend of the mountain chain. The two focal mechanisms outside the Pyrenees show a different stress regime (Fig. 2): strike slip and east–west extension.

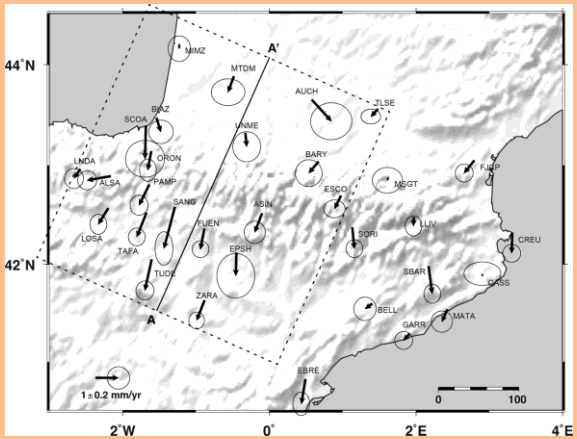

Figure 4. Map of the GPS horizontal velocities of the Pyrenees. The velocities are presented in Eurasia-fixed reference frame with 95 per cent confidence limits. A–A' shows the orientation and stations included in the velocity profile shown in Fig. 5.

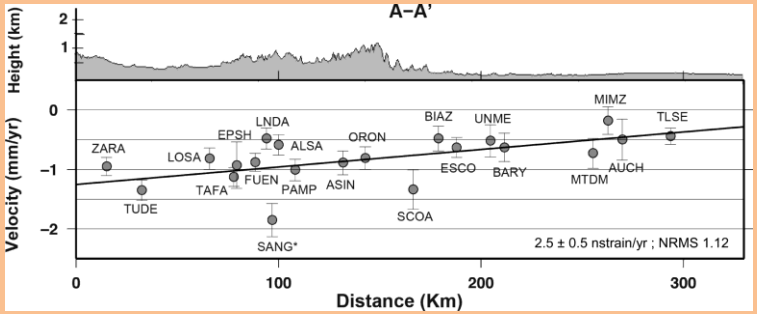

Figure 5. GPS velocities projected onto a N024°E profile, approximately perpendicular to the strike of the Pyrenees in the western and central regions (see Fig. 4). Topography is shown with 16 × vertical exaggeration. Station SANG* is shown but excluded from the estimation of the slope and the statistics.

(2002) gives the recurrence interval T for an earthquake scalar moment M_0

$$T(M_0) = \left[\frac{1}{1-\beta}\right] \frac{M_0^{\beta} M_{\rm cm}^{1-\beta}}{\dot{M}_{\rm g}} \tau(2-\beta)\varepsilon_{\rm m},$$

where $M_{\rm cm}$ is the scalar moment for the MCE, $\beta = \frac{2}{3} b_{\rm value}$, τ is a gamma function and $\varepsilon_{\rm m} = \exp(M_0/M_{\rm cm})$ and $\dot{M}_{\rm g}$ is the geodetic moment rate, given by (Savage & Simpson 1997):

$$\dot{M}_{\rm g} = 2\mu H S \text{Max}\left|\dot{\varepsilon}_1\right|, \left|\dot{\varepsilon}_2\right|, \left|\dot{\varepsilon}_1 + \dot{\varepsilon}_2\right|,$$

where μ is the shear modulus, S represents an area within a geodetic polygon at the Earth's surface and H is the seismogenic depth. For our calculation, we compute both M_0 and $M_{\rm cm}$ from the magnitude of the maximum earthquake in the seismic record for Pyrenees region ($M_{\rm w} = 6.5$; (Olivera *et al.* 1992) using

$$\log M_0 = 1.5 M_{\rm w} + 16$$

(Hanks & Kanamori 1979).

We assume a universal $b_{\rm value}$ of 1 for the Pyrenees (Secanell *et al.* 2008), a shear modulus of 30 GPa and a seismogenic depth of 15 km (Perea 2009). If we use our estimate of the average strain rate (2.7 nstrain yr^{-1}) for the entire region of significant seismicity (160 km × 75 km), we obtain a recurrence time for an $M_{\rm w}$ 6.5 earthquake of ∼2500 yr. If a higher strain rate (9 nstrain yr^{-1}) is valid for the western region of highest seismicity, bounded by stations BIAZ, UNME, ORON and ASIN (100 km × 40 km), then the estimated recurrence interval is ∼2200 yr.

6 CONCLUSIONS

We analysed data from 49 CGPS over a 3.5 yr period to assess deformation rates across and within the Pyrenees. Stations south of the western and central Pyrenees have velocities with respect to western Europe between 0.5 and 1.5 mm yr^{-1} and show a relatively coherent pattern unaffected by modelling assumptions. A profile across this region shows extension perpendicular to the

Transform Faults

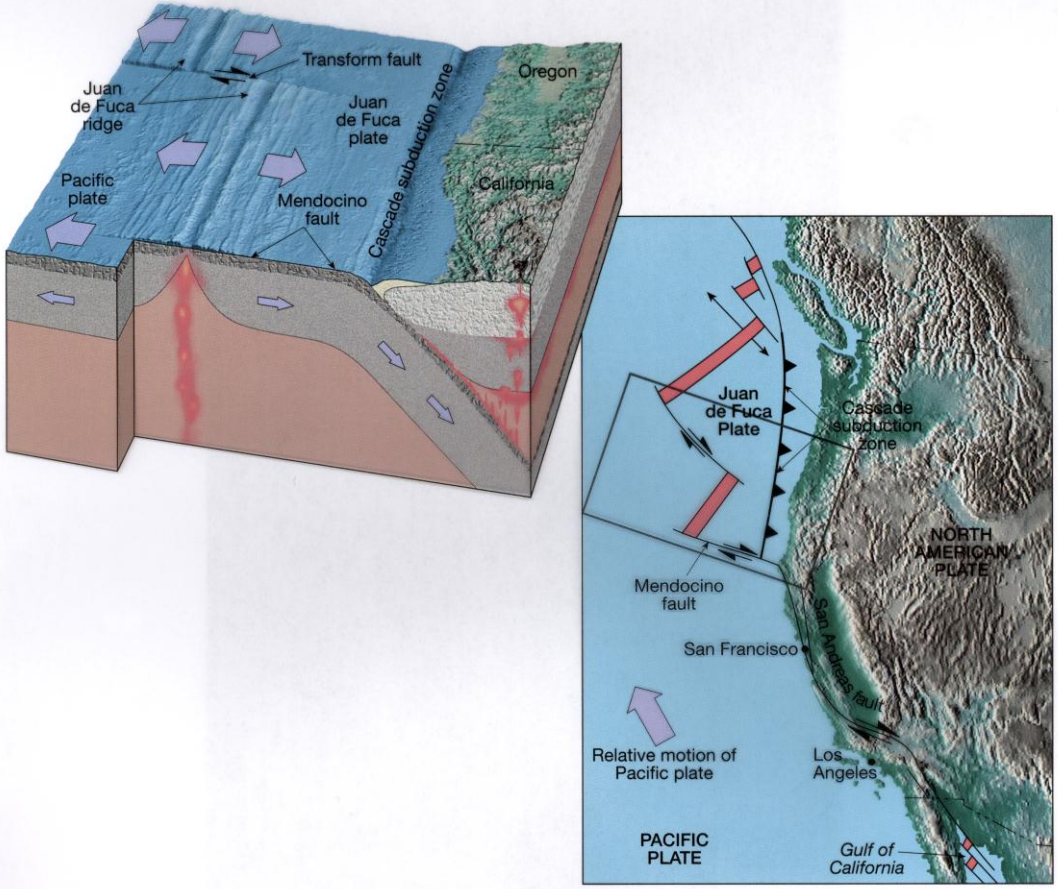

EARTH; AN INTRODUCTION TO PHYSICAL GEOLOGY 6E
by Tarbuck and Lutgens

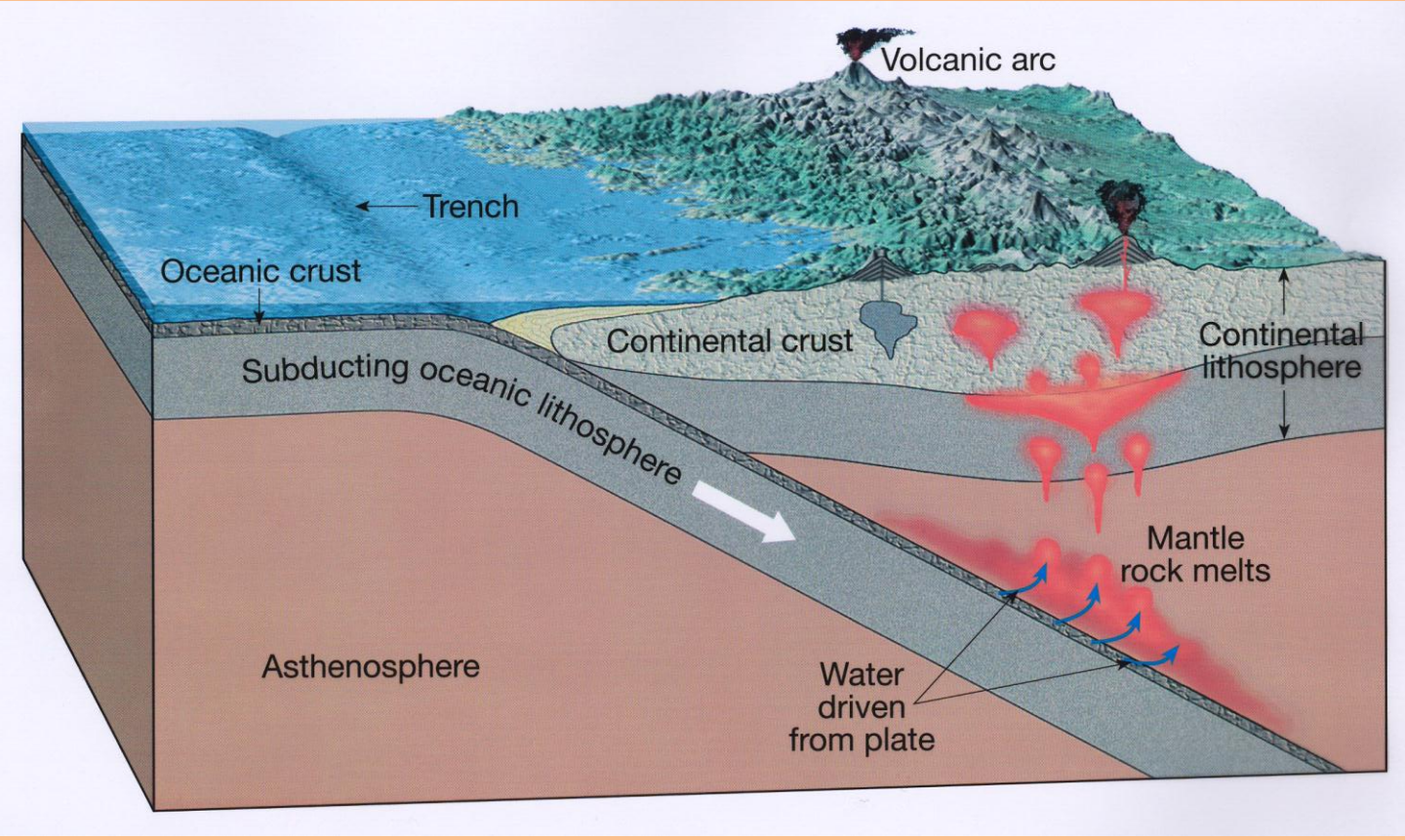
Volcanic arc
Trench
Oceanic crust
Continental crust
Continental lithosphere
Subducting oceanic lithosphere
Mantle rock melts
Asthenosphere
Water driven from plate

T-29

Regional Metamorphism

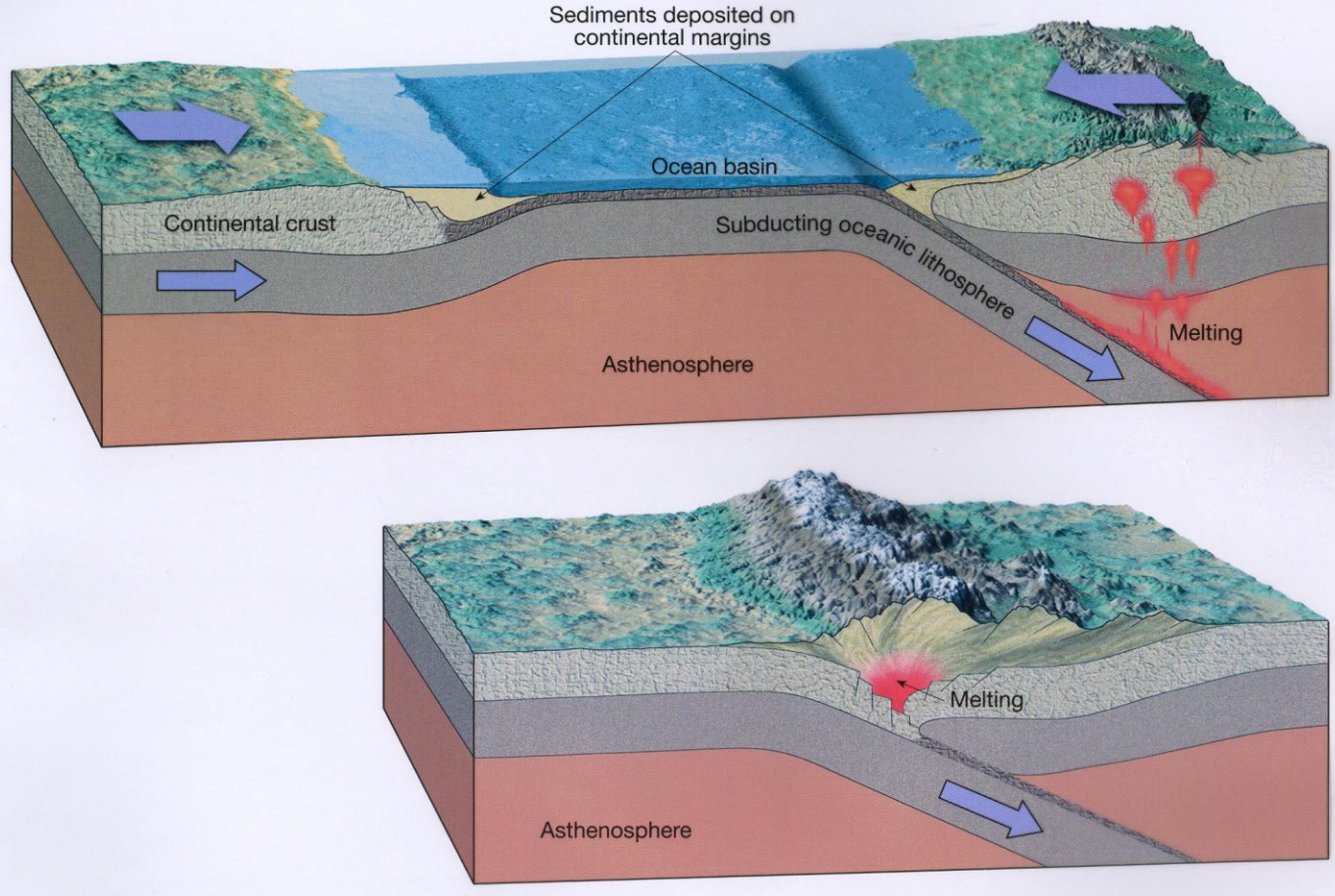

EARTH; AN INTRODUCTION TO PHYSICAL GEOLOGY 6E
by Tarbuck and Lutgens

T-149

Transforming Asthenosphere into Continental Crust

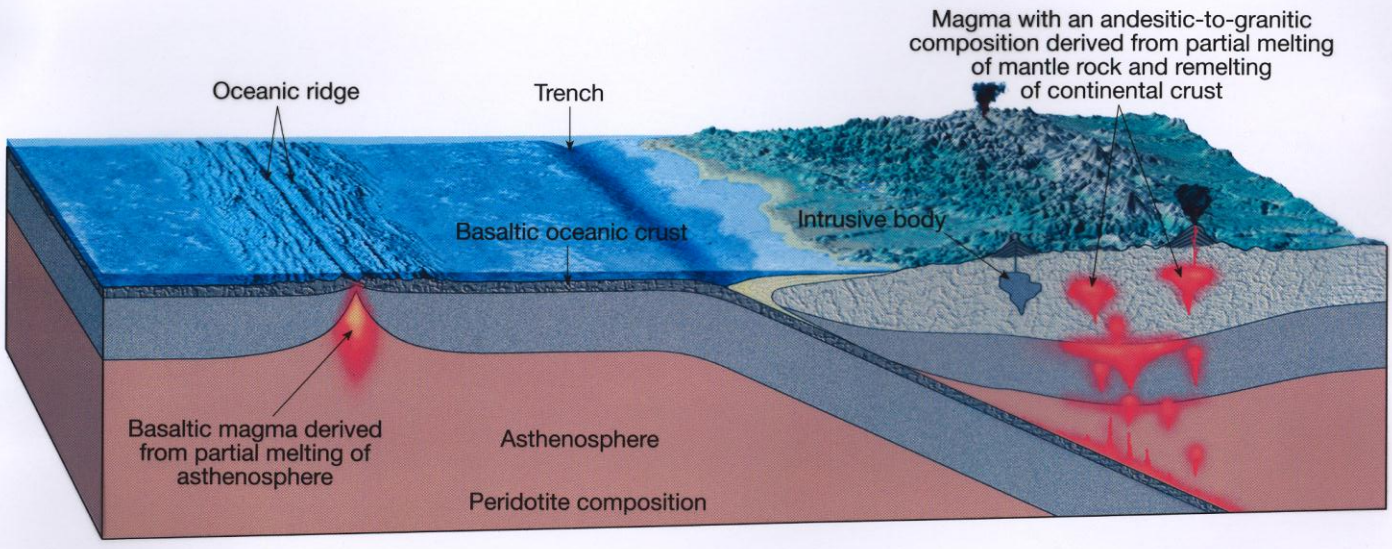

EARTH; AN INTRODUCTION TO PHYSICAL GEOLOGY 6E
by Tarbuck and Lutgens

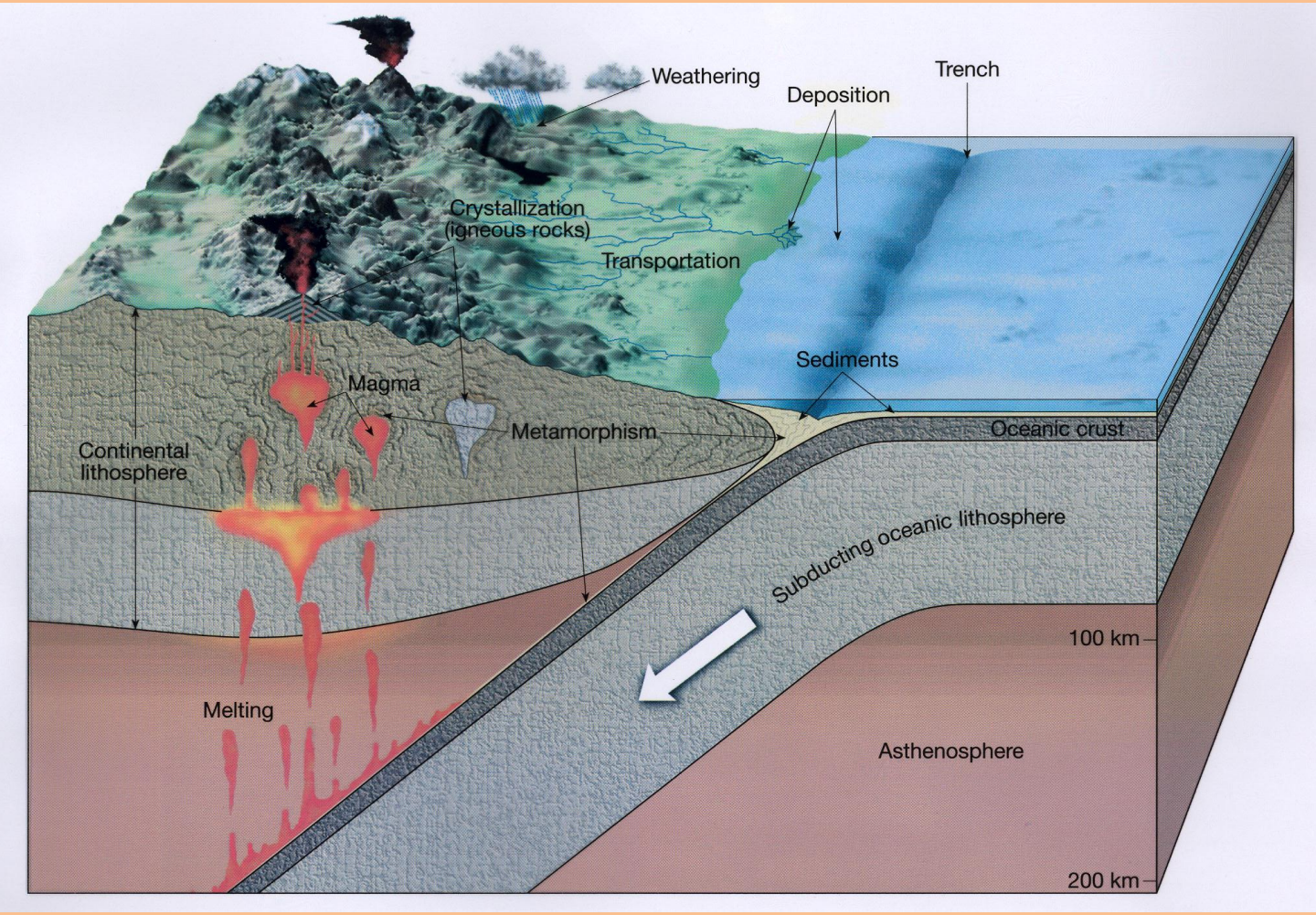
Weathering
Deposition
Trench
Crystallization
(igneous rocks)
Transportation
Sediments
Magma
Metamorphism
Oceanic crust
Continental
lithosphere
Subducting oceanic lithosphere
100 km
Melting
Asthenosphere
200 km

T-147

Orogenesis at Andean-type Subduction Zone

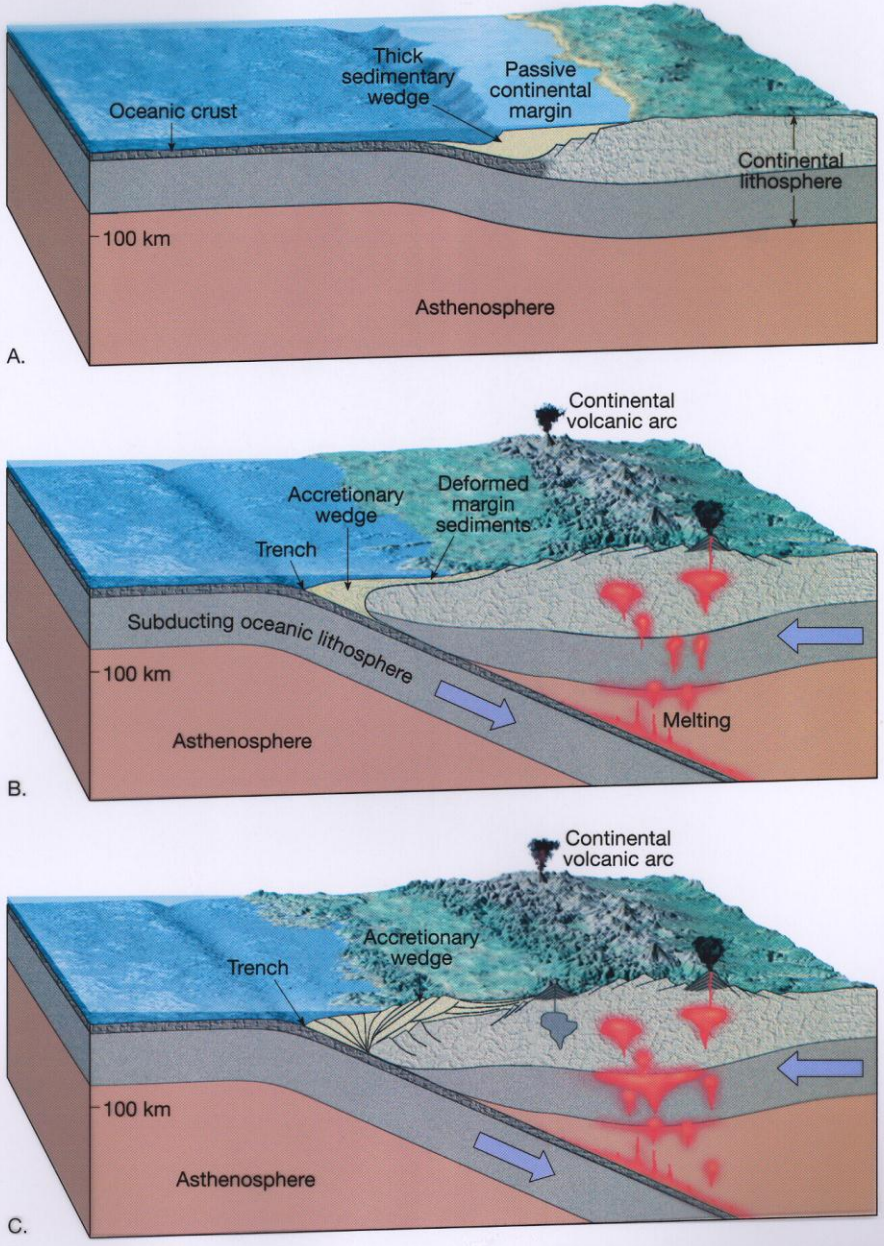

EARTH; AN INTRODUCTION TO PHYSICAL GEOLOGY 6E
by Tarbuck and Lutgens

T-6

Relationship Between Divergent and Convergent Plates

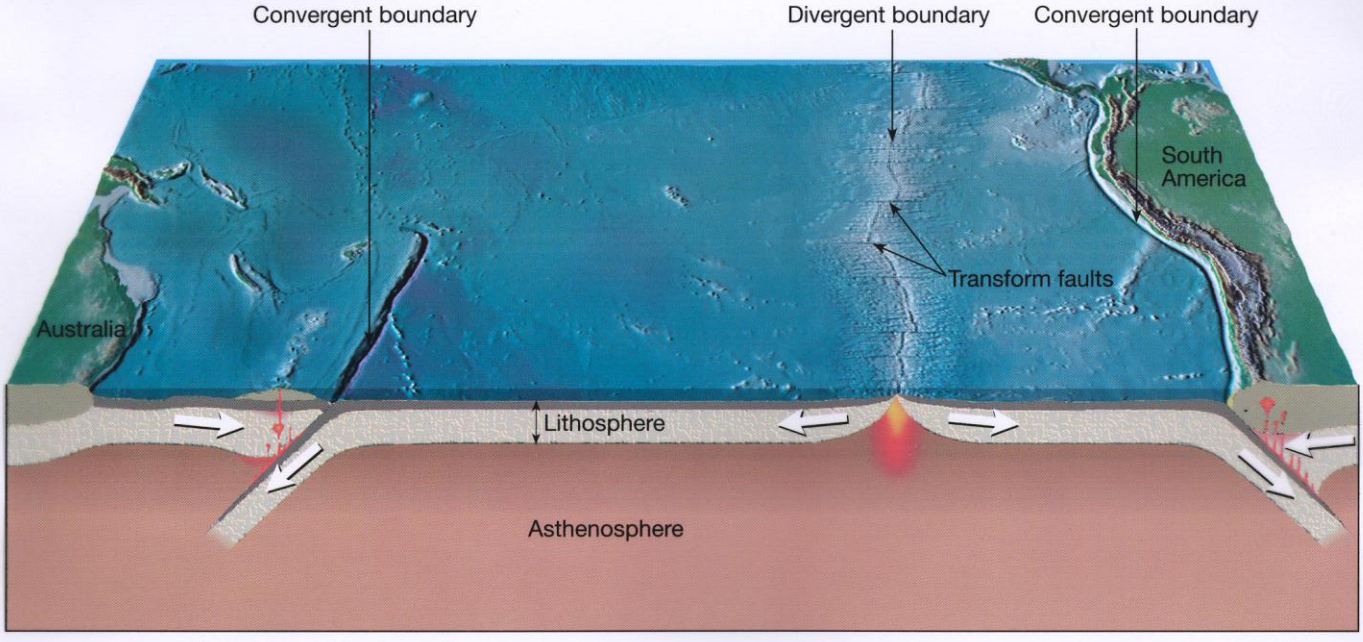

EARTH; AN INTRODUCTION TO PHYSICAL GEOLOGY 6E
by Tarbuck and Lutgens

T-136

East African Rift Valleys

EARTH; AN INTRODUCTION TO PHYSICAL GEOLOGY 6E
by Tarbuck and Lutgens

Rock Cycle

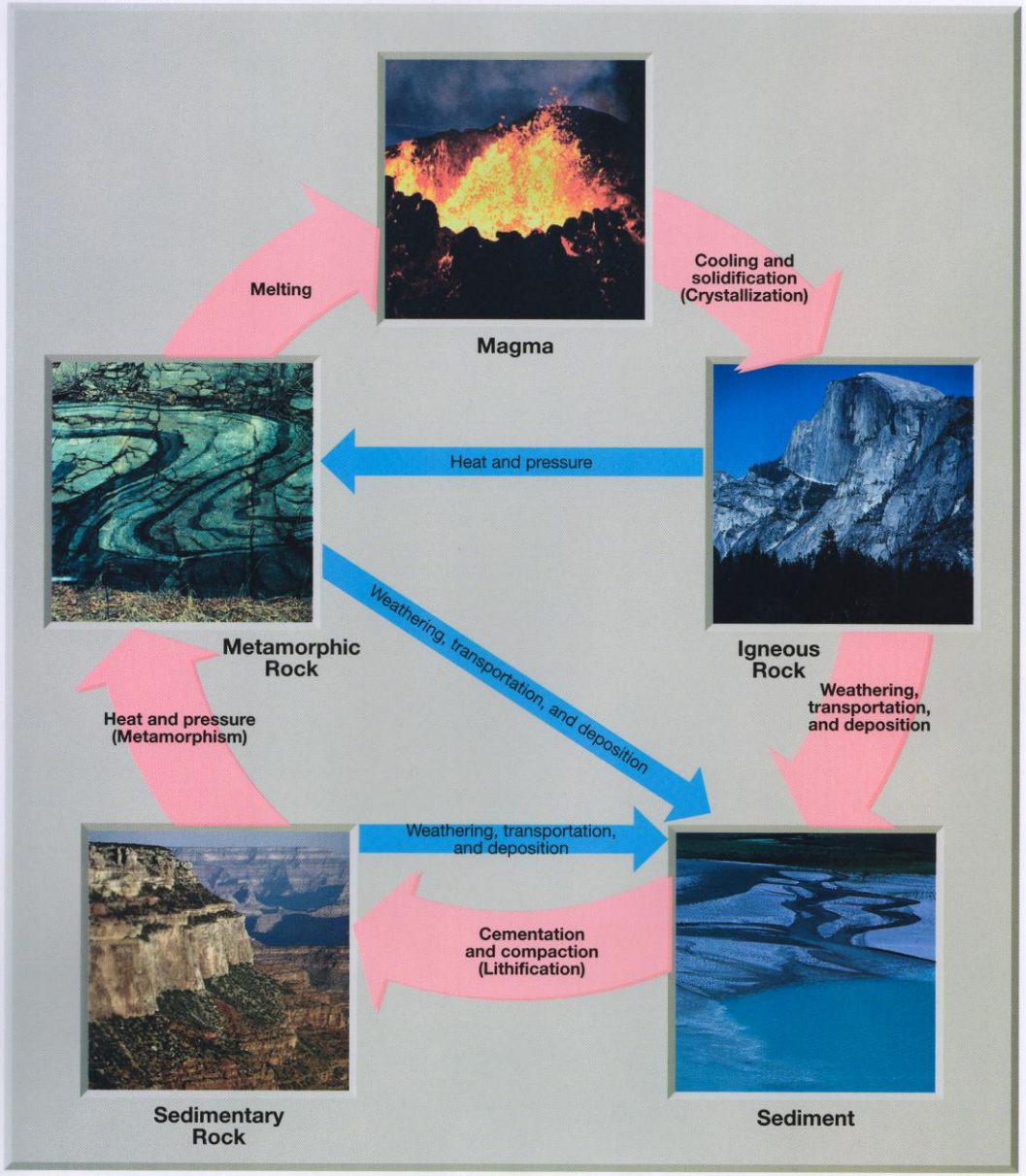

EARTH; AN INTRODUCTION TO PHYSICAL GEOLOGY 6E
by Tarbuck and Lutgens

James P. M. Syvitski
University of Colorado at Boulder

Article

Anthropocene Metamorphosis of the Indus Delta and Lower Floodplain

James P.M. Syvitski, Albert J. Kettner, Irina Overeem, Liviu Giosan, G. Robert Brakenridge, Mark Hannon, Roger Bilham

Anthropocene 01/2014;

ABSTRACT The Indus River/Delta system is highly dynamic, reflecting the impacts of monsoonal-driven floods and cyclone-induced storm surges, earthquakes ranging up to Mw = 7.8, and inundations from tsunamis. 19th century Indus discharge was likely larger than today, but upstream seasonal spillways limited the maximum flood discharge. Upstream avulsions during the 2010 flood similarly reduced the downstream discharge, so that only 43% of the floodwaters reached the delta. The present-day Indus River is wider with larger meander wavelengths (~13 km) compared to the 4 km to 8 km meander wavelengths for the super-elevated historical channel deposits. The Indus River is presently affected by: 1) artificial flood levees, 2) barrages and their irrigation canals, 3) sediment impoundment behind upstream reservoirs, and 4) inter-basin diversion. This silt-dominated river formerly transported 270+ Mt/y of sediment to its delta; the now-transformed river carries little water or sediment (currently ~13 Mt/y) to its delta, and the river often runs dry. Modern-day reduction in fluvial fluxes is expressed as fewer distributary channels, from 17 channels in 1861 to just 1 significant channel in 2000. Abandoned delta channels are being tidally reworked. Since 1944, the delta has lost 12.7 km2/y of land altering a stunning 25% of the delta; 21% of the 1944 delta area was eroded, and 7% of new delta area formed. The erosion rate averaged ~69 Mt/y, deposition averaged ~22 Mt/y, providing a net loss of ~47 Mt/y particularly in the Rann of Kachchh area that is undergoing tectonic subsidence. [less]

ANTHROPOCENE WORKING GROUP: PROGRAMME FOR 2013

- SQS in conjunction with SACOM-INQUA is sponsoring a full-day special session "The Quaternary System and its Formal Subdivision" during the First International Congress on Stratigraphy - *Strati 2013*, in Lisbon, Portugal, 1-7 July, 2013. See: http://www.strati2013.org . The conveners for this special session are Martin J. Head (Chair, SQS), Philip L. Gibbard (President, SACOM-INQUA), and Thijs van Kolfschoten (former Secretary SQS). There will be a special session on the Anthropocene at which Jan Zalasiewicz will be presenting. A special issue of **Quaternary International** is planned for contributions to the Quaternary session.

- International Geosphere-Biosphere Programme (IGBP): James P Syvitski reports on a workshop to be held in the fall of 2013 on the Anthropocene. The writing meeting and the subsequent workshop is being sponsored by IGBP, IHDP, DIVERSATAS, and WCRP, the four Global Environmental Change Programmes under ICSU. These programmes are merging into something called Future Earth and we want the Anthropocene to be a concept that makes this

Newsletter of the Anthropocene Working Group

Volume 4:Report of activities 2012 **June 2013**

Humans as Geologic Agents

Edited by Judy Ehlen, William C. Haneberg, and Robert A. Larson

Year Published: 2005

Total Pages: 168

Product Code: REG016

Homo sapiens is the only known species to consciously effect change to the Earth's geologic environment. We reshape the Earth; intensify erosion; modify rivers; change local climates; pollute water resources, soils and geologic media; and alter soils and the biosphere. We dig holes in it, remove parts of it, and bury highly toxic materials in it. In this volume, the authors explore human impact on the Earth and attempt to answer the following questions. What have we done to Terra? How fast have we effected change? Are the changes permanent? Are they good, or have we inadvertently caused more damage? Can we, should we, repair some or all of these changes? These are important questions for the geoscience community because, as those most knowledgeable about the Earth and its resources, geologists play a major role in sustaining and preserving the Earth.

Table of Contents - Reviews in Engineering Geology (REG016)

Preface
v
1. George A. Kiersch: Engineering geology applied to anthropomorphic problems
Allen W. Hatheway
2. Effects of human activity on lineation analysis
Judy Ehlen
3. Disconnected rivers: Human impacts to rivers in the United States
Ellen Wohl
4. The history of the use and effectiveness of instream structures in the United States
Douglas M. Thompson
5. Impact of military activities on local and regional geologic conditions
Edward P.F. Rose
6. Human influence on the Columbia River littoral cell
Richard W. Galster
7. Impacts of coal mining
Robert J. Turka and Richard E. Gray
8. Impacts of land subsidence caused by withdrawal of underground fluids in the United States
Thomas L. Holzer and Devin L. Galloway
9. Salt dissolution and subsidence or collapse caused by human activities
Kenneth S. Johnson
10. The Glen Creek Landslide: A case study in the misuse of the Jahnsian steps during hillside development
Philip L. Johnson

comfortable levels", but no value! In the last OPEC Annual Statistical bulletin 2010-2011 edition "spare capacity is only mentioned in a note page 10 quoting 2005 OPEC Conference.
It is only in OPEC World Oil Outlook that a graph on spare capacity is given since 2009 http://www.opec.org/opec_web/en/data_graphs/646.htm, stating for WOO2011 that OPEC spare capacity was around 4 Mb/d in 2011 (against 2 Mb/d for EIA) and should be 8 Mb/d in medium term.
Figure 4: OPEC spare capacity by OPEC WOO 2011

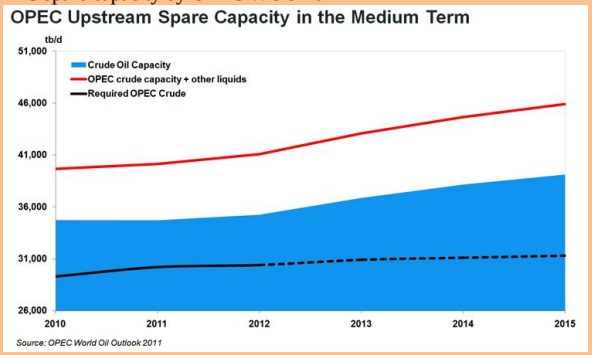

To estimate the spare capacity, it is necessary to know exactly what is the production?
It appears that OPEC does not agree on what is their production. This graph uses **secondary sources** data, but it should be quite different using **direct communication** data!
There are discrepancies on capacity and on production between OPEC presentations: Ch.Khelil "Oil production capacity" Sept 2006 OPEC seminar
http://www.opec.org/opec_web/static_files_project/media/downloads/press_room/Chakib_Khelil.pdf
and Dr Nimat B. Abu Al-Soof "Upstream Oil Industry Analyst OPEC " May 2007
http://www.opec.org/opec_web/static_files_project/media/downloads/publications/OPEC%20Spare%20Capacity.pdf.
For 2003 Khelil reports OPEC capacity at 29 Mb/d when al-Soof at 31 Mb/d
The inaccuracy on OPEC capacity is more than 2 Mb/d
Figure 5: OPEC spare capacity by Khelil 2007

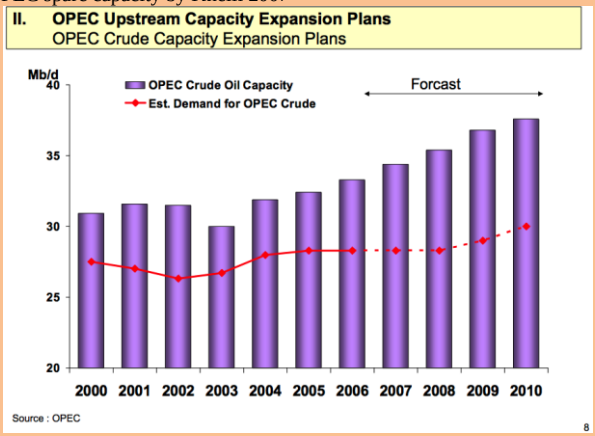

Figure 6: OPEC spare capacity by al-Soof 2006

OPEC spare capacity is reported by EIA http://www.eia.gov/analysis/requests/ndaa/pdf/ndaa.pdf in this graph showing the inverse correlation with WTI real oil price (in 2010$/b) and if OPEC capacity is shown, the title is for world spare oil production capacity! EIA assumes that the non-OPEC production has no spare capacity.

Figure 2: OPEC spare capacity by EIA 2001-2012 and WTI crude oil price

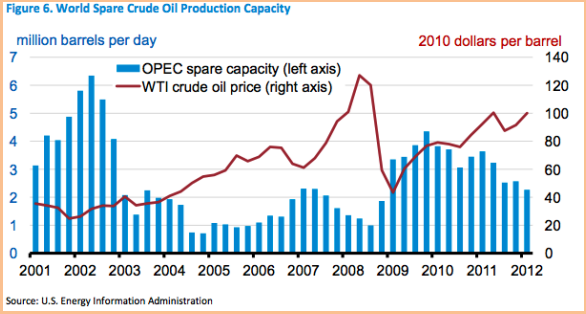

EIA provides data since 1990 and a better presentation can be plotted for WTI shown as negative value. The relationship between OPEC spare capacity and WTI may seem good by period, but it is not very reliable. It is obvious that the "*unprecedented upsurge of oil production capacity*" claimed by Maugeri is the OPEC increase in 2009 (from 1 to 5 Mb/d) correlating well with the decrease in WTI from 120 $/b to 50 $/b. The meaning is clear for 2009: low oil price is connected to high oil spare capacity. But, like egg and chicken, which starts first? Spare capacity being a guess, it is difficult to time exactly the increase, depending on the brains of the author!

OPEC annual spare capacity from EIA was 3.05 Mb/d in 2000 and 2.99 Mb/d in 2011: it means the same on a long period. For the period 1990-2012 the EIA average is about 3 Mb/d with up to 6 and down to 1: usually a surge follow a fall! For long term forecast, extrapolation from the past has to be done on long term and not on short term!

Figure 3: OPEC spare capacity by EIA/AEO & STEO 1990-2013 and WTI price in negative scale

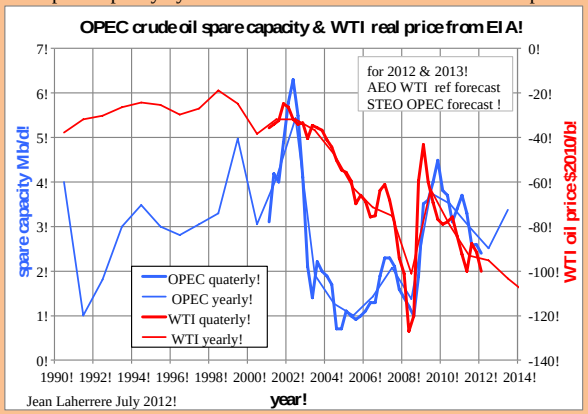

OPEC in its monthly oil market report does not mention OPEC spare capacity and in its annual report there is only this sentence "*OPEC crude oil spare capacity is also expected to remain at*

Figure 1: World oil production capacity to 2020
(Crude oil and NGLs, excluding biofuels)

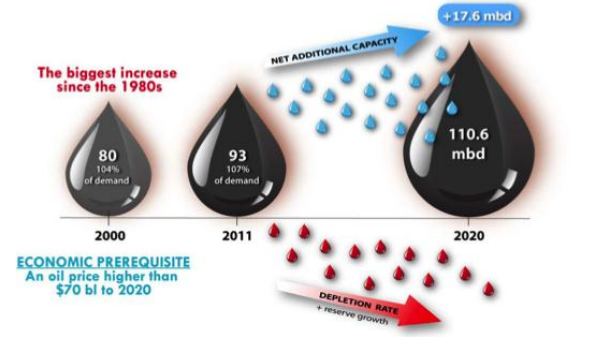

The oil production capacity is a very badly defined value and the data for OPEC spare capacity from EIA and IEA differs widely, as shown by Rembrandt Koppelaar in these two graphs from 2003 to 2009 (http://europe.theoildrum.com/node/5787).
EIA reports very little UAE spare capacity in 2003 when IEA reports more than 2 Mb/d.
Figure 1: OPEC spare capacity by EIA & IEA from Koppelaar 2003-2009

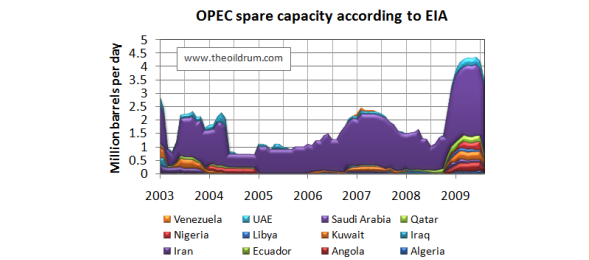

Figure 1 - OPEC spare capacity according to the Energy Information Administration from January 2003 to August 2009

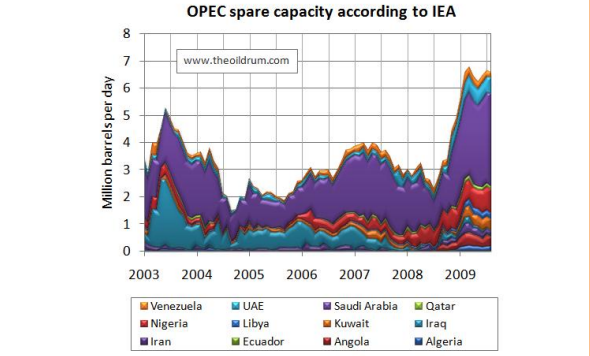

Figure 2 - OPEC Spare Capacity from January 2003 to August 2009 according to the International Energy Agency

Table 3: Additional production from U.S. shale/tight oil plays by 2020 (million barrels per day)

Shale play	Additional, unrestricted production	Additional adjusted production
Bakken/Three Forks	2.5	1.5
Eagle Ford	2.1	1.47
Permian	1	0.7
Utica	0.2	0.1
Niobrara/Codell	0.2	0.1
Others	0.6	0.3
Total	***6.6***	***4.17***

The term shale oil is now old fashion and replaced by tight oil! The word shale is now connected to hydraulic fracturation (called fracking in the medias) and has bad reputation. It is time to use a better term!

Maugeri forecasts an increase of tight oil production of 4.17 (admire the accuracy!) Mb/d from 2010 to 2020, when AEO 2012 (figure 55) forecasts an increase of 0.8 Mb/d in reference case and a maxi of 1.9 Mb/d, less than half of Maugeri's claim!

Like I always say, when more than two significant digits are given, it means that the second is surely wrong and likely the first one, because the author has a very poor understanding of the accuracy of the data!

Figure 46: AEO 2012 forecast on US tight oil production 2000-2035

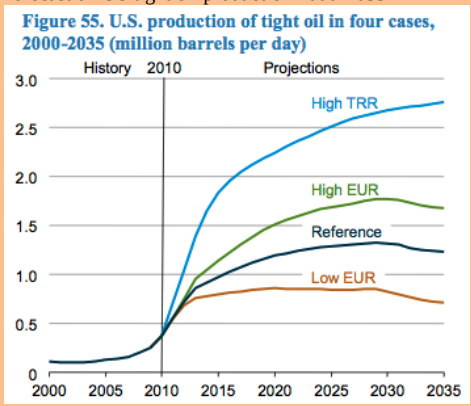

-page 64

The oil market is already adequately supplied with spare capacity of around 4 mbd

IEA Oil market report for July 2012 states: "OPEC's effective spare capacity in June was 2.35 mb/d", far from Maugeri's 4 Mb/d. But this 2.35 Mb/d is also wrong!

-page 66

The shale/tight oil boom in the United States is ***not a temporary bubble****, but the most important revolution in the oil sector in decades.*

Bakken production in Montana (see figure 17) looks a temporary bubble as it was for the peak in 1968.